Dissertation zur Erlangung des Doktorgrades
der Fakultät für Chemie und Pharmazie
der Ludwig-Maximilians-Universität München

GroEL Ring Separation and Exchange in the Chaperonin Reaction

Xiao Yan

aus

Qian'an, China

2018

Erklärung

Diese Dissertation wurde im Sinne von §7 der Promotionsordnung vom 28. November 2011 von Herrn Prof. Dr. F. Ulrich Hartl betreut.

Eidesstattliche Versicherung

Diese Dissertation wurde eigenständig und ohne unerlaubte Hilfe erarbeitet.

München, 07. November 2018

Xiao Yan

Dissertation eingereicht am	15.11.2018
1. Gutachterin / 1. Gutachter:	Prof. Dr. F. Ulrich Hartl
2. Gutachterin / 2. Gutachter:	Dr. Dejana Mokranjac
Mündliche Prüfung am	28.01.2019

Acknowledgements

Foremost I would like to express my deepest gratitude to my supervisors Dr. Manajit Hayer-Hartl and Prof. Dr. F. Ulrich Hartl who provided me with an opportunity to work on this extremely interesting project. I am very thankful to them for the constant support and advice throughout the entire period of my study. Importantly, working with them allowed me to see how scientists of great eminence work, which will be invaluable throughout my career.

Very special thanks to Dr. Qiaoyun Shi, Dr. Andreas Bracher, Dr. Goran Miličić, and Amit. K. Singh for their collaboration on exploring the nature of ring separation and exchange in the chaperonin reaction.

Thanks to Dr. Amit. J. Gupta, Dr. Shubhasis Haldar, Dr. David Balchin, Dr. Javaid. Y. Bhat, and Dr. Harald Aigner for experimental help and productive discussions. I thank Dr. Amit. J. Gupta, Dr. Shubhasis Haldar, Dr. Sneha Kumar, Dr. Niti Kumar, Dr. Rajat Gupta, and Dr. Gopal Jayaraj for friendship, moral support, and their scientific expertise. Thanks to Dr. Neysan Donnelly and Dr. Lucas Cairo for kindly correcting the thesis.

I thankfully acknowledge the great professional help of the Hartl-lab technical staff: Emmanuel Burghardt, Nadine Wischnewski, Albert Ries, Romy Lange, Anastasia Jungclaus, and Silvia Gaertner.

Thanks to all hartl-fighters, especially Dr. Young-Jun Choe, Dr. Sae-Hun Park, Dr. Prasad Kasturi, and Chandhuru Jagadeesan for their helpful suggestions and the true atmosphere of science, which I will always remember.

Finally, my deepest thanks go to my family and especially my father. Without their love, patience and constant support this work would not exist.

Contents

List of abbreviations

aa	Amino acid
ADP	Adenosine 5’-diphosphate
Ala	Alanine
Apy	Apyrase
ATP	Adenosine 5’-triphosphate
CDTA	1,2-Cyclohexylenedinitrilotetraacetic acid
CTD	C-terminal dimerization domain in Hsp90
Cys	Cysteine
Da	Dalton
DapA	Dihydrodipicolinate synthase
dcFCCS	Dual-color fluorescence cross-correlation spectroscopy
DM-MBP	Double-mutant maltose binding protein
DNA	Deoxyribonucleic acid
DOL	Degree of labeling
DTT	Dithiothreitol
DUB	Deubiquitinating enzyme
E. coli	*Escherichia coli*
ER	Endoplasmic reticulum
ERAD	Endoplasmic reticulum-associated degradation
FCS	Fluorescence correlation spectroscopy
FRET	Fluorescence resonance energy transfer
GuHCl	Guanidine hydrochloride
Hop	Hsc70/Hsp90 organizing protein

HS buffer	High-salt buffer
Hsp	Heat shock protein
IPTG	Isopropyl β-D-thiogalactopyranoside
Kan	Kanamycin
LB	Lysogenic broth
MD	Middle domain in Hsp90
β-ME	β-mercaptoethanol
mMDH	Mitochondrial malate dehydrogenase
MOPS	3-morpholinopropane-1-sulfonic acid
MPIB	Max Planck Institute of Biochemistry
NAC	Nascent chain-associated complex
NADH	Nicotinamide adenine dinucleotide, reduced form
NBD	N-terminal nucleotide-binding domain in Hsp70
NEF	Nucleotide exchange factor
NTD	N-terminal nucleotide-binding domain in Hsp90
PCR	Polymerase chain reaction
PEP	Phosphoenolpyruvate
Pfd	Prefoldin
PN	Proteostasis network
RAC	Ribosome-associated complex
Rho	mitochondrial rhodanese
SBD	C-terminal substrate-binding domain in Hsp70
SDS-PAGE	Sodium dodecyl sulfate-polyacrylamide gel electrophoresis
SEC	Size-exclusion chromatography
Ser	Serine

TCA	Trichloroacetic acid
TF	Trigger factor
TPR	Tetratricopeptide repeat
Tris	2-Amino-2-hydroxymethyl-propane-1,3-diol
Ub	Ubiquitin
UPS	Ubiquitin-proteasome system

1 Summary

The bacterial chaperonin GroEL and its cofactor GroES form a nano-cage for a single molecule of substrate protein (SP) to fold in isolation. GroEL and GroES undergo an ATP-regulated interaction cycle that governs the closing and opening of the folding cage. GroEL consists of two heptameric rings, stacked back-to-back, and displays intra-ring positive allosteric cooperativity and inter-ring negative allostery. Previous reports have suggested that ring separation and exchange can occur between the non-covalently bound rings of GroEL; however, the mechanism and physiological function of this phenomenon had yet to be explained.

Here I show that GroEL undergoes transient ring separation, resulting in ring exchange between complexes. Through the ATPase cycling of GroEL/ES, ring separation is shown to occur upon ATP-binding to the *trans*-ring of the asymmetric GroEL:7ADP:GroES complex in the presence or absence of SP. Ring separation is a consequence of inter-ring negative allostery. To address the physiological function of this phenomenon, I created a novel mutant with the two rings connected by disulfide bonds. This GroEL mutant, unable to perform ring separation, is folding-active but populates symmetric GroEL:$GroES_2$ complexes with GroES bound to both rings of GroEL, where both GroEL rings function simultaneously rather than sequentially. As a consequence, SP binding and release from the folding chamber is inefficient, and *E. coli* growth is impaired. My results suggest that transient ring separation is an integral part of the chaperonin mechanism to ensure sequential GroEL/ES cycling and effective SP folding.

2 Introduction

Proteins are macromolecules consisting of one or more long chain of amino acid residues. Proteins perform almost all of the physiological activities inside cells: they form key structural elements (molecules of the cytoskeleton, epidermal keratin, collagen, viral coat proteins), catalyze metabolic reactions (enzymes), transport molecules (ion channels, specific transporters and pumps), and are involved in the regulation of cell signaling and gene expression (kinases, hormones, receptors, DNA-binding proteins), communication with the environment (sensor proteins), cell movement and changes in shape (myosin, kinesin, flagellum), defense against viral and bacterial infection (the immune system), and in the storage of nutrients and energy (casein, ovalbumin, gluten).

Just as a piece of paper can fly only when it is folded into a paper plane, a protein must fold into a specific and precise structure to fulfill its designated physiological function. The process in which a polypeptide assumes its unique three-dimensional structure is called protein folding.

2.1 Protein folding

2.1.1 Protein structure

Proteins are synthesized from varying combinations of 20 different amino acids. This obeys a universal feature of nature: A few types of building blocks can be combined in different ways to produce a huge variety of complicated structures. According to the central dogma of molecular biology, proteins are specified by their amino acid sequences, which are encoded in the DNA.

An amino acid consists of an amino group ($-NH_3^+$) and a carboxylate group ($-COO^-$), as well as a side chain known as an R group with variable chemical properties (hydrophobic, polar, charged). The peptide bond formed between the $-COO^-$ of one amino acid and the $-NH_3^+$ of the successive one links amino acids together to form a polypeptide. The amino acid sequence is the first level of protein structure and is called the primary structure.

The conformation of the polypeptide backbone, excluding the side chains, is known as the secondary structure. Due to its partial (~40%) double-bond character, the peptide bond cannot rotate. Therefore, the repeating Cα-C-N-Cα chemical structure can be considered as a series of planar groups (Figure 2.1). The flexibility of the peptide backbone stems from its rotation around a single bond of N-Cα (angle ϕ) and Cα-C (angle Ψ). The steric interference between the polypeptide backbone and side chains limits the possible combinations of torsion angles, which is described by the Ramachandran diagram. The amide groups and carbonyl oxygens involved in the peptide bonds are strongly polar and show a high tendency to form hydrogen bonds. Under physiological conditions, the polypeptide chain readily folds to satisfy as many of these hydrogen-bonding requirements as possible. Meanwhile, the polypeptide backbone and side chains must adopt a conformation to minimize their steric strain. As a result, two types of secondary structure are commonly found in proteins: the α-helix and the β-sheet.

The three-dimensional shape of a protein is defined as its tertiary structure, and is determined by the secondary structure (the overall folding of its peptide backbone) and the spatial arrangement of all the side chains. The tertiary structure of a protein is mainly stabilized by hydrophobic interactions. The nonpolar side chains are located predominantly in the interior of a protein and form the hydrophobic core that stabilizes the folded protein. Unfolding or exposing the

interior core would be entropically unfavorable. In addition, hydrogen bonds, van der Waals interactions between atoms, and cross-links (e.g., ion pairs, disulfide bonds, and inorganic ions) also help to fine-tune the folded conformation of a protein.

Many proteins, once folded, assemble with other polypeptide subunits to form homo- or hetero-oligomeric complexes. The spatial arrangement of these subunits is known as the quaternary structure. The forces that keep subunits together are similar to those that stabilize the tertiary structure of the individual subunits. Cells synthesize extremely large proteins for more complicated functions by assembling multiple-subunit complexes. The production of such large proteins would be virtually impossible if they were synthesized only as single large polypeptides. In addition, the interactions between subunits provide for allosteric regulation.

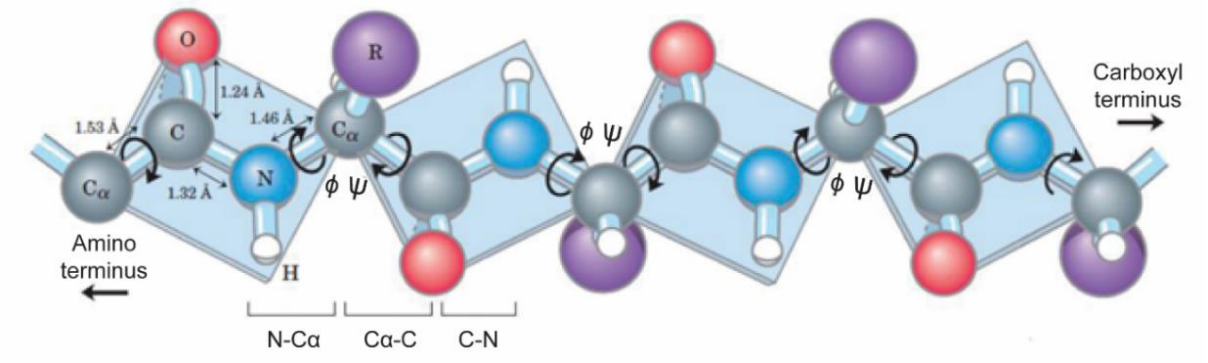

Figure 2.1 Torsion angles in the protein backbone.
Schematic of a protein backbone with indicated torsion angles between peptide bond planes. Each peptide bond is planar and cannot rotate. N-Cα and Cα-C bonds can rotate, with assigned bond angles of ϕ and ψ, respectively. Figure modified from Nelson and Cox (2005).

2.1.2 The complexity of protein folding

One of the key questions in biochemistry is how a linear polypeptide folds into its native structure. Pioneering experiments by Christian Anfinsen on the refolding of ribonuclease A indicated that all the information required for protein folding is stored within its amino acid sequence (Anfinsen, 1973; Anfinsen et al., 1955).

However, there are no completely reliable methods to predict a protein's structure and function only from its amino acid sequence.

The primary sequence determines the final native structure of a protein, which is usually the most thermodynamically stable state. However, Anfinsen's theory cannot tell us about the folding trajectory of a polypeptide. The famous Levinthal's paradox indicates that a 100-aa polypeptide in principle can adopt 10^{100} possible conformations. Exploring the entire conformational space to find the single conformation of the native state would take ~10^{77} years, exceeding by far the timescale of the universe (Levinthal, 1968). However, protein folding is usually very fast (at least for small proteins ≤ 100 amino acids), occurring within milliseconds to seconds, and *E. coli* cells, for example, divide approximately every 20 minutes, having doubled and folded their proteome. Therefore, protein folding cannot be a random process but must occur through one or a few preferred trajectories (folding pathways). During the folding process, small elements of secondary structure form first, and then these coalesce under the predominant hydrophobic effect to produce a molten globular intermediate with a still fluctuating hydrophobic core. Final rearrangements yield the native structure (Figure 2.2A) (Goldberg, 1985; Teufel et al., 2011). Future advances in computational folding simulation will contribute to a more detailed description of the folding trajectory.

One influential approach to energetically describe the global folding trajectory is that a protein progresses on a funnel-shaped potential energy landscape with several downhill routes (Figure 2.2B) (Hartl et al., 2011; Schultz, 2000). Chain collapse and a progressive increase in native interactions rapidly restrain the conformational space that needs to be explored *en route* to the native state. However, the free energy of the folding landscape is usually rugged, suggesting that polypeptides have to overcome substantial kinetic barriers to reach their native states.

As a consequence, partially folded intermediates may transiently populate kinetically trapped species, either as disorganized globules maintaining large configurational entropy but lacking specific native interactions, or as intermediates stabilized by non-native contacts. In the former case, searching for crucial native contacts within the globule will limit the folding rate, whereas in the latter instance, breaking non-native contacts may become rate limiting. Long-lived folding intermediates, which typically expose hydrophobic residues and unstructured polypeptide backbone regions, would readily form aggregates in a concentration-dependent manner (Figure 2.2B). Aggregation formation is largely driven by hydrophobic interactions and primarily results in amorphous structures. Alternatively, highly ordered amyloid fibrils defined by cross-β-strand structure, eventually impair cellular functions (Woerner et al., 2016) and are hallmarks of degenerative disorders such as Alzheimer's disease, Parkinson's disease, Huntington's disease, and amyotrophic lateral sclerosis (ALS) (Kim et al., 2013; Labbadia and Morimoto, 2015).

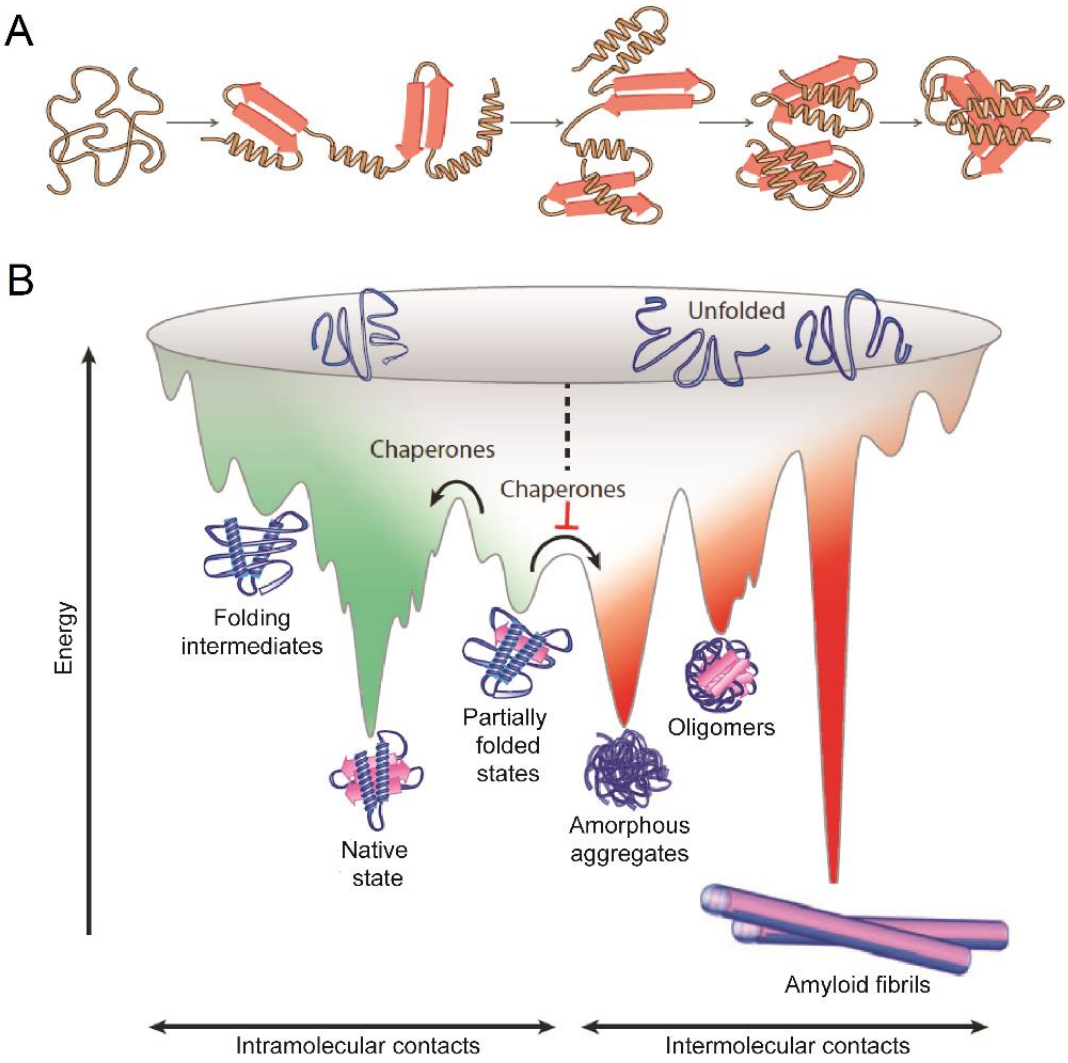

Figure 2.2 Model for protein folding.

(A) The polypeptide first forms secondary structure elements (α-helices and β-sheets). These structures collapse into a single molten globule, and rearrangement steps generate the final tertiary structure. (B) Schematic of a funnel-shaped folding energy landscape. Proteins that are folded from an unfolded polypeptide to the native conformation can proceed through local energy minima and kinetic traps along the downhill pathway. Protein folding is driven by the formation of native intramolecular interactions. In cases where several polypeptides fold in the same space (e.g., the cytosol), intermolecular interactions can occur. The folding energy landscape can overlap with that of intermolecular aggregation. Aggregates can happen as small oligomers, amorphous or fibrillar deposits. Chaperones will interact with various intermediate states, either preventing their aggregation formation, assisting their productive folding, or even accelerating the degradation of aggregates. Figure B modified from Hartl et al. (2011) and Kim et al. (2013).

2.2 Protein folding in the cell

2.2.1 The challenge of protein folding *in vivo*

Many small proteins refold into their specified three-dimensional structures after the removal of the denaturant *in vitro*, a process which is guided by the information encoded within their amino acid sequences. Although the Anfinsen principle generally holds true, the folding process is more complex inside the living cell. Research over the past decades has firmly established that *in vivo*, protein folding becomes considerably more challenging due to macromolecular crowding. Compared with the dilute conditions *in vitro*, total cytosolic proteins reach a concentration of 300–400 g L^{-1}, which leads to considerable excluded volume effects (Ellis, 2001; Ellis and Minton, 2006). These excluded volume effects, while favoring the functional interactions between macromolecules, strongly enhance the tendency of non-native and structurally flexible proteins to aggregate (Ellis and Minton, 2006; van den Berg et al., 1999).

Protein folding *in vivo* is further complicated by the vectorial synthesis of polypeptide chains from the N-terminus to the C-terminus on ribosomes. The nascent chain must be maintained in a folding-competent state in which (mis)folding is delayed, until substantial segments or a complete domain have emerged from the ribosome exit tunnel. This is especially true for those proteins with significant long-range interactions that are necessary for cooperative domain folding. Particularly in such proteins, nascent chains may undesirably engage in non-native intra- and inter-chain interactions during the delay in folding (Zhang and Ignatova, 2011). In addition, many nascent chains, prior to complete folding, need to be transported into specific subcellular compartments, e.g., the endoplasmic reticulum (ER), mitochondria, and cell membranes (Young et al., 2003). Therefore, the translocation

process also increases the risk of protein misfolding and aggregation (Gloge et al., 2014).

To ensure that proteins successfully navigate the complex free-energy landscape and are maintained in soluble yet conformationally dynamic states under crowding conditions, and also in order to cope with harmful aggregation, cells have evolved a comprehensive protein homeostasis (proteostasis) network. This system coordinates protein synthesis, folding, disaggregation, and degradation to suppress protein aggregation (Powers et al., 2009).

2.2.2 The proteostasis network

Proteostasis is ensured by the coordinated activity of a diverse set of proteins collectively known as the proteostasis network (PN). The PN is generally defined as a network of proteins with a role in protein synthesis, folding, disaggregation, and degradation, encompassing the translational machinery, molecular chaperones and cochaperones, the ubiquitin-proteasome system (UPS), and the autophagy-lysosome system (Figure 2.3) (Labbadia and Morimoto, 2015). Also, some other components, e.g., transcription factors, chromatin remodelers, structural components, signaling pathway components, metabolic factors, transport machinery, and regulators of posttranslational modifications, are indirectly involved in proteostasis and are considered critical and essential auxiliary factors of the PN (Akerfelt et al., 2010; Labbadia and Morimoto, 2015; Walter and Ron, 2011).

The PN is a multi-compartmental system and is integral to cell viability and organismal health. Subnetworks of the PN in different subcellular compartments have evolved accordingly in response to the specific proteomes that they encounter. Temporal and spatial changes in the composition and activity of PN can influence

proteostasis, aging, and disease. In fact, loss of proteostasis is a common characteristic associated with aging and disease, which is defined by the accumulation of non-native protein aggregates in different tissues (Labbadia and Morimoto, 2015). Therefore, a better understanding of the temporal and spatial properties of the PN will guide future efforts to develop effective pharmacological treatments in protein conformational diseases. Here, I will focus on how molecular chaperones and cochaperones assist protein folding and maintain proteostasis.

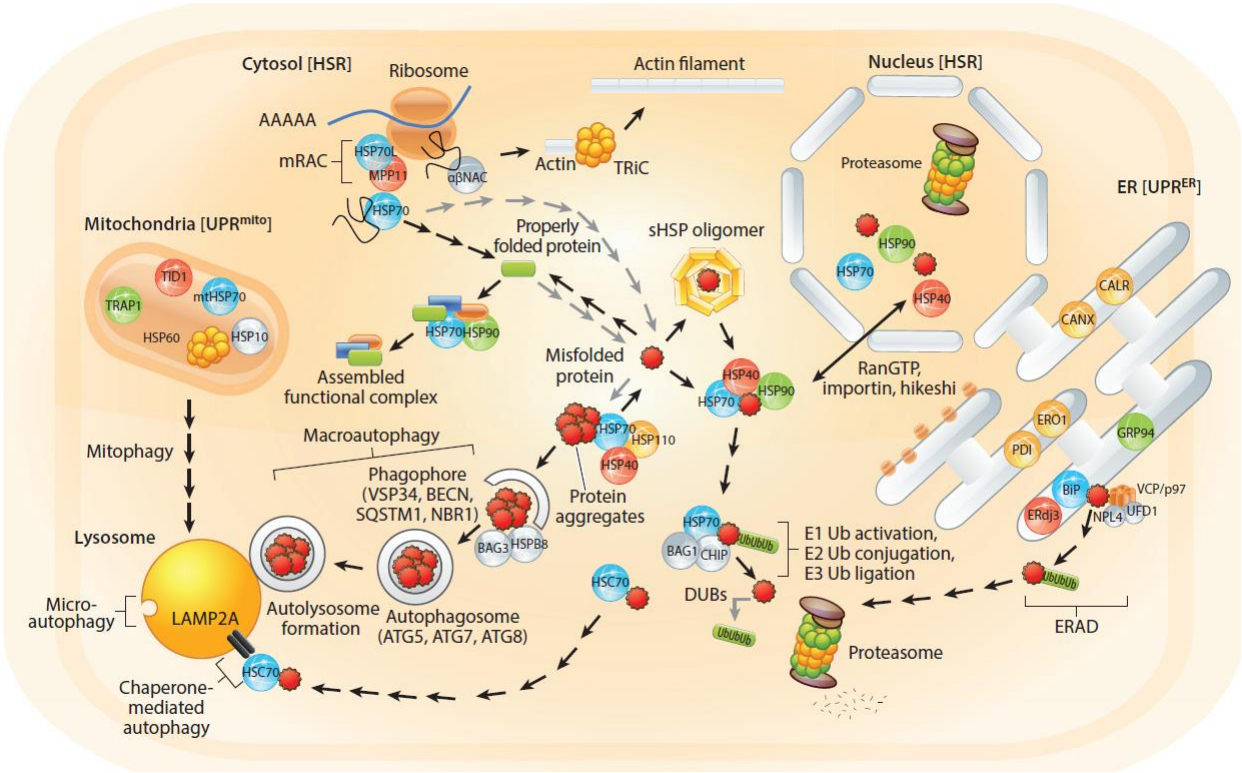

Figure 2.3 Overview of the proteostasis network.
Molecular chaperones of the Hsp70 (blue spheres), Hsp40/DNAJ (red spheres) and Hsp90 (green spheres) families are present in all major cellular compartments, where they cooperate with cochaperones (gray spheres) as central hubs to promote folding of nascent chains, assembly of protein complexes, disaggregation and refolding of misfolded proteins (serrated red spheres), and degradation of terminally misfolded substrates by the proteasome and autophagy. Small heat shock protein (sHsp) oligomers bind misfolded proteins and keep them in a folding-competent state for Hsp70 and other chaperone systems. If refolding fails, Hsp70, in cooperation with the nucleotide exchange factor Bcl2-associated athanogene 1 (BAG1) and the E3 ubiquitin ligase C-terminus of HSC70-interacting protein (CHIP), can lead protein substrates to the proteasome for degradation.

The Hsp60 family of chaperones is indispensable for mitochondrial proteostasis (in collaboration with the cochaperone Hsp10) and for folding of cytoskeletal components via the TCP-1 ring complex (TRiC) in the cytosol. Some chaperones and cochaperones show specialized or compartment-specific functions (orange spheres). For instance, in the ER, ER oxidoreductin 1 (ERO1) and protein disulfide isomerase (PDI) work together to stimulate disulfide bond formation. Specific stress response pathways, e.g., the heat shock response and unfolded protein responses of the ER (UPR_{ER}) and mitochondria (UPR_{mito}), can be activated upon protein misfolding and boost chaperone levels. Sometimes misfolded proteins can form aggregates deleterious to cells. Hsp110 together with Hsp70/Hsp40 act as a disaggregase. Finally, the unsolved aggregates are passed to the ubiquitin-proteasome system (UPS) for degradation, while even larger aggregates can be eliminated by the lysosome through autophagy. Gray arrows indicate processes which are active at low levels in healthy cells. Abbreviations: DUB, deubiquitinating enzyme; ERAD, ER-associated degradation; mRAC, mammalian ribosome-associated complex; NAC, nascent chain–associated complex; Ub, ubiquitin. Figure modified from Labbadia and Morimoto (2015).

2.3 Molecular chaperones network

A molecular chaperone can be defined as any protein that interacts with, stabilizes, or helps another client protein to reach its functionally active state, without being part of its final structure (Hartl, 1996). Chaperones were first discovered as proteins whose expression increase upon heat stress and were therefore dubbed heat shock proteins (Hsp) (Tissieres et al., 1974). Pioneering work on molecular chaperone functions in protein folding and/or assembly of certain client proteins represents a quantum leap in understanding cellular protein folding in addition to Anfinsen's theory (Cheng et al., 1989; Goloubinoff et al., 1989; Ostermann et al., 1989).

Chaperones are broadly classified according to molecular weight into the Hsp40, Hsp60, Hsp70, Hsp90, Hsp100, and small Hsp families (Hartl et al., 2011; Kim et al., 2013). They are now known to play key roles in a multitude of aspects of proteome maintenance, including *de novo* folding, disaggregation and refolding of stress-denatured proteins, oligomeric assembly, protein transport, and support in proteolytic degradation (Hartl et al., 2011; Kim et al., 2013). Moreover, chaperones

robustly buffer unstable proteins, especially mutants with compromised stability, and therefore allow the evolution of new functions for these proteins and of novel phenotypic traits (Rutherford and Lindquist, 1998; Tokuriki and Tawfik, 2009). In general, many chaperones recognize the exposed hydrophobic residues of client proteins and regulate folding process through ATP- and cofactor-regulated binding and release cycles (Mayer, 2010).

The general organization of the chaperone network is conserved throughout evolution (Kim et al., 2013) (Figure 2.4). In all domains of life, ribosome-associated chaperones, e.g., trigger factor (TF) in bacteria, ribosome-associated complex (RAC) and nascent chain-associated complex (NAC) in eukaryotes, are the first chaperones encountered by a newly synthesized polypeptide. These upstream chaperones prevent the emerging polypeptides from premature (mis)folding and maintain them in a non-aggregated and folding-competent state (Kaiser et al., 2006). Non-ribosome-bound members of the Hsp70 system, in cooperation with cochaperones (Hsp40s and nucleotide exchange factors), can mediate the folding of longer nascent chains co- or posttranslationally (Calloni et al., 2012). Some proteins require further assistance for folding from downstream chaperone systems, e.g., the chaperonin system (Kerner et al., 2005) and Hsp90 (Wandinger et al., 2008). Overall, the translational machinery and molecular chaperones have been highly optimized and coordinated through evolution, which ensures efficient folding for the bulk of newly synthesized proteins (Vabulas and Hartl, 2005).

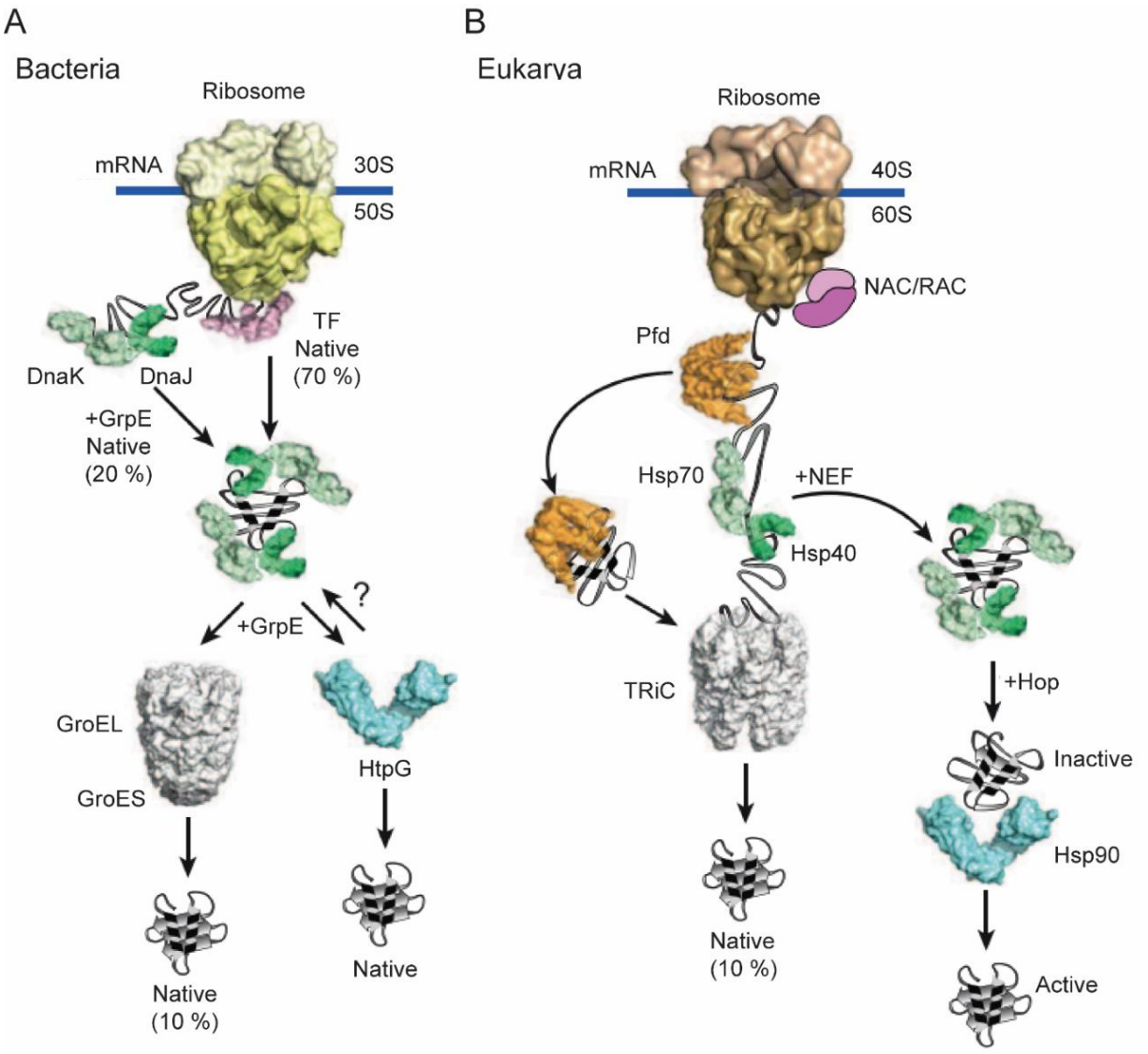

Figure 2.4 Organization of chaperone network in the cytosol.
In bacteria (A) and eukaryotes (B), ribosome-associated chaperones, e.g., trigger factor (TF) in bacteria, ribosome-associated complex (RAC), and nascent chain-associated complex (NAC) in eukaryotes, initially assist folding cotranslationally by interacting with hydrophobic segments on the emerging nascent polypeptides. Non-ribosome-bound members of the Hsp70 family (DnaK in bacteria and Hsc70 and Hsp70 in eukaryotes), together with Hsp40s (DnaJ in bacteria) and nucleotide exchange factors (NEFs; GrpE in bacteria), function as second-tier chaperones to fold longer nascent chains co- or posttranslationally. Partially folded substrates can also be transferred to downstream chaperones that assist folding into native structures, such as the chaperonin (GroEL/ES in bacteria and TRiC in eukaryotes) and Hsp90 (HtpG in bacteria). Substrate transfer from Hsc70 to Hsp90 is facilitated by the coupling cochaperone Hsc70/Hsp90 organizing protein (Hop). Percentages indicate the approximate protein flux of the whole proteome through the chaperone network. Figure modified from Balchin et al. (2016) and Kim et al. (2013).

2.3.1 Ribosome-associated chaperones

The nascent polypeptide chain is topologically restricted on the ribosome until the C-terminal region of the protein is released to engage in long-range interactions. Therefore, ribosome-associated chaperones cotranslationally prevent the emerging nascent polypeptides from unfavorable intra- and intermolecular interactions, typically by protecting exposed hydrophobic segments (Kim et al., 2013). Such chaperones include trigger factor (TF) in prokaryotes, ribosome-associated complex (RAC) and nascent chain-associated complex (NAC) in eukaryotes (Bukau et al., 2000; Preissler and Deuerling, 2012).

TF (~50 kDa) has an elongated three-domain structure and binds to the ribosome in a 1:1 stoichiometry using ribosomal protein L23 as the major docking site (Hoffmann et al., 2010). By localizing directly at the ribosomal exit site, TF binds to hydrophobic stretches in nascent chains, presumably delaying chain collapse and keeping them in folding-competent states. As a result, TF slows down the rate of cotranslational folding but increases the folding yield. For longer nascent chains, TF cooperates with the downstream DnaK/DnaJ system (Figure 2.4). The release of nascent chains from TF is not ATP-dependent but is governed by the propensity to bury hydrophobic segments during translation. Deletion of TF in *E. coli* is only lethal upon co-deleting DnaK (Hsp70 protein) at temperatures above 30°C, and *vice versa*, indicating that these proteins show functional redundancy (Genevaux et al., 2004).

In eukaryotes, RAC and NAC fulfill a similar role to that of TF in nascent chain folding, even though they are structurally irrelevant (Figure 2.4). RAC in *Saccharomyces cerevisiae* and other fungi, consisting of the specialized Hsp70 Ssz1 and Hsp40 zuotin (Hsp70L1 and Mpp11 in mammals), assists nascent chain folding in cooperation with the ribosome-binding Hsp70 isoforms Ssb1 and Ssb2 (Koplin et

al., 2010; Preissler and Deuerling, 2012; Willmund et al., 2013). NAC, a heterodimer consisting of α (31 kDa) and β (22 kDa) subunits, docks on the ribosome via the β subunit and binds short nascent chains. Recent findings show that NAC is not only important for cotranslational folding of nascent chains, but is also required for proper intracellular protein sorting (del Alamo et al., 2011; Gamerdinger et al., 2015).

2.3.2 The Hsp70 machinery

A large fraction of proteins are not able to reach their native states with the help of ribosome-associated chaperones alone. For these proteins (≥ 30% of the proteome), the next level of assisted folding is carried out by the Hsp70 system. Hsp70 (DnaK in bacteria) acts as a central hub in the cytosolic chaperone network and participates in a wide range of cellular processes, including protein folding, refolding, disaggregation, and protein trafficking to cellular compartments or the proteolytic machinery (Calloni et al., 2012).

Hsp70 has two domains connected via a hydrophobic linker region: an N-terminal nucleotide-binding domain (NBD, ~40 kDa) and a C-terminal substrate-binding domain (SBD, ~30 kDa) (Figure 2.5A). The SBD consists of a β-sandwich domain with the substrate binding site and an α-helical lid segment. A peptide substrate with a 5- to 7-aa motif enriched in hydrophobic resides binds in a groove of the β-sandwich domain. The NBD harbors the nucleotide binding pocket and regulates the functional substrate protein (SP) cycling via ATP binding and hydrolysis (Mayer, 2010).

The Hsp70 reaction cycle is closely regulated by the cochaperone Hsp40 and nucleotide exchange factors (NEFs) (Figure 2.5B). Hsp40 (also known as DnaJ in bacteria) functions in recognizing and delivering substrates to Hsp70 in its ATP-

bound state, where the hydrophobic linker and the α-helical lid of the SBD are contacted with the NBD, resulting in the SBD in an open conformation with high *on* and *off* rates for substrates. The interaction of Hsp40 with the Hsp70 NBD as well as with the hydrophobic linker segment strongly stimulates ATP hydrolysis (>1000-fold) in the NBD. The hydrolysis of ATP to ADP allosterically leads to α-helical lid closure and thus traps the bound SP tightly with low *on* and *off* rates (Mayer, 2013). Subsequent NEF (GrpE in bacteria) binding to the NBD catalyzes ADP-ATP exchange, resulting in α-helical lid opening and SP release for folding or transfer to downstream chaperones or the degradation machinery (Balchin et al., 2016). By going through consecutive cycles of high and low SP binding affinity, i.e., binding and release of extended hydrophobic segments, Hsp70 prevents off-pathway aggregation and reverses misfolding by eliminating abnormal long-range interactions present in the folding intermediate (kinetic partitioning mechanism) (Hartl et al., 2011).

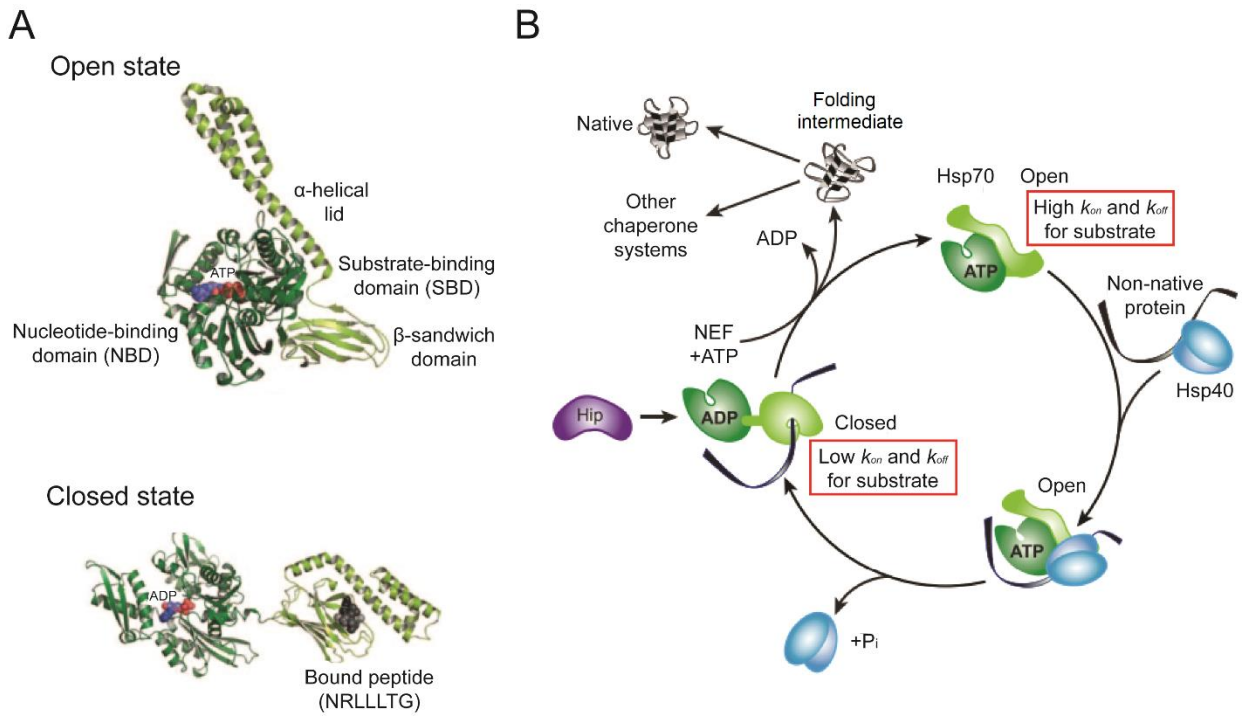

Figure 2.5 Hsp70 reaction cycle.

(A) Structure of DnaK, the bacterial Hsp70. A large conformational change in Hsp70 is driven by ATP binding and hydrolysis at the nucleotide-binding domain (NBD). ATP binding induces the open state (left: PDB 4B9Q), where the α-helical lid of the substrate-binding domain (SBD) is attached to the NBD with high on and off rates for the peptide substrate. Upon ATP hydrolysis to ADP, Hsp70 changes to the closed state (right: PDB 2KHO), where the SBD separates from NBD, and the α-helical lid is closed over the peptide binding cleft with low on and off rates for the substrate. (B) The Hsp70 system cycle. A nonnative protein first interacts with Hsp40 and is transferred to ATP-bound Hsp70 (open state). ATP hydrolysis on Hsp70 is accelerated by interaction with Hsp40, and Hsp70 transits to the closed state. ADP release is catalyzed by nucleotide exchange factor (NEF), and subsequent ATP recruitment triggers SP release for folding or further transfer to downstream chaperones. Hip in metazoans delays SP release by stabilizing the ADP-bound state. Figure modified from Balchin et al. (2016).

2.3.3 The Hsp90 machinery

In eukaryotes, Hsp90 constitutes a proteostasis hub that manages numerous important signaling pathways (Taipale et al., 2010). Besides protein folding, Hsp90 also supports conformational maturation and maintenance of a range of important signaling proteins, including proto-oncogenic kinases, transcription factors, and steroid hormone receptors (Balchin et al., 2016; Taipale et al., 2012). Hsp90 effectively buffers destabilizing mutations in its client proteins, thereby allowing the acquisition of new evolutionary traits (Lindquist, 2009; Rutherford and Lindquist, 1998).

Hsp90 functions as a dimer, and each subunit consists of an N-terminal nucleotide-binding domain (NTD, ~25 kDa), a C-terminal dimerization domain (CTD, ~12 kDa), and a middle domain (MD, ~40 kDa) bridging the NTD and CTD (Ali et al., 2006; Karagoz and Rudiger, 2015; Verba et al., 2016) (Figure 2.6A). The Hsp90 dimer undergoes an ATP-driven reaction cycle accompanied by conformational rearrangement (Figure 2.6B). These dynamic conformations are selectively stabilized by nucleotides, client proteins, and various cochaperones. In the absence of ATP, Hsp90 is in an open state. ATP binding triggers the lid segment

of the NTD to close over the bound nucleotide, resulting in NTD dimerization via strand exchange. A flexible loop from the MD interacts with the NTD, resulting in a twisted closed state with residues from the MD accelerating ATP hydrolysis (Rohl et al., 2013). After ATP hydrolysis and ADP release, Hsp90 transits to the open conformation (Figure 2.6B). The rate-limiting step for the Hsp90 cycle is not ATP hydrolysis but the large conformational rearrangement from open to closed (Hessling et al., 2009).

Hsp90 cooperates with different cochaperones to regulate its ATPase activity and recruit substrates. Many cochaperones use tetratricopeptide repeat (TPR) domains to bind Hsp90 (Scheufler et al., 2000). For example, Hop facilitates client transfer from upstream Hsp70 to Hsp90, and Cdc37 works as an adapter for kinase proteins. Therefore, both Hop and Cdc37 will stabilize the open state of Hsp90, inhibit ATPase activity, and facilitate client binding (Scheufler et al., 2000; Verba et al., 2016). In contrast, Aha1 binds to the NTD and MD of an Hsp90 dimer in an asymmetrical way, facilitating a transition to the closed state and thereby stimulating ATPase activity (Retzlaff et al., 2010). In addition, p23 acts towards the end of the cycle and accelerates the maturation of clients by stabilizing the closed conformation of Hsp90 before ATP hydrolysis (Li et al., 2012). No cochaperone has yet been discovered for the bacterial Hsp90, HtpG.

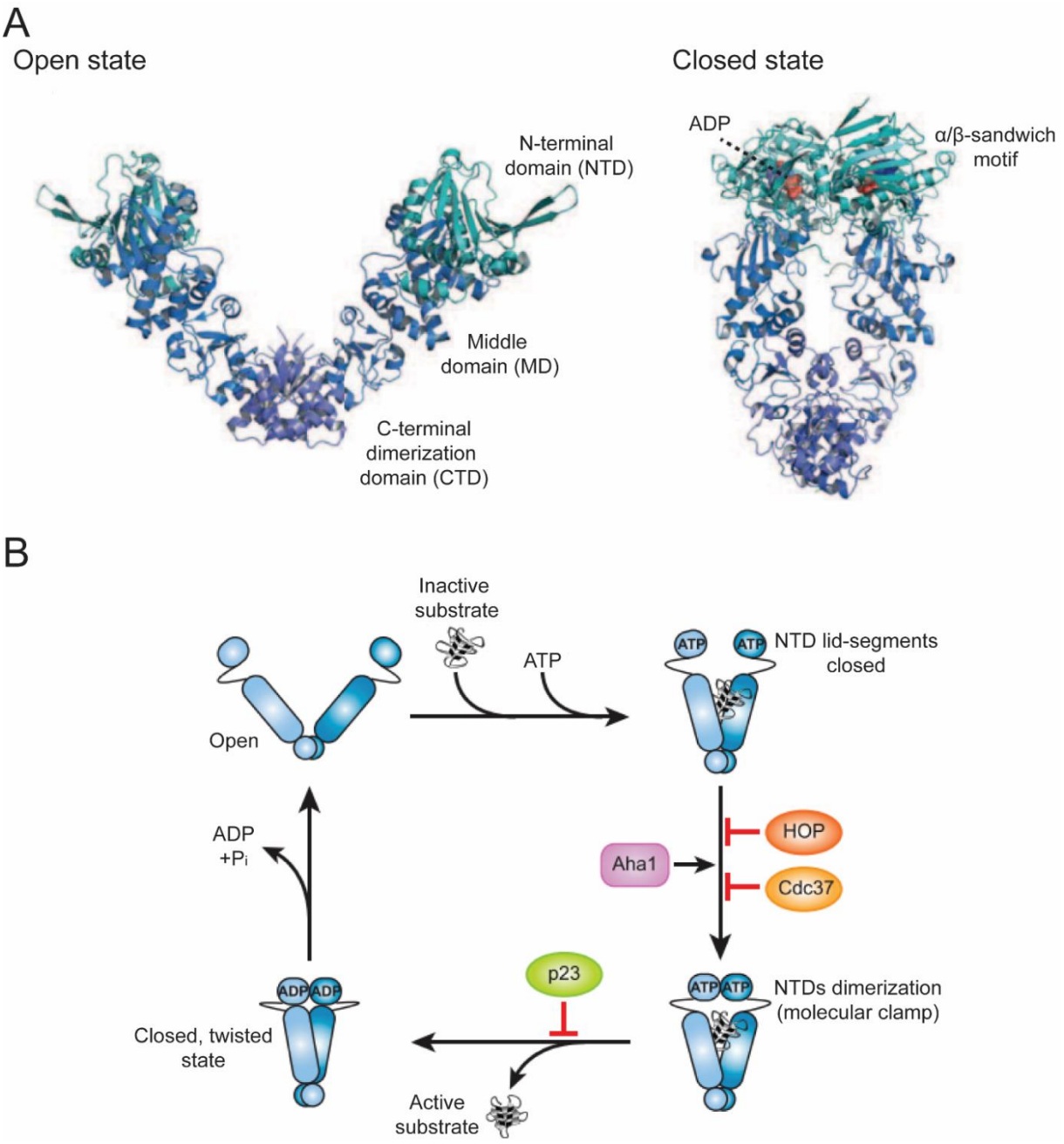

Figure 2.6 Hsp90 reaction cycle.

(A) Crystal structures of bacterial Hsp90 in an open state (left: PDB 2IOQ) and of yeast Hsp90 in a closed state (right: PDB 2CG9). Each subunit consists of an N-terminal nucleotide-binding domain (NTD), a middle domain (MD), and a C-terminal dimerization domain (CTD). (B) The cycle of the Hsp90 system. Inactive client protein binds to Hsp90 dimer. ATP binding transfers the conformational equilibrium from the open state to the closed state which is accompanied by the NTD dimerization. This metastable state is committed to ATP hydrolysis, inducing a yet further closed, twisted state. ADP and P_i release revert Hsp90 to the open conformation. Various

cochaperones, e.g., Hop, Cdc37, Aha1, and p23, cooperate with Hsp90 to regulate its ATPase activity and recruit clients. Figure modified from Balchin et al. (2016) and Hartl et al. (2011).

2.3.4 The Hsp60 machinery

The Hsp60 family, also known as the chaperonins, are unique protein folding machines in that they form nano-cages for single protein molecules up to ~60 kDa to fold in isolation. They form large double-ring complexes of 800–900 kDa with 7–9 subunits of ~60 kDa per ring. Chaperonins are essential in all three branches of life and are divided into two distantly related groups: group I and group II (Balchin et al., 2016; Horwich et al., 2007; Kim et al., 2013).

Group I chaperonins have seven-membered rings and are present in bacteria (known as GroEL), mitochondria (Hsp60), and chloroplasts (Cpn60). Group I chaperonins functionally cooperate with the cochaperone Hsp10 (GroES in bacteria, Hsp10 in mitochondria, and Cpn10/Cpn20 in chloroplasts) which forms the lid of the folding cavity. Group II chaperonins in archaea (thermosome) and the eukaryotic cytosol (TRiC, also known as CCT) usually have rings of 8–9 subunits per ring. They are independent of Hsp10 factors, possessing a built-in lid domain that can replace GroES to close the cage (Balchin et al., 2016; Hartl et al., 2011). Although group I and group II chaperonins share a common architecture, they cannot fold substrates interchangeably, indicating significant differences in SP folding mechanisms.

2.4 The *Escherichia coli* Hsp60 machinery: GroEL and GroES

GroEL in bacteria has been studied intensely. It is involved in the folding of ~10% of the *E. coli* proteome, including those proteins that cannot be folded by the upstream chaperones (Kerner et al., 2005; Saibil et al., 2013). The cylindrical GroEL

and the dome-shaped GroES, a heptameric ring of ~10 kDa subunits, form a nano-cage for folding. GroES binds to the ends of the GroEL cylinder, forming the lid of the cage.

GroEL consists of two heptameric rings of ~57 kDa subunits stacked back-to-back. Each subunit consists of an equatorial ATPase domain (residues 6–133, 409–523), an intermediate hinge-like domain (residues 134–190, 377–408), and an apical domain (residues 191–376). The equatorial domain mediates intra- and inter-ring interactions, and the apical domain binds non-native SP and GroES (Braig et al., 1994) (Figure 2.7A). The disordered C-terminal tail (residues 524–548, ending with four repeats of Gly-Gly-Met) protrudes from the equatorial domains into the central cavity, thereby blocking the free passage between the two rings (Hayer-Hartl et al., 2016).

The apical domains form the flexible ring opening and helices H (residues 233–243) and I (residues 255–267) expose hydrophobic residues towards the central cavity for the binding of molten globule-like folding intermediates. Each equatorial domain has an ATP binding pocket. ATP binding and hydrolysis transmit allosteric signals through the hinge-like intermediate domain causing large *en bloc* conformational changes of the apical domain (Figure 2.7B). The two rings are aligned with each other in a staggered configuration (1:2) across the equatorial plane, with every subunit in one ring contacting two subunits in the opposite ring (Saibil et al., 2013). As a large multimeric assembly with a hierarchical structure, GroEL displays intra-ring positive allosteric cooperativity and inter-ring negative cooperativity described by a nested allosteric model (Gruber and Horovitz, 2016; Saibil et al., 2013; Yifrach and Horovitz, 1995).

GroES is a dome-shaped heptameric ring of ~10 kDa subunits. It binds to the ends of GroEL in a nucleotide-regulated way, thereby forming the cage for SP

encapsulation and folding. Each GroES subunit consists of nine β-strands and one 22-amino acid mobile loop which forms the binding motif with helices H and I of the GroEL apical domains (Landry et al., 1993) (Figure 2.7B).

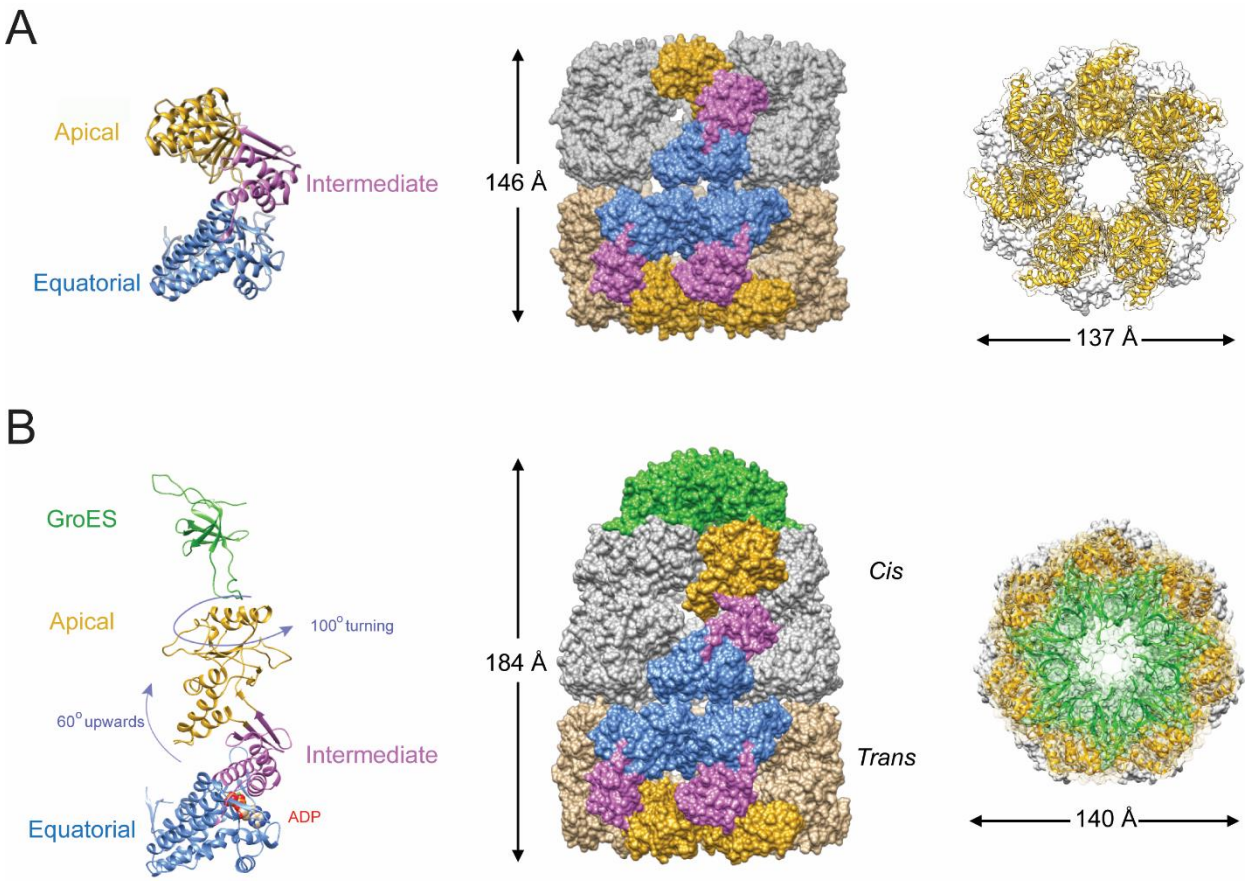

Figure 2.7 Structure of bacterial chaperonin.
Apo GroEL (PDB 1XCK) (A) and GroEL/ES complex (PDB 1AON) (B). Side view (middle panel) and top view (right panel) are shown in space-filling representations. One subunit in each ring (left panel) is displayed with the equatorial domain in blue, the intermediate domain in magenta, the apical domain in orange, and GroES in green.

2.4.1 The GroEL/ES protein folding cycle

The nucleotide-free ring (so called *trans*-ring) of the GroEL/ES complex is the acceptor state for a non-native SP (Figure 2.8A). Collapsed folding intermediates in the "molten globule" state, lacking stable tertiary elements and thus exposing

hydrophobic segments, usually engage two or more apical domains within one ring for efficient binding (Hartl, 1996; Sharma et al., 2008). Binding to GroEL is accompanied by a rapid conformational expansion of collapsed substrates ($t_{1/2}$ ~100 ms) as measured by fluorescence resonance energy transfer (FRET) (Lin et al., 2008; Sharma et al., 2008). Upon binding of ATP, the *trans*-ring undergoes a dramatic upward and clockwise movement in its apical domain, which may further expand tightly bound substrate segments and release weakly bound segments (Hayer-Hartl et al., 2016). The ATP-triggered expansion is very transient ($t_{1/2}$~15 ms) and closely followed by GroES binding ($t_{1/2}$~200 ms), resulting in displacement of the SP into an enclosed chamber (the so-called *cis*-ring) (Clare et al., 2012). The GroEL/ES cage (~175 000 $Å^3$) is approximately twice the size of that of an apo GroEL ring without GroES, and is sufficiently large to encapsulate SPs up to ~60 kDa in size. Importantly, upon GroES binding, the inner wall of the GroEL/ES cage changes from hydrophobic to hydrophilic and becomes net-negatively charged, providing an environment permissive for folding (Xu et al., 1997). The SP is free to fold inside this cage for ~2–7 s (dependent on temperature), the time needed for ATP hydrolysis. ATP binding also triggers the dissociation of ADP and GroES and the release of the SP from the former *cis*-ring, resulting in a new *trans*-ring. Incompletely folded protein is rapidly recaptured by GroEL for another folding attempt (Rye et al., 1999). Certain proteins that are too large for encapsulation in the GroEL/ES cage can fold by binding and release from the *trans*-ring without encapsulation (Chaudhuri et al., 2009).

2.4.2 Sequential versus simultaneous model of chaperonin reaction

In the chaperonin cycle described above, the two rings of GroEL fold SPs sequentially, and mainly asymmetrical GroEL:GroES complexes are populated. The

trans-ring can bind ATP and GroES only after the *cis*-ring has hydrolyzed its bound ATP (Rye et al., 1999). This asymmetry is due to the negative allosteric coupling of the GroEL rings, with communication between two rings being transferred by critical interactions at the inter-ring interface of the equatorial domains (Gruber and Horovitz, 2016; Saibil et al., 2013; Yan et al,. 2018). However, symmetric GroEL:$GroES_2$ complexes with GroES binding simultaneously to both GroEL rings, have also been reported in the absence or presence of SPs (Sameshima et al., 2008; Schmidt et al., 1994; Yang et al., 2013; Ye and Lorimer, 2013). The functional importance of the symmetric complexes has been debated. Based on the symmetric GroEL:$GroES_2$ complexes, a non-sequential model has been proposed (Figure 2.8B), in which GroES binds simultaneously to both GroEL rings and dissociates stochastically upon ATP hydrolysis, with SP accelerating nucleotide exchange (Hayer-Hartl et al., 2016; Yang et al., 2013). SP binding to the *trans*-ring would stimulate the rate-limited ADP dissociation and thereby allow fast ATP and GroES binding before the *cis*-ring has hydrolyzed ATP (Ye and Lorimer, 2013). Notably, these studies applied the same FRET measurement to calibrate GroEL:$GroES_2$ complexes but generated quite different results depending on the fluorophore pairs for labeled GroEL and GroES. A more robust study applying a novel dual-color fluorescence cross-correlation spectroscopy (dcFCCS) and avoiding GroEL labeling, strongly suggested that symmetric GroEL:$GroES_2$ is disfavored in the presence of foldable SPs and at a physiological ATP:ADP ratio (Haldar et al., 2015). Therefore, the two rings of chaperonin are more likely to function sequentially and asymmetric GroEL:GroES complexes are populated *in vivo*.

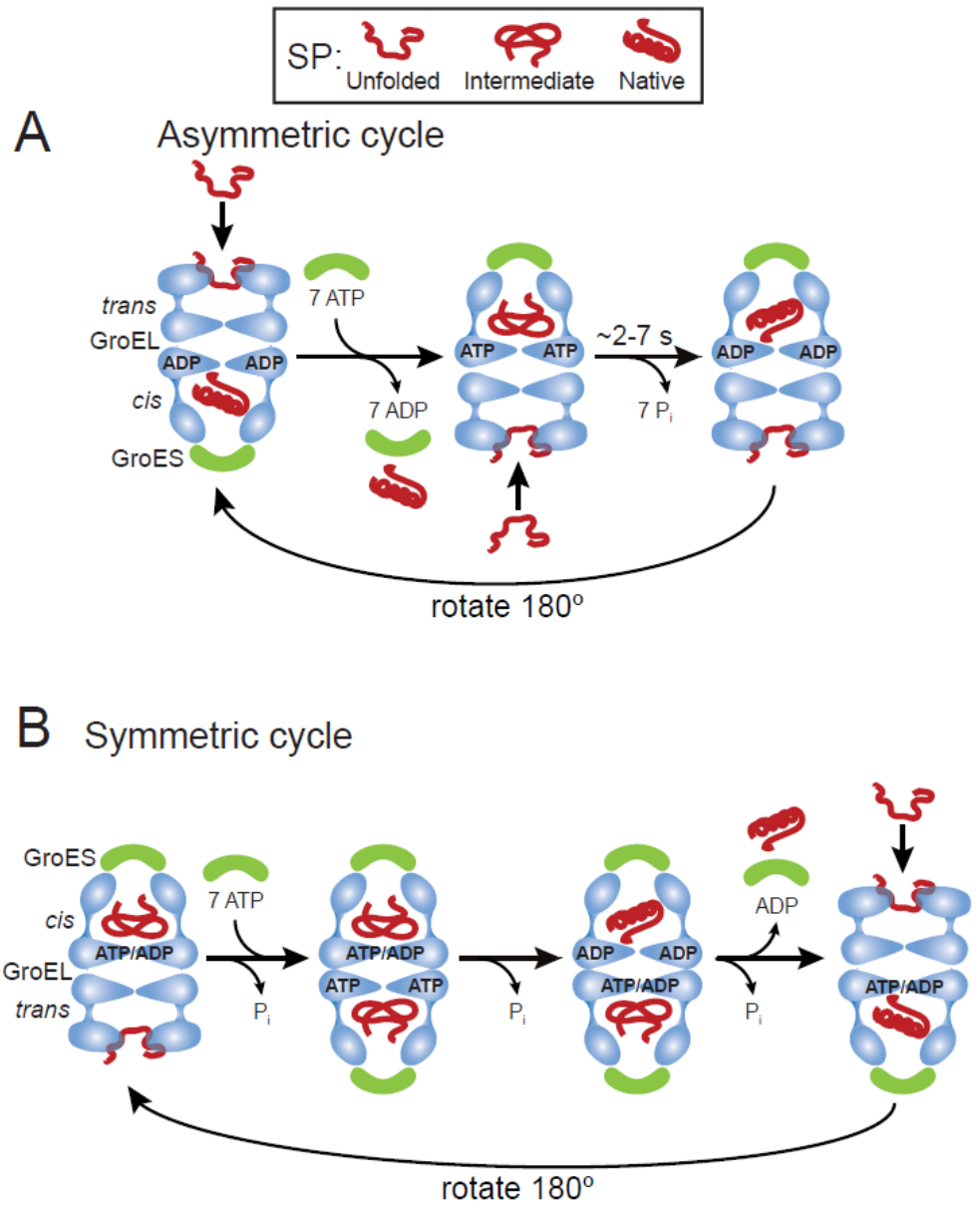

Figure 2.8 GroEL/ES reaction cycle.
Models of the asymmetric (A) and symmetric (B) GroEL/ES reaction cycles. Conformational transitions of SP are indicated. Modified from Hayer-Hartl et al. (2016) and Yan et al. (2018).

2.4.3 *In vivo* substrates of GroEL

GroEL/ES is essential for *E. coli* growth under all conditions (Georgopoulos, 2006), suggesting that folding of some essential proteins strictly depends on the chaperonin system. A set of ~250 proteins in *E. coli*, including 67 essential proteins, was

identified as interactors of GroEL upon translation *in vivo*, corresponding to ~10% of the total cytosolic proteome (Kerner et al., 2005). The size distribution of most GroEL substrates is ~35–60 kDa, consistent with the size of the GroEL/ES cage. Some identified larger substrates may use GroEL for aggregation prevention and apply *trans*-ring binding for folding but not global encapsulation (Chaudhuri et al., 2001). A subset of ~80 GroEL interactors, including 13 essential proteins, strictly depends on GroEL/ES for folding and occupies ~75–80% of the total chaperonin capacity (Figure 2.9) (Kerner et al., 2005). Notably, upon deletion of GroEL, a subset of ~50 of these proteins was confirmed to be obligate chaperonin substrates (Fujiwara et al., 2010). The obligate substrates typically feature α/β or α+β domain topologies. Interestingly, substrates with a $(\beta/\alpha)_8$-TIM barrel topology are strongly enriched and maintained by many long-range contacts in their native states. Therefore, such special proteins are likely to form kinetically trapped intermediates as they navigate the folding energy landscapes (Dobson et al., 1998; Hayer-Hartl et al., 2016).

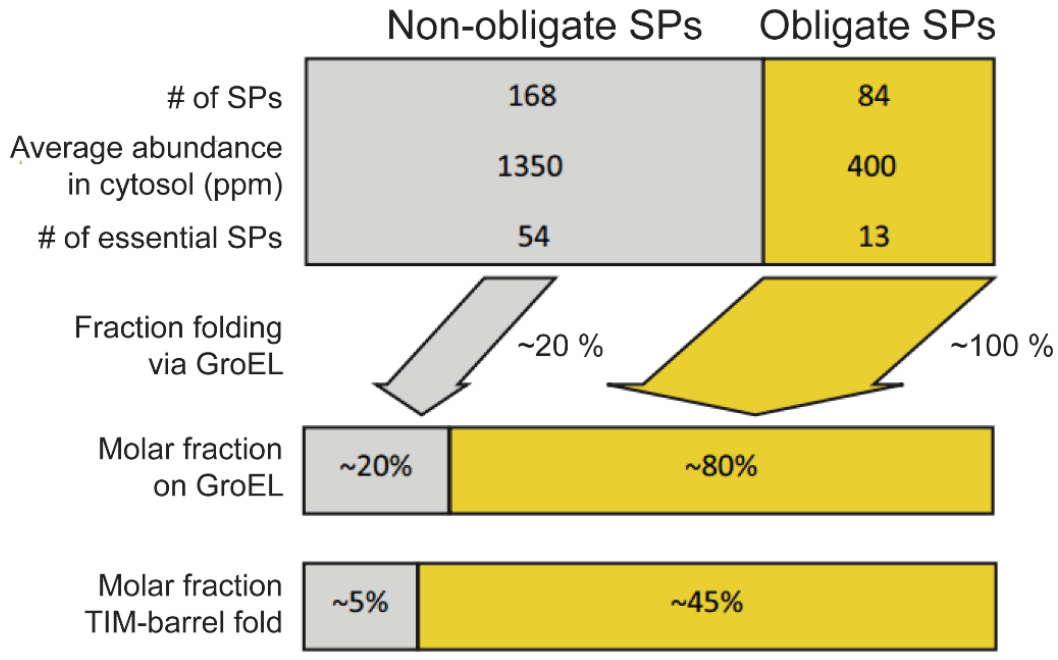

Figure 2.9 *In vivo* substrates of chaperonin.

Number of non-obligate and obligate SPs and their molar occupancy of GroEL folding capacity. Non-obligate SPs are generally folded by upstream chaperones. Figure modified from Hayer-Hartl et al. (2016).

2.4.4 Mechanisms of GroEL/ES-mediated protein folding

Effective assisted in-cage folding requires ATP and the co-chaperone GroES. The exact mechanism of chaperonin-catalyzed folding is still a matter of debate. Three models have been proposed to explain chaperonin-assisted protein folding, which either propose that the reaction proceeds only passively by preventing off-pathway aggregation (passive cage), or by additionally accelerating protein folding by active (mutually non-exclusive) mechanism (active cage and iterative annealing) (Hartl and Hayer-Hartl, 2002; Hayer-Hartl et al., 2016; Jewett and Shea, 2010; Todd et al., 1996) (Figure 2.10).

The passive cage model (also referred to as the "Anfinsen cage" model) suggests that protein folding inside the GroEL/ES cage occurs at the same kinetics as in free solution at infinite dilution where aggregation is prevented (Horwich et al., 2009). The passive cage model successfully explains the higher folding yield observed upon encapsulation of the substrate inside the GroEL central cavity. However, it is not in agreement with a large body of evidence that the chaperonin accelerates the folding rate of various SPs over their spontaneous folding, even when spontaneous folding happens very effectively (Brinker et al., 2001; Georgescauld et al., 2014; Gupta et al., 2014; Lin et al., 2008; Tang et al., 2006; Weaver et al., 2017). The proponents of the passive cage model have rationalized this accelerated assisted folding by claiming that chaperonin encapsulates SP and thus prevents transient but reversible aggregation which would otherwise slow the spontaneous folding (Apetri and Horwich, 2008; Horwich et al., 2009; Tyagi et al., 2011). The key idea of the passive cage model is that folding occurs with full yield upon a single round of

encapsulation, and the chaperonin-assisted rate will equal the spontaneous refolding rate in the absence of aggregation. However, there is no evidence for the existence of such reversible aggregation intermediates, and irreversible aggregates only reduce the yield but does not slow the spontaneous folding rate (Chakraborty et al., 2010; Georgescauld et al., 2014; Tang et al., 2006). Significantly, recent experiments conducted using single molecule spectroscopy demonstrated an accelerated folding process by chaperonin under conditions where aggregation during spontaneous refolding was prevented by extreme dilution (Georgescauld et al., 2014; Gupta et al., 2014; Weaver et al., 2017).

The active cage model proposes that, besides aggregation prevention, the physical environment of the GroEL cage accelerates the folding process by modulating the folding energy landscape (Figure 2.10). This is attributed to an effect of steric confinement of kinetically trapped folding intermediates which are entropically stabilized due to dynamic conformations (Baumketner et al., 2003; Brinker et al., 2001; Chakraborty et al., 2010; Hayer-Hartl et al., 2016; Lucent et al., 2007; Tang et al., 2006). Such intermediates are produced through indiscriminate hydrophobic collapse of large domain that are stabilized by many long-range interactions in the native state (Hayer-Hartl et al., 2016; Lin and Zewail, 2012). Three features of the *cis*-ring have been implicated as being crucial in the active cage model. The first is the volume of the cage relative to the size of the substrate, which would exert steric confinement on the substrate (Tang et al., 2006). This confinement accelerates folding by limiting the conformational freedom to be explored during folding and favoring the formation of local and long-range interactions, resulting in a smoothening of the folding energy landscape (Georgescauld et al., 2014; Gupta et al., 2014; Hartl et al., 2011; Kim et al., 2013). The second feature is the high net charge of the cage (total -42, 189 negatively and 147 positively charged residues)

(Chakraborty et al., 2010; Gupta et al., 2014; Tang et al., 2006). The highly charged cavity would thermodynamically favor compaction of hydrophobic residues through ordering water structure inside the cavity (England et al., 2008; Gupta et al., 2014). The third feature is the flexible and mildly hydrophobic C-terminal Gly-Gly-Met repeats that protrude from the equatorial domains into the central cavity (Tang et al., 2006; Weaver et al., 2017; Weaver and Rye, 2014). They may engage in mildly hydrophobic interactions and entropic excluded volume effects to facilitate SP remodeling (Jewett et al., 2004; Kinoshita, 2006). Taken together, the key idea of the active cage model is that accelerated folding occurs with full yield upon a single round of encapsulation.

The iterative annealing model suggests an alternate explanation for the accelerated folding process (Figure 2.10). Substrate binding and release from GroEL in the ATP-driven cycle would accelerate the folding through periodically unfolding kinetically trapped states, which would afford intermediates a chance to partition between rapid productive folding and reformation of the kinetically trapped state (Corsepius and Lorimer, 2013; Hayer-Hartl et al., 2016; Thirumalai and Lorimer, 2001). In this model, accelerated folding occurs inside or outside the GroEL/ES cage by forced unfolding, with substrate encapsulation being a mere byproduct of the unfolding reaction (Yang et al., 2013; Ye and Lorimer, 2013). A clear conformational change of SP upon binding to GroEL and ATP-induced apical domain movements have been measured; however, it is hard to evaluate whether these conformational changes are compulsory for the accelerated folding process (Clare et al., 2012; Lin et al., 2008; Sharma et al., 2008). Importantly, in the case of a single step of SP binding followed by stable encapsulation with GroES (a single ring mutant of GroEL), enhancement of folding kinetics by chaperonin was also observed, suggesting that forced unfolding only contributes to a minor extent (if at all) to the accelerated folding.

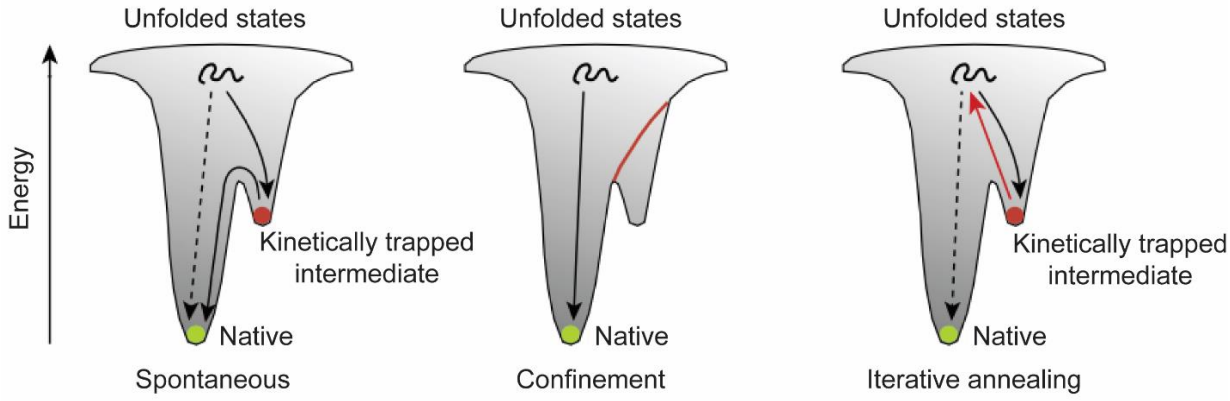

Figure 2.10 Mechanisms of accelerated folding.
A simple funnel-shaped energy landscape is depicted for a substrate populating a kinetically trapped state during spontaneous folding, resulting in a slow conversion to the native state (left). Confinement in the hydrophilic GroEL/ES cage will smoothen the energy landscape to avoid the formation of certain trapped intermediates (middle). In the iterative annealing model, this intermediate is actively unfolded by GroEL and allowed to repartition between fast folding to the native conformation and reformation of the kinetically trapped intermediate (right). Figure modified from Hayer-Hartl et al. (2016).

2.5 Aim of the study

Despite being the subject of intense research, the functional coordination between the two rings of GroEL in the chaperonin reaction cycle is only partially understood. In the 1990s, an equatorial split at the plane between the two rings of GroEL was observed with Tcpn60, the chaperonin of *Thermus thermophilus* (Ishii et al., 1995), and *E. coli* GroEL (Burston et al., 1996; Taguchi et al., 1997). Ring separation and exchange occurs in an ATP-, K^+- and Mg^{2+}-dependent manner (Taguchi et al., 1997). A small population of single GroEL rings was also observed using electron microscopy (Llorca et al., 1998; Ranson et al., 2006). In addition, some group I chaperonins, e.g., mammalian mitochondrial Hsp60 (Levy-Rimler et al., 2001; Nisemblat et al., 2015; Viitanen et al., 1992) and GroEL from *Thermoanaerobacter brockii* (Todd et al., 1995), were purified in single-ring form and shown to dimerize to double-ring conformations in the presence of ATP and the cochaperone Hsp10

(Levy-Rimler et al., 2002). Taken together, ring separation and exchange appears to be conserved chaperonin features warranting further investigation.

Here, I describe the results of a series of biochemical and biophysical experiments performed to investigate ring separation and exchange. Two main questions were studied: how does ring separation and exchange happen, and what is the physiological significance of these steps? My findings incorporate transient ring separation into the GroEL cycle and define it as a critical step in chaperonin function.

3 Materials and methods

3.1 Materials

3.1.1 Chemicals

Chemicals and reagents used were of pro analysis quality or ACS quality.

Table 3.1 Chemicals

CHEMICALS	SOURCE	IDENTIFIER
Acetic acid	Sigma-Aldrich	Cat#537020
Acrylamide/Bis Solution, 37.5:1 (30% w/v)	Serva Electrophoresis GmbH	Cat#10688
Adenosine 5′-diphosphate sodium salt (ADP)	Sigma-Aldrich	Cat#A2754
Adenosine 5′-triphosphate disodium salt trihydrate (ATP)	Roche	Cat#10127523001
Agarose	Cambrex	Cat#50004
2-Aminobenzaldehyde (ABA)	Sigma-Aldrich	Cat#A9628
Ammonium persulfate (APS)	Sigma-Aldrich	Cat#A3678
Ampicillin sodium salt	Carl Roth	Cat#K029.3
Atto532	ATTO-TEC	Cat#AD 532-41
Atto647N	ATTO-TEC	Cat#AD 647N-41
Atto655	ATTO-TEC	Cat#AD 655-41
Bacto agar	Difco	Cat#214030
Chloramphenicol	Sigma-Aldrich	Cat#C0378
cOmplete Protease Inhibitor Cocktail	Roche	Cat#04693159001
1,2-Cyclohexylenedinitrilotetraacetic acid (CDTA)	Sigma-Aldrich	Cat# 319945
1,4-Dithiothreitol (DTT)	Roche	Cat#10197777001
Ethanol	Sigma-Aldrich	Cat#32205
Glycerol	Carl Roth	Cat#4043.2
Glycine	Carl Roth	Cat#3908.3
Guanidine-HCl Solution (8M in H_2O)	Thermo Fisher Scientific	Cat#24115
Hydrochloric acid (37%)	Sigma-Aldrich	Cat#H1758
Isopropyl β-D-1-thiogalactopyranoside (IPTG)	Carl Roth	Cat#CN08.2
Kanamycin	Sigma-Aldrich	Cat#K4000
α-Ketopropionic acid (Pyruvic acid)	Sigma-Aldrich	Cat#107360
L-aspartate-beta-semialdehyde	MBIP Microchemistry Core Facility	N/A
Magnesium chloride hexahydrate ($MgCl_2$)	Sigma-Aldrich	Cat#M9272
2-mercaptoethanol	Sigma-Aldrich	Cat#M6250
Methanol	Carl Roth	Cat# HN41.2
3-Morpholinopropane-1-sulfonic acid (MOPS)	Sigma-Aldrich	Cat#M1254

β-Nicotinamide adenine dinucleotide, reduced dipotassium salt (NADH)	Sigma-Aldrich	Cat#N4505
Oligonucleotides	Metabion Int. AG	N/A
Phospho(enol)pyruvic acid monopotassium salt (PEP)	Sigma-Aldrich	Cat#P7127
Potassium chloride (KCl)	Carl Roth	Cat#6781.1
SERVA Blue G	Serva Electrophoresis GmbH	Cat#35050
Sodium chloride (NaCl)	VWR	Cat#27810.295
Sodium dodecyl sulfate (SDS)	Sigma-Aldrich	Cat#436143
Sodium hydroxide (NaOH)	VWR	Cat#28245.298
SYBR™ Safe DNA Gel Stain	Thermo Fisher Scientific	Cat#S33102
N,N,N',N'-Tetramethylethylenediamine (TEMED)	Sigma-Aldrich	Cat#411019
2-Amino-2-(hydroxymethyl)-1,3-propanediol (Tris base)	Sigma-Aldrich	Cat#10708976001
Tween-20	Sigma-Aldrich	Cat#P9416
Urea ReagentPlus® (≥99.5%)	Sigma-Aldrich	Cat#E001250

3.1.2 Proteins, enzymes, and kits

Table 3.2 Proteins, enzymes, and kits

REAGENT or RESOURCE	SOURCE	IDENTIFIER
Antibodies		
Rabbit polyclonal anti-rhodanese	(Hayer-Hartl et al., 1996)	N/A
Rabbit polyclonal anti-pig heart mMDH	(Figueiredo et al., 2004)	N/A
Rabbit polyclonal anti-GroEL	(Ewalt et al., 1997)	N/A
Kits		
CopyRight v2.0 pEZ BAC Blunt Cloning Kit with Electrocompetent Cells	Lucigen	Cat#42009-1
4-20% Mini-PROTEAN™ TGX Stain-Free ™ Protein Gels	Bio-Rad	Cat#4568095
Novex 6% Tris-Glycine Mini Gels	Invitrogen	Cat#XP00065BOX
QIAprep Spin Miniprep Kit	Qiagen	Cat#27106
QIAquick PCR Purification Kit	Qiagen	Cat#28106
QuikChange Site-Directed Mutagenesis Kit	Agilent Technologies	Cat#200519
Proteins and Enzymes		
Apyrase from potatoes	Sigma-Aldrich	Cat#A6535
Benzonase Nuclease	Merck	Cat#70746
Bovine mitochondrial rhodanese	Sigma-Aldrich	Cat#R1756
Bovine Serum Albumin (BSA)	SERVA	Cat#11924
DapA	(Kerner et al., 2005)	N/A
DM-MBP	(Tang et al., 2006)	N/A
GroEL variants	This work	N/A
GroES variants	This work	N/A
Lysozyme	Sigma-Aldrich	Cat#L6876
mitochondrial MDH from pig heart	Roche	Cat#10127256001

Pfu DNA Polymerase	Promega	Cat#M774A
Pyruvate Kinase/Lactic Dehydrogenase enzymes from rabbit muscle	Sigma-Aldrich	Cat#P0294
Restriction enzymes	New England Biolabs	N/A
T4 DNA ligase	New England Biolabs	Cat#M0202S

3.1.3 Instruments and software

Table 3.3 Instruments and software

INSTRUMENTS	**SUPPLIER**
Äkta Explorer, Äkta Purifier, Äkta Ettan, chromatography, columns (DEAE, MonoQ, Sephacryl S200, Heparin)	GE Healthcare
Amicon centrifuge filter units, steritop filter units	Milipore
Applied Photo Physics SX 18MV	Applied Photophysics
Benchtop centrifuges 5415D and 5417R	Eppendorf
Benchtop centrifuge GS-6	Beckman Coulter
CM200 FEG electron microscope	Philips
Electrophoresis power supply Power PAC 300	Bio-Rad
Eppendorf BioSpectrometer kinetic	Eppendorf
FluoroLog 3 spectrofluorometer	Horiba Yvon
High capacity centrifuge J6-MI	Beckman Coulter
Innova 44 incubator	New Brunswick Scientific
Luminescent Image Analyzer LAS-3000	FujiFilm
MicroTime 200 time resolved, confocal fluorescence microscope	PicoQuant
Mini Trans-Blot Electrophoretic Transfer Cell	Bio-Rad
NanoDrop 1000	Thermo Fisher Scientific
PCR thermocycler	Biometra
pH meter	WTW
µ-slide 8 well chambered microscope coverslip	Ibidi
Sonicator 3000	Misonix
SteriTop filter units	Merck
Ultracentrifuge Optima L-90K	Beckman Coulter
Ultracentrifuge rotor type 45 Ti	Beckman Coulter
Thermomixer comfort	Eppendorf
V-560 Spectrophotometer	Jasco
Vivaspin concentrator	GE Healthcare
Vortex Mixer Genie 2	Scientific Industries
SOFTWARE	
AIDA Image Analyzer version 4.15.025	Raytest
CCP4i	http://www.ccp4.ac.uk/ccp4i_main.php
Chimera	http://www.cgl.ucsf.edu/chimera
COOT	https://www2.mrc-lmb.cam.ac.uk/personal/pemsley/coot/
ImageJ	National Institutes of Health

MolProbity	http://molprobity.biochem.duke.edu/
MOLREP	http://www.ccp4.ac.uk/html/molrep.html
OriginPro 9.1	OriginLab
PyMOL 0.99	DeLano Scientific, http://www.pymol.org
REFMAC5	http://www.ccp4.ac.uk/html/refmac5.html
SymPhoTime64	PicoQuant

3.1.4 Buffers and media

All buffers for protein refolding, purification, and storage were filtered using SteriTop filter units. The buffers used for protein purification are described in the respective section.

Table 3.4 Buffers and media

REAGENT or RESOURCE	COMPASITION
Buffer	
Coomassie gel destaining solution	10% ethanol, 7% acetic acid
Coomassie gel staining solution	40% ethanol, 8% acetic acid, 0.1% (w/v) Serva Coomassie Blue R-250
DapA refolding buffer	20 mM Tris-HCl pH 7.5, 100 mM KCl, 10 mM $MgCl_2$
HS buffer	20 mM MOPS-NaOH pH 7.4, 150 mM KCl, 10 mM $MgCl_2$
Native-PAGE running buffer	3.03 g L^{-1} Tris, 14.4 g L^{-1} Glycine
SDS-PAGE running buffer	3.03 g L^{-1} Tris, 14.4 g L^{-1} Glycine, 1 g L^{-1} SDS
Media	
Lysogeny broth medium (LB)	10 g L^{-1} tryptone, 5 g L^{-1} yeast extract, 10 g L^{-1} NaCl purchased from AMRESCO (15 g L^{-1} agar added for agar plates)
SOC medium	20 g L^{-1} tryptone, 5 g L^{-1} yeast extract, 0.5 g L^{-1} NaCl, 0.186 g L^{-1} KCl, 0.95 g L^{-1} $MgCl_2$, 20 ml of 1 M glucose (filter-sterilized)

3.1.5 Strains and plasmids

Table 3.5 Strains and plasmids

REAGENT or RESOURCE	SOURCE	IDENTIFIER
Bacterial and Virus Strains		
E. coli DH5α	Thermo Fisher Scientific	Cat#18265017
E. coli BL21 (DE3) Gold	Stratagene	Cat#200131
E. coli MC4100	(Genevaux et al., 2004)	N/A
E. coli MC4100 SC3	(Kerner et al., 2005)	N/A
Plasmids		

pET11a-EL-WT and pET11a-EL mutants	This work	N/A
pEZ BAC	Lucigen	Cat#42009-1
pEZ BAC lac-SL	This work	N/A
pEZ BAC lac-SL-A109C	This work	N/A
pEZ BAC lac-SL-A109S	This work	N/A

3.2 Molecular biology methods

3.2.1 Plasmid transformation of competent *E. coli* cells

Plasmid or DNA ligation mixture was added to 100 µl of competent cells and incubated on ice for 15 min. The mixture was heat shocked at 42°C for 90 s and cold shocked on ice for 2 min, followed by incubation with constant agitation in 950 µl SOC medium at 37°C for 1 h. The cells were plated on pre-heated and antibiotic-containing LB plates. LB plates were incubated at 37°C overnight.

3.2.2 Plasmid construction

Amino acid mutations in proteins were introduced by site-directed mutagenesis to plasmids. Primers carrying the desired mutation were self-complementary aligned with template DNA. PCR for the full-length plasmid DNA was carried out using Pfu DNA polymerase and the following conditions for 20 cycles: 95°C for 40 s, 68°C for both annealing and extension (500 bp/min). The PCR product was treated with DpnI to digest the template plasmid at 37°C for 3 h. The remaining DNA was then transformed into competent *E. coli* DH5α cells. Mutations were confirmed by DNA sequencing.

3.3 Biochemical methods

3.3.1 GroEL and GroES purification

Buffer A: 50 mM Tris/HCl pH 7.5, 30 mM NaCl, 1 mM CDTA, and 1 mM DTT.

Buffer B: 50 mM Tris/HCl pH 7.5, 500 mM NaCl, 1 mM CDTA, and 1 mM DTT.

Buffer C: 20 mM MOPS/NaOH pH 7.4, 100 mM NaCl, and 10% glycerol.

Buffer D: 20 mM Imidazole pH 5.8 and 10 mM NaCl.

Buffer E: 20 mM Imidazole pH 5.8 and 1 M NaCl.

GroEL variants were expressed and purified in *E. coli* BL21 (DE3) Gold as described previously with minor modifications (Hayer-Hartl et al., 1996). Cells were grown to an OD_{600} of 0.4–0.6 at 37°C (~2–3 h). 1 mM IPTG was added to induce protein expression for a further 6 h at 37°C. The cells were harvested by centrifugation, re-suspended in buffer A, and frozen in liquid nitrogen. Thawed *E. coli* were lysed for 30 min at 4°C in the presence of complete protease inhibitor cocktail (Roche), 1 mg ml^{-1} lysozyme (Sigma), and 10 U ml^{-1} Benzonase (Noagen). The predigested cells were sonicated with a tip sonicator at a power of 45 W, using 30 s pulses with 40 s pauses for 20 cycles, while the lysis was cooled on ice to prevent protein aggregation.

After removal of cell debris and membranes by centrifugation (Beckman Ti45 rotor, 40 000 rpm, 45 min, 4°C), the supernatant was fractioned using FPLC on a DEAE column (~160 ml, self-made) equilibrated in buffer A with a gradient to buffer B. The GroEL fractions were collected for overnight dialysis to buffer A. The desalted sample containing GroEL was applied to HiPrep Heparin FF 16/10 (20 ml, GE Healthcare) equilibrated in buffer A with a gradient to buffer B. The sample containing GroEL was dialyzed to buffer A and loaded on Mono Q HR 16/10 (20 ml, GE Healthcare) equilibrated in buffer A with a gradient to buffer B. The collected GroEL was applied to HiPrep 26/60 Sephacryl S-300 (320 ml, GE Healthcare) equilibrated in buffer C. The pool of GroEL fractions was concentrated with a Vivaspin 20 concentrator (100 kDa cutoff, GE Healthcare). The concentration of GroEL was measured with a NanoDrop at 280 nm and stored at -80°C.

After each chromatography step, the GroEL fractions were analyzed using SDS-PAGE. The final check for the quality of GroEL was an assay of its ATPase activity in the absence or presence of GroES (Poso et al., 2004).

GroES expression and cell lysis were carried out as for GroEL. After removal of cell debris and membranes by centrifugation, the supernatant in buffer A was applied to a DEAE sepharose column (~160 ml, self-made) equilibrated in buffer A with a gradient to buffer B. The GroES fractions were collected for overnight dialysis to buffer D and next applied to Mono Q HR 16/10 (20 ml, GE Healthcare) equilibrated in buffer D with a gradient to buffer E. The collected GroES was applied to HiLoad 26/600 Superdex 200 (320 ml, GE Healthcare) equilibrated in buffer C. The pool of GroES fractions was concentrated with a Vivaspin 20 concentrator (10 kDa cutoff, GE Healthcare). The concentration of GroES was measured with a NanoDrop at 280 nm and stored at -80°C. After every chromatography step, the GroES fractions were checked using SDS-PAGE. The purification quality of GroES was checked by the ATPase activity originating from impurities and its inhibitory effects on the ATPase activity of GroEL (Poso et al., 2004).

The concentrations of all the proteins shown in this thesis were based on the oligomeric forms unless indicated.

3.3.2 GroEL and GroES maleimide labeling

The GroEL cysteine mutant (EL-E315C or EL-E315C/A109C) and the GroES mutant 98C (ES-98C, with an additional cysteine residue attached to the C-terminus) were incubated with 10 mM DTT for 30 min and buffer exchanged to 20 mM MOPS pH 7.4, 100 mM NaCl and 10% glycerol on a Bio-Spin 6 column (BioRad). The reduced GroEL or GroES was immediately mixed with fluorescent probes (ATTO-TEC) using maleimide chemistry for 30 min at 25°C (Haldar et al., 2015). Note that

the endogenous three cysteine residues of GroEL were preserved as they are important for negative cooperativity and were found not to be accessible for fluorophore labeling within 30 min. The labeling reaction was quenched by the addition of 10 mM DTT. Free dye was removed using a Bio-Spin 6 column equilibrated in buffer C containing 10 mM DTT.

The degree of labeling (DOL) was measured by absorption spectroscopy (GroEL: ε_{280} = 146 020 M^{-1} cm^{-1}; GroES: ε_{280} = 10 430 M^{-1} cm^{-1}; Atto532: ε_{max} = 115 000 M^{-1} cm^{-1}, CF_{280} = 0.09; Atto647N: ε_{max} = 150 000 M^{-1} cm^{-1}, CF_{280} = 0.03; Atto655: ε_{max} = 125 000 M^{-1} cm^{-1}, CF_{280} = 0.08), using the following equation (1):

$$\mathrm{DOL}=\frac{A_{dye}/\varepsilon_{dye}}{(A_{280}-A_{dye}\times CF_{280})/\varepsilon_{protein}} \quad (1)$$

The absence of free dye in the sample was ascertained using fluorescence correlation spectroscopy (FCS).

3.3.3 ATPase assay and data fitting

The ATPase activity of GroEL (100 nM) was measured in HS buffer at 25°C in the absence or presence of GroES (200 nM) using an NADH-coupled enzymatic assay (1 mM phosphoenolpyruvate, 20 U ml^{-1} pyruvate kinase, 20 U ml^{-1} lactate dehydrogenase and 0.25 mM NADH) at different ATP concentrations (Poso et al., 2004). Allosteric properties with respect to ATP were analyzed by fitting the data to equations (2) and (3) (Yifrach and Horovitz, 1995).

$$V_0=\frac{0.5V_{max1}L_1([S]/K_R)(1+[S]/K_R)^{N-1}+V_{max2}L_1L_2([S]/K_R)(1+[S]/K_R)^{2N-1}}{1+L_1(1+[S]/K_R)^{N}+L_1L_2(1+[S]/K_R)^{2N}} \quad (2)$$

where V_0 is the observed initial rate of ATP hydrolysis; [S] is ATP concentration; L_1 and L_2 are apparent allosteric constants; K_R is the dissociation constant of ATP; N is the number of ATP binding sites; V_{max1} and V_{max2} are the maximal initial rates of ATP hydrolysis by one ring and by both rings of GroEL, respectively.

$$V_0 = \frac{V_{max} K[S]^n}{1 + K[S]^n} \quad (3)$$

where V_0 and V_{max} are the initial and maximal rates of ATP hydrolysis, respectively; [S] is ATP concentration; K is the apparent ATP binding constant; n is the Hill coefficient.

3.3.4 Aggregation prevention and protein refolding

Rhodanese (Rho; 100 μM) was denatured in 6 M Guanidine hydrochloride (GuHCl)/10 mM DTT for 60 min at 25°C and diluted 200-fold into HS buffer in the absence or presence of GroEL variants (0.5 μM). Aggregation was monitored by measuring turbidity at 320 nm.

Rho, mMDH and DapA refolding assays were performed as described previously with minor modifications (Hayer-Hartl, 2000; Kerner et al., 2005; Weber and Hayer-Hartl, 2000). GuHCl/10 mM DTT-denatured Rho and mMDH were diluted 200-fold into GroEL/ES-containing HS buffer to a final concentration of 0.5 μM, and denatured DapA was diluted 200-fold into GroEL/ES-containing buffer (20 mM Tris-HCl, pH 7.5, 100 mM KCl, and 10 mM $MgCl_2$) to a final concentration of 0.2 μM. GroEL and GroES were at concentrations of 1 μM and 2 μM, respectively. Refolding was initiated by addition of ATP (10 mM). When indicated, chaperonin action was stopped by addition of CDTA (50 mM). Enzymatic assays of Rho, mMDH, and DapA were performed as described (Hayer-Hartl, 2000; Kerner et al., 2005; Weber and Hayer-Hartl, 2000). Spontaneous refolding of Rho and mMDH was inefficient (<10% yield) due to aggregation. For dimeric mMDH and tetrameric DapA, enzymatic activity was measured after 1 h incubation to allow the productive assembly of the native enzyme. The obtained enzymatic activity data was normalized to a native control and fitted with a single exponential rate.

3.3.5 Analysis of protein encapsulation

Refolding reactions were performed as above and stopped after 40 min (Rho) or 60 min (mMDH) by addition of 1 mM BeF_x to allow binding of GroES to both GroEL rings, resulting in stable encapsulation of SP. Reactions were then separated on a Superdex 200 PC3.2/30 column (Amersham Biosciences) equilibrated in HS buffer containing 1 mM BeF_x and 20 μM ATP. Fractions were collected and analyzed using immunoblotting against Rho or mMDH antibodies, followed by densitometry. The total amount of detected SP was set to 100%.

3.3.6 Mixed-ring (MR) formation

EL-WT (or GroEL variant) and EL-379 (1 μM each) were mixed in HS buffer with or without GroES (4 μM). Reactions were initiated by addition of 10 mM ATP or ADP at 25°C and stopped by the addition of CDTA (80 mM) after 5 min unless otherwise indicated. For MR formation in the presence of non-native SPs, GuHCl-denatured DM-MBP (4 μM; final GuHCl concentration 60 mM), Rho (1 μM; final GuHCl concentration 30 mM), and mMDH (1 μM; final GuHCl concentration 30 mM) were added to MR formation reactions for 5 min. MR formation was analyzed on 6% native-PAGE. MR was purified on a MonoQ 10/100 GL anion-exchange column (GE Healthcare Life Sciences) with a NaCl gradient of 30–500 mM. For the generation of scrambled rings, EL-WT and EL-379 were mixed at a 1:1 molar ratio (1 μM each) and dissociated into subunits by incubation in 3.5 M urea, followed by 30-fold dilution into HS buffer containing ATP (5 mM) and $(NH_4)_2SO_4$ (600 mM) for reassembly (Shiseki et al., 2001). After reassembly for 60 min at 25°C, the reconstituted GroEL complexes were purified using size exclusion chromatography (Superdex 200 Increase 3.2/300, Amersham Biosciences) and analyzed on 6% native-PAGE. As a control, the same procedure was performed using EL-WT and EL-379 alone.

In the experiments testing the effects of nucleotide analogs, EL-WT and EL-379 (1:1 molar ratio) were mixed in HS buffer containing GroES, 1 mM ADP, and 1 mM BeF_x (generated by combining 1 mM $BeSO_4$ and 10 mM KF), AlF_x (generated by combining 1 mM $Al(NO_3)_3$ and 10 mM KF), or Na_3VO_4 for 10 min at 25°C. For ATP binding to a preformed GroEL:7ADP:GroES complex, EL-WT (or EL-D398A) and EL-379 were incubated with GroES and 1 mM ADP for 10 min. Then, ATP (10 mM) was added, and the reactions were stopped by addition of CDTA (50 mM) within 10 s.

3.3.7 *In vivo* complementation assay

A GroEL-depleted strain, MC4100 SC3 Kan^R, in which the chromosomal groE promoter is replaced with the araC gene and the pBAD promoter, was used (Tang et al., 2008). GroES and variants of GroEL were constructed in the single-copy vector backbone of pEZ BAC (Lucigen) under the Lac UV5 promoter. *E. coli* MC4100 SC3 cells transformed with pEZ BAC lac-SL plasmids for the expression of GroES and either EL-WT, EL-A109C (EL-SS), or EL-A109S were grown in LB medium containing 0.1 mM IPTG at 37°C to an OD_{600} of 0.5–1. Serial dilutions (10^1- to 10^5-fold) of cell suspension were spotted onto LB-kanamycin-chloramphenicol plates with or without IPTG (0.2 mM). Plates were incubated at 25°C, 37°C, or 42°C.

To verify that the expression of GroEL was similar for all the plasmid constructs, cells harboring the respective plasmids were grown in LB medium containing 0 mM or 0.2 mM IPTG at 37°C to an OD_{600} of ~1. The MC4100 strain with endogenous GroEL was used as a control. Equivalent amounts of cells (determined by cell density at OD_{600}) were collected from the liquid culture, and the level of GroEL was quantified by immunoblotting using GroEL antibodies, followed by densitometry.

3.3.8 Thiol-trapping

Thiol-trapping to detect the presence of inter-ring disulfide bonds in EL-A109C *in vivo* was performed according to Leichert and Jakob (2004) with modifications. EL-WT and mutant cells were grown with 0.2 mM IPTG to an OD_{600} of 0.6 at 37°C. Then, 1.5 ml of the cell culture was harvested directly into 200 µl of ice-cold 100% (w/v) trichloroacetic acid (TCA) and stored on ice for at least 30 min. The TCA-treated cells were centrifuged (13 000 g, 4°C, 30 min), and the resulting pellet was washed with 500 µl of ice-cold 10% (w/v) TCA followed by a wash with 200 µl of ice-cold 5% (w/v) TCA. The supernatant was removed completely, and the pellet was resuspended in 60 µl of denaturing buffer (6 M urea, 200 mM Tris-HCl pH 8.5, 10 mM CDTA, and 0.5% (w/v) SDS) supplemented with 100 mM iodoacetamide to alkylate free thiol groups. After 10 min of incubation at 25°C, the reaction was stopped by adding 60 µl of ice-cold 20% (w/v) TCA. After 20 min of incubation on ice, the alkylated proteins were centrifuged again, and the pellet was washed with TCA as described before. The protein pellet was then dissolved in 20 µl of denaturing buffer without or with 10 mM DTT, followed by 4–20% SDS-PAGE (Bio-Rad) and anti-GroEL immunoblotting.

3.4 Biophysical methods

3.4.1 Fluorescence correlation spectroscopy (FCS)

FCS using pulsed interleaved excitation (PIE) (Muller et al., 2005) was performed on a Microtime 200 inverse time-resolved fluorescence microscope (PicoQuant). Picosecond-pulsed diode lasers at 530 nm (LDH-P-FA-530) and 640 nm (LDH-PC-640B) were applied to excite green and red fluorescent dyes, respectively. Each laser had a 60 µW power measured before the major dichroic mirror. The pulse of the lasers was set to 26.6 mHz. The excitation light was guided into the sample cuvette

(Ibidi) through a water immersion objective (60×1.2 NA, Olympus). The emission fluorescence and excitation light were separated by a dichroic mirror (Z532/635RPC). The emitted light was guided through a pinhole (75 µm) and split according to wavelength by a beam splitter (600 DCXR) onto photon avalanche diodes (SPADs) (PDM series, MPD). The emission light was cleaned by emission bandpass filters (HQ 690/70 and HQ 580/70, Chromas) in front of the respective detector. Detection was performed with time-correlated single photon counting, in which any given photon was properly correlated with the excitation source. Recorded fluorescence traces were cross-correlated and fitted to equation (4).

$$G_{GR}(\tau)=\frac{\langle \delta F_G(t)\cdot \delta F_R(t+\tau)\rangle}{\langle F_G(t)\rangle\cdot\langle F_R(t)\rangle} \quad (4)$$

where δF_G and δF_R denote the fluctuation of the signal of green and red fluorescence between the time points t and $t+\tau$, respectively.

The amplitude of the cross-correlation is proportional to the concentration of double-labeled particles, which was fitted to equation (5). The average concentration of double-labeled particles is proportional to the amplitude of cross-correlation $G_{GR}(0)$, where V_{eff} denotes the volume of the focal spot.

$$\langle C_{GR}\rangle=\frac{G_{GR}(0)}{G_G(0)\cdot G_R(0)\cdot V_{eff}} \quad (5)$$

3.4.2 Dual-color fluorescence cross-correlation spectroscopy (dcFCCS)

dcFCCS was employed to study the kinetics of GroEL ring exchange and the proportions of asymmetric and symmetric GroEL/ES particles.

To study MR formation in the dcFCCS assay, EL-E315C labeled with Atto532 and EL-E315C labeled with Atto655 (0.5 µM each) were incubated with GroES (2 µM). The reaction was started by adding denatured DM-MBP (1 µM) and ATP (5 mM). At each time point, a 10 µl aliquot of the reaction was stopped by addition of

2.5 U apyrase (Apy) and diluted 15-fold for the dcFCCS assay. To study MR dissociation in the dcFCCS assay, double-labeled MR was first prepared by mixing equimolar concentrations of EL-E315C (Atto532) and EL-E315C (Atto655) (1 µM each) with ATP for 5 min. ATP was removed using two Bio-spin 6 columns. Double-labeled MR (5 nM) was incubated with unlabeled EL-WT (1 µM), GroES (2.1 µM), and DM-MBP (1 µM). The reaction was started by adding ATP (5 mM). At each time point, a 10 µl aliquot of the reaction was taken, stopped by addition of 2.5 U Apy, and diluted 15-fold for dcFCCS assay.

Analysis of asymmetric and symmetric GroEL/ES complexes was performed essentially as described (Haldar et al., 2015). Atto655- and Atto532-labeled GroES mutant 98C (50 nM each; denoted ES-655 and ES-532, respectively) were mixed with GroEL (50 nM) in HS buffer containing 10 mM ATP and 0.05% Tween 20. The measurements were performed in the absence of SP for 60 min and in the presence of SP (0.5 µM DM-MBP) for 30 min. Formation of GroEL:$GroES_2$ complexes with EL-D398A was set to 100% as a positive control. To follow GroES dissociation, GroEL:$GroES_2$ complexes containing ES-655 and ES-532 were incubated with a 20-fold excess of unlabeled GroES (2 µM).

3.4.3 Stopped-flow fluorescence resonance energy transfer (Stopped-flow FRET)

Stopped-flow FRET experiments were carried out using an Applied Photo Physics SX 18MV with a 1:1 mixing ratio at 25°C. The donor (Atto532) was excited at 532 nm with a slit width of 10 nm, and the acceptor (Atto647N) fluorescence was recorded with a 645-nm cutoff filter. Kinetic traces shown are averages of 4–6 independent measurements. For steady-state dissociation experiments, GroEL/ES complexes were formed by mixing acceptor-labeled GroEL (EL_A; 0.2 µM with ~2.2 fluorophores per tetradecamer), donor-labeled ES-98C (ES_D; 0.4 µM heptamer with

~1.1 fluorophores per heptamer), and 10 mM ATP for 1 min. The steady-state GroEL/ES reaction was then rapidly mixed with a 20-fold excess of unlabeled, competitor GroES (4 µM) in the absence or presence of a 10-fold excess of non-native DM-MBP (2 µM). The final GuHCl concentration in the presence of non-native DM-MBP was 15 mM. The loss of energy transfer as ES_D is replaced by unlabeled GroES is measured as a decrease in the acceptor fluorescence intensity.

To obtain pseudo-first-order association kinetics of GroES and GroEL, a 10-fold excess of ES_D (2 µM) over EL_A (0.2 µM) was used in the absence or presence of non-native DM-MBP (2 µM). The gain of energy transfer as ES_D binds to EL_A is measured as an increase in the acceptor fluorescence intensity.

3.4.4 Crystallography

Robotic crystal screening using the Protein Complex Suite 1 screen (Radaev and Sun, 2002) was performed at the MPIB crystallization facility. Crystals grew by the sitting-drop vapor diffusion method at 18°C in drops containing a protein solution of 40 mg ml^{-1} in HS buffer. Crystals of EL-A109C (EL-SS) were obtained with a precipitant containing 0.1 M sodium citrate pH 5.5 and 15% PEG6000 (Protein Complex Suite 1, condition D7). EL-SS:$GroES_2$ was crystallized in the presence of 10 mM ATP and 3 mM BeF_x with a precipitant containing 0.1 M Tris-HCl pH 8.0, 0.2 M NaCl and 20% PEG4000 (Protein Complex Suite 1, condition C8). The crystals were transferred in a step-wise manner into cryo buffers containing 20% PEG-6000, 0.1 M sodium-citrate pH 5.5, and 15% glycerol, and 20% PEG-4000, 0.1 M Tris-HCl pH 8.0, 0.2 M NaCl, 10% glycerol, 10 mM ATP, and 3 mM BeF_x, respectively. The crystals were cryo-cooled with liquid nitrogen after 15 min incubation.

Diffraction data were collected at the automatic beamline MASSIF-1 (ID30A-1) of the European Synchrotron Radiation Facility (ESRF) in Grenoble, France

(Bowler et al., 2015). The structures were solved by molecular replacement with the MOLREP program (Vagin and Isupov, 2001), using the coordinates of previously published crystal structures PDB 4WSC and 4PKN (Fei et al., 2013) as search templates. In iterative cycles, the structure models were alternatingly manually altered with Coot (Emsley and Cowtan, 2004) and refined with Refmac5 (Murshudov et al., 2011), employing the local NCS and TLS options. GroES and the apical, intermediate, and equatorial domains of GroEL served as TLS groups. In the model of EL-SS:$GroES_2$, linker regions with poor density were omitted. The stereochemical quality of the models was assessed with the MolProbity program (Chen et al., 2010).

3.4.5 Electron microscopy

After incubation for 2 min at 25°C, a mixture of GroEL (50 nM) and GroES (100 nM) in HS buffer containing 1 mM ATP was applied to freshly plasma-cleaned, carbon-coated grids (Quantifoil), followed by negative staining with 2% uranyl acetate. Images were collected under low-dose conditions on a Philips CM200 FEG electron microscope at 160 kV equipped with a TemCam F415MP 4k detector at a magnification of 50 000x.

4 Results

4.1 GroEL ring separation and exchange in the chaperonin reaction

GroEL ring separation and exchange was first observed with Tcpn60 of *T. thermophilus* (Ishii et al., 1995) and *E. coli* GroEL (Burston et al., 1996; Taguchi et al., 1997). In order to distinguish between the two rings of GroEL in the chaperonin reaction, I exploited earlier experiments that GroEL hybrids can be made by mixing wild-type GroEL (EL-WT) with GroEL mutant EL-379. EL-379 carries three mutations, Y203E/G337S/I349E, in the apical domain. This mutant GroEL is ATPase-active but was shown to fail in binding SP and GroES (Burston et al., 1996). On native-PAGE, the EL-379 migrates more slowly than EL-WT, and the mixed ring (MR) complex migrates between EL-379 and EL-WT (Figure 4.1A, lanes 1–2). A similar behavior was observed for a MR complex between GroEL and Tcpn60 (Taguchi et al., 1997). Interestingly, MR could not only be efficiently generated at 42°C, as reported previously (Burston et al., 1996), but also formed at 25°C (Figure 4.1A, lanes 1–3). MR formation was ATP-dependent, as no MR was observed with EL-379 and ATP-binding defective mutant EL-D87K (Fenton et al., 1994) (Figure 4.1A, lane 4).

To demonstrate that MR consists of distinct rings from EL-379 and EL-WT but not of scrambled subunits, I dissociated the two types of GroEL into subunits by incubation with 3.5 M urea and then reassembled the subunits in the presence of ATP, Mg^{2+} and Ammonium sulfate (Ybarra and Horowitz, 1995) (Figure 4.1B). This produced scrambled complexes moving as multiple bands on native-PAGE between EL-379 and EL-WT (Figure 4.1C), but not as a well-defined single band as observed for MR (Figure 4.1A). MR was also detected and purified by anion-exchange

chromatography (Figure 4.1D). Intriguingly, incubation of MR with ATP resulted in redistribution of the rings into the typical three-band pattern at a molar ratio of EL-WT:MR:EL-379 of 1:2:1 (Figures 4.1A, lanes 5–6). This suggested that, once formed, the MR complex is not a stable entity but possesses dynamic characteristic.

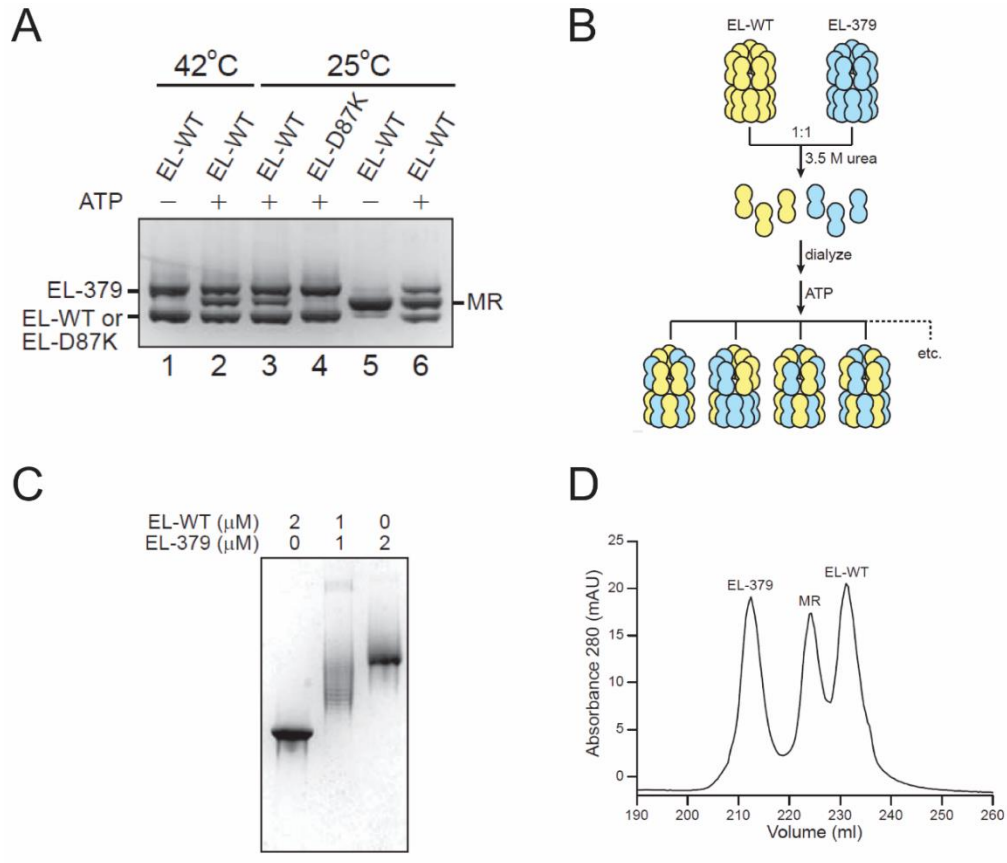

Figure 4.1 GroEL ring separation and exchange.
(A) Formation of mixed ring GroEL (MR) monitored by native-PAGE. EL-WT or EL-D87K was incubated with EL-379 (1 μM each) in HS buffer, in the absence or presence of ATP for 5 min at 42°C or 25°C (lanes 1–4). Reactions were stopped by addition of CDTA and analyzed on 6% native-PAGE. MR of EL-WT and EL-379 produced at 42°C was purified (lane 5) and incubated with ATP for 5 min at 25°C (lane 6). MR migrates between EL-WT (or EL-D87K) and EL-379. (B) Schematic of subunit exchange between GroEL complexes (as opposed to ring exchange). EL-WT and EL-379 were mixed (1 μM each) and dissociated into subunits by incubation in 3.5 M urea. The subunits were diluted 30-fold into HS buffer and allowed to reassemble in the presence of ATP, $MgCl_2$, and $(NH_4)_2SO_4$ for 60 min at 25°C. Reassembled GroEL tetradecamers were purified using size-exclusion chromatography. As a control, the same procedure was performed using EL-WT and EL-379 alone. Figure modified from (Shiseki et al., 2001). (C) Analysis on 6% native-PAGE of the reassembled GroEL tetradecamers

described in (B). (D) Purification of MR complex. EL-WT and EL-379 (5 µM each) were mixed in HS buffer containing 10 mM ATP for 5 min at 42°C. CDTA was added to stop the reaction. The sample was fractionated on a Mono Q 10/100 GL anion-exchange column with a NaCl gradient from 30 to 500 mM.

Time course measurements showed that MR formed with kinetics comparable to the ATPase rate of GroEL at 25°C (an apparent $t_{1/2}$ of ~50 s, i.e., ~3 rounds of ATP hydrolysis per tetradecamer) (Figures 4.2 and 4.5A). Interestingly, MR formation also occurred with similar kinetics in the presence of crowding agent Ficoll 70 (30%) (Figures 4.2), which would mimic the excluded volume effects prevailing in the cellular environment (Zimmerman and Minton, 1993). Taken together, these findings suggested that ring separation and exchange can take place during the GroEL ATPase cycle.

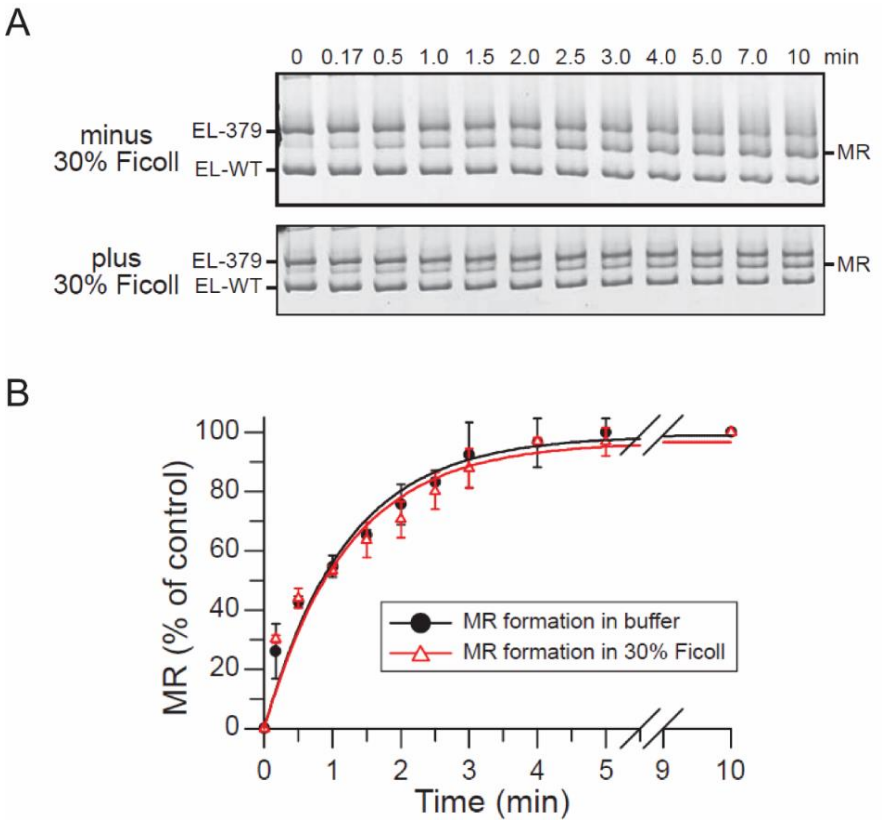

Figure 4.2 Kinetics of MR formation monitored using native-PAGE.
(A-B) EL-WT and EL-379 were incubated in ATP-containing HS buffer in the absence or presence of 30% Ficoll 70 at 25°C. Reactions were stopped by addition of CDTA at different

time points, and MR formation was monitored on 6% native-PAGE (A), followed by densitometry. The amount of MR at 10 min was set to 100%. Data represent the mean ± SEM of three independent experiments (B).

4.2 MR formation in the presence of ATP, GroES, and SPs

Next, I analyzed the requirement of nucleotides and also the effect of GroES on ring separation and exchange. MR formed was efficient in the presence of ATP but inefficient with ADP (Figure 4.3A, lanes 1–3). Note that ADP stocks may contain trace amounts of ATP (Hayer-Hartl et al., 1996). When GroES was involved in the reaction, ring separation and exchange occurred again only with ATP (Figure 4.3A, lanes 4–5). To distinguish between a requirement for ATP binding or hydrolysis in causing ring exchange, I next resorted to EL-D398A, a GroEL mutant binding ATP but hydrolyzing it at a very slow rate compared to EL-WT (less than 2%) (Rye et al., 1997). ATP-dependent MR formation of EL-D398A with EL-379 (Figure 4.3B) was as efficient as for EL-WT (Figure 4.3A), indicating that ATP binding but not hydrolysis is required for ring separation.

Ring separation and exchange was further analyzed in the presence of unfolded SP and GroES. A range of SPs varying in size and folding properties were utilized, including double-mutant maltose binding protein (DM-MBP; ~41 kDa), mitochondrial rhodanese (Rho; ~33 kDa), and mitochondrial malate dehydrogenase (mMDH; ~35 kDa). Note that DM-MBP refolds spontaneously with slow kinetics ($t_{1/2}$ ~30 min) and the folding intermediate binds GroEL tightly (Tang et al., 2006), which would allow the chaperonin cycle to be examined under conditions of SP saturation (Haldar et al., 2015); mitochondrial rhodanese (Rho; ~33 kDa) and mitochondrial malate dehydrogenase (mMDH; ~35 kDa) aggregate rapidly upon dilution from denaturant into refolding solution without GroEL (Martin et al., 1991; Ranson et al., 1995). Since EL-379 does not bind substrates (Burston et al., 1996),

SP concentrations were applied according to EL-WT. Efficient MR formation was observed with all the three substrates (Figure 4.3C). Therefore, ring separation and exchange occurs in the course of the functional chaperonin-assisted folding reaction.

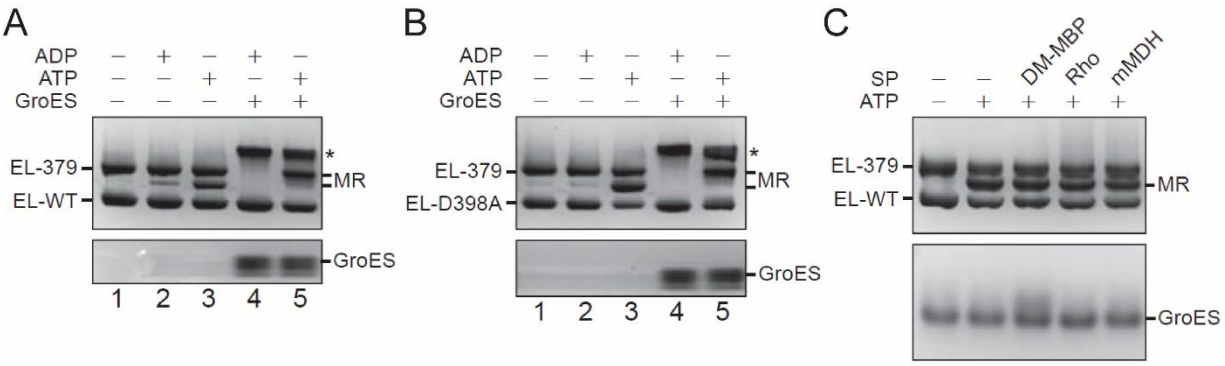

Figure 4.3 MR formation in the presence of ATP, GroES, and SPs.
(A and B) Nucleotide requirement for MR formation in the absence or presence of GroES assayed on native-PAGE. EL-WT (A) or EL-D398A (B) was incubated with EL-379 (1 µM each) for 5 min at 25°C in the absence or presence of nucleotide and GroES (4 µM). Reactions were stopped by addition of CDTA. (C) MR formation in the presence of SPs. MR formation of EL-WT and EL-379 was performed at 25°C in the absence of SP or presence of unfolded DM-MBP (4 µM), Rho (1 µM), or mMDH (1 µM). Reactions were stopped by addition of CDTA.

4.3 ATP binding to GroEL:7ADP:GroES causes ring separation

To address the exact step in the GroEL/ES reaction cycle at which the GroEL rings separate, I took advantage of previous reports that complexes of ADP with metal fluoride or vanadate ion can mimic distinct states of the γ-phosphate along the reaction coordinate of ATP hydrolysis. Specifically, ADP·BeF_x mimics the bound ATP prior to hydrolysis, ADP·AlF_x the transition state of ATP hydrolysis, and ADP·VO_4 the post-hydrolysis state (Chaudhry et al., 2003; Ditzel et al., 1998; Leitner et al., 2012). Asymmetric GroEL:GroES complexes were reported to form with these nucleotide analogs bound in the *cis*-ring (Haldar et al., 2015; Yang et al., 2013). Neither EL-WT nor EL-D398A showed MR formation in the presence of these nucleotides (Figures 4.4A and 4.4B). After Pi release, ADP also failed to

trigger ring separation (Figure 4.3). Thus, the action of ATP solely in the *cis*-ring obviously does not trigger ring separation, suggesting that ATP-binding to the *trans*-ring would cause ring separation upon ATP hydrolysis in the *cis*-ring.

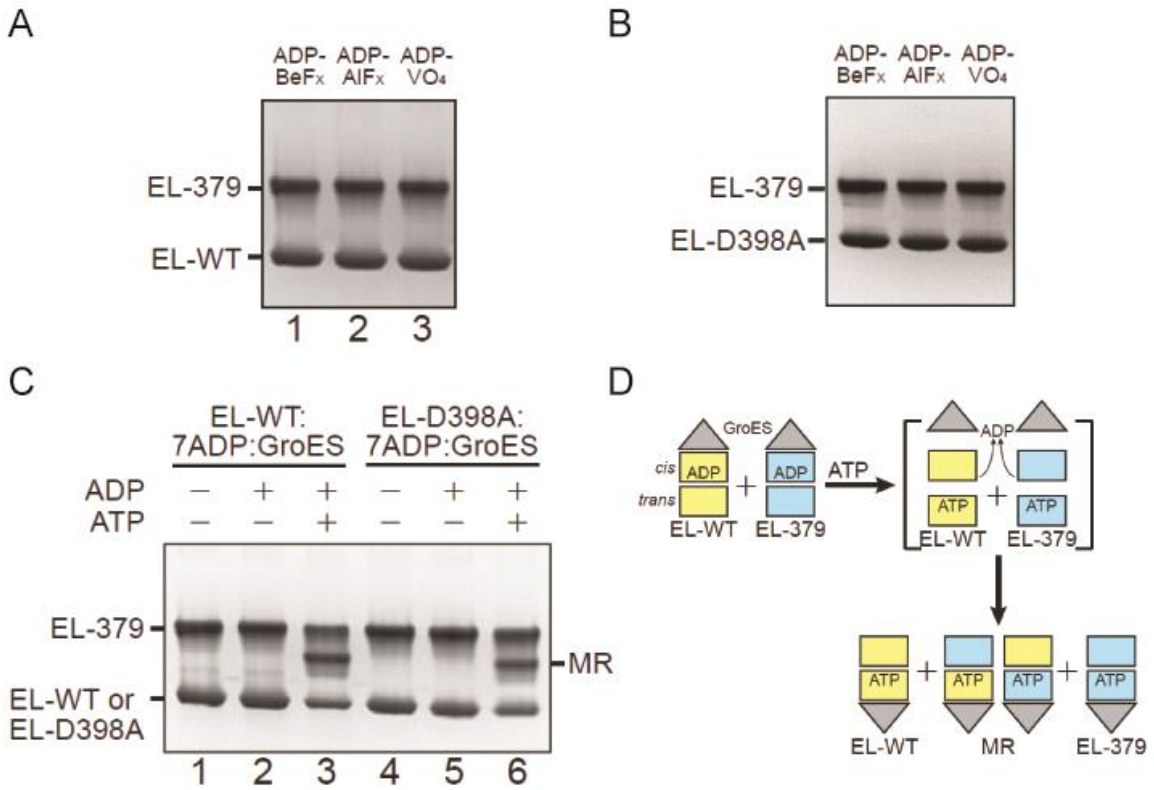

Figure 4.4 GroEL ring separation upon ATP binding to the *trans*-ring of the GroEL:7ADP:GroES complex.
(A and B) No MR formation in the presence of nucleotide analogs. EL-WT (A) or EL-D398A (B) and EL-379 were incubated in the presence of GroES and ADP together with either BeF_x, AlF_x or Na_3VO_4 (lanes 1–3, respectively). (C) ATP binding to GroEL:7ADP:GroES causes ring separation. EL-WT (lanes 1–3) or EL-D398A (lanes 4–6) and EL-379 were incubated with GroES and ADP for 10 min at 25°C to form GroEL:7ADP:GroES complexes. MR formation was initiated by addition of ATP and stopped by addition of CDTA within 10 s (lanes 3 and 6). (D) Hypothetical model for ATP binding to the *trans*-ring of a GroEL:7ADP:GroES complex triggering transient ring separation coupled with the dissociation of ADP and GroES from the *cis*-ring and possible MR formation.

To test this hypothesis directly, I first generated the asymmetric GroEL:7ADP:GroES complex by incubating GroEL and GroES in the presence of ADP. Addition of ATP to this complex, resulting in ATP binding to the *trans*-ring,

efficiently triggered ring separation and MR formation within 10 s (Figure 4.4C, lanes 1–3). Remarkably, MR formation within seconds was also detected upon ATP binding to the *trans*-ring of ATPase-defective EL-D398A:7ADP:GroES complex (Figure 4.4C, lanes 4–6). Note that EL-D398A needs ~40 min to hydrolyze one round of 14 ATP molecules (Rye et al., 1997; Yang et al., 2013). Taken together, ATP binding to the *trans*-ring of the GroEL:7ADP:GroES complex is the critical step to trigger ring separation (Figure 4.4D), which is concomitant with ADP dissociation and GroES release from the *cis*-ring.

4.4 Negative inter-ring allosteric cooperativity is required for ring separation

In the GroEL/ES nano-machine, ordered conformational changes fueled by ATP binding and hydrolysis result in highly organized temporal and spatial functions (Yifrach and Horovitz, 2000). The ATPase cycle is regulated by a system of nested cooperativity, which can be deduced from the steady-state measurements of ATPase rates at different ATP concentrations (Horovitz and Willison, 2005). ATP binds to one GroEL ring with positive cooperativity shown by the sigmoid pattern at lower ATP concentration (Hill coefficient n = ~2.8), and there is negative allosteric cooperativity between rings (Figure 4.5A). Considering that ring separation is caused by ATP binding to the *trans*-ring, it seemed reasonable that the inter-ring negative allostery was required for this event. Inter-ring negative cooperativity is displayed by a small but clearly measurable decrease in the ATPase activity from its maximum as the ATP concentration is enhanced above ~20 μM (Gruber and Horovitz, 2016) (Figure 4.5A).

I analyzed the efficiency of MR formation with a series of GroEL mutants showing defects in either positive or negative cooperativity. The D155A mutation switches the ATP-induced intra-ring allostery from concerted to sequential by breaking one intra-subunit salt bridge (D155-R395) (Danziger et al., 2003). This results in reduced positive cooperativity (n = ~1.5), while preserving the negative inter-ring allostery (Figure 4.5B). A GroEL mutant essentially lacking positive cooperativity was created by combining D155A with the R197A mutation (Figure 4.5C). The latter breaks one of the inter-subunit salt bridges (R197-E386), diminishing positive allostery (Fridmann et al., 2000; White et al., 1997). EL-D155A/R197A nevertheless maintained the negative inter-ring cooperativity (Figure 4.5C). Both EL-D155A and EL-D155A/R197A formed MR complexes in the presence of GroES and ATP with a similar efficiency as EL-WT (Fig. 4.5E), suggesting that intra-ring positive cooperativity is not essential for ring separation and exchange. In contrast, the mutant EL-E461K has completely lost negative inter-ring allostery but largely maintained positive intra-ring cooperativity (n = ~2.3) (Fig. 4.5D). This mutant is deprived of the critical inter-ring salt-bridges (E461-R452 and K105-E434) of the equatorial domains, and the two rings are rearranged in a 1:1 subunit interaction (Cabo-Bilbao et al., 2006; Sewell et al., 2004). Strikingly, no MR occurred with EL-E461K (Fig. 4.5E). As a conclusion, structural changes underlying negative inter-ring allostery of ATP binding are significant in triggering ring separation.

The structural basis for negative allosteric cooperativity is primarily steric effects (Cui and Karplus, 2008). When nucleotide binding occurs simultaneously in both rings, the twisting of the equatorial domains upon ATP binding would result in severe van der Waals clashes. However, the mutant EL-E461K reduces ~50% of the inter-ring contact surface compared to EL-WT due to deficient inter-ring salt bridges

thus realigning the two rings in a 1:1 subunit interaction (Cabo-Bilbao et al., 2006). Lacking of strong inter-ring interactions, EL-E461K cannot generate strong van der Waals clashes upon nucleotides binding and thus fails to trigger ring separation. Therefore, it is plausible that the steric clashes arising from negative inter-ring cooperativity structurally determine ring separation and exchange.

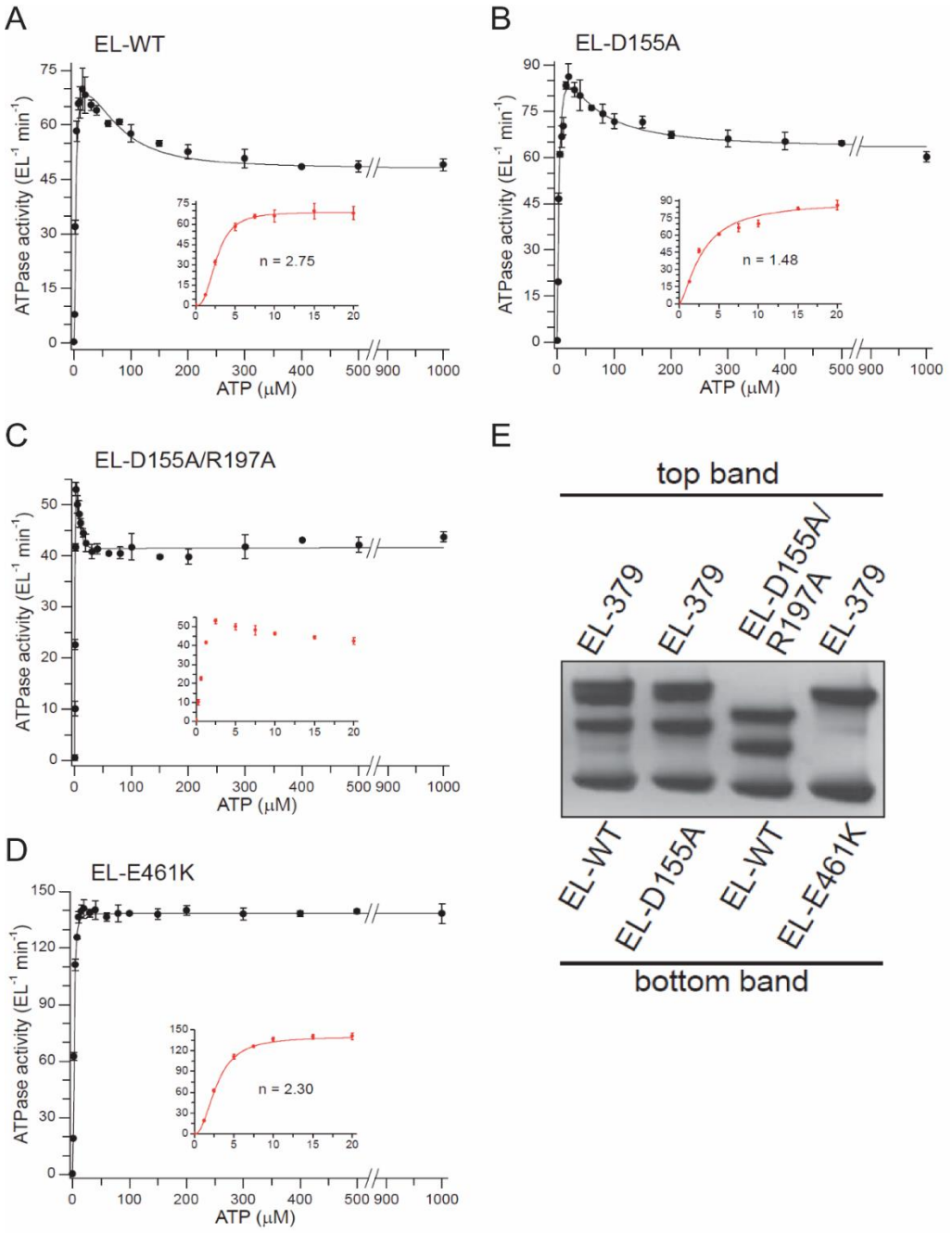

Figure 4.5 Negative inter-ring cooperativity is required for ring separation.

(A-D) ATPase activities of EL-WT (A), EL-D155A (B), EL-D155A/R197A (C) and EL-E461K (D) as a function of ATP concentration. ATPase activities were measured photometrically using a NADH-coupled enzymatic assay at 25°C. The data were fitted using equation (1) (see Methods for details). Inserts show the ATPase rates at low ATP concentrations up to 20 µM and fitted to the Hill equation (2) (see Methods for details) where possible. Data represent the mean ± SEM of three independent experiments. (E) MR formation in the presence of GroES between EL-379 and EL-D155A (defective in positive intra-ring cooperativity), between EL-WT and EL-D155A/R197A (defective in positive intra-ring cooperativity), and between EL-379 and EL-E461K (defective in negative inter-ring cooperativity). MR formation between EL-379 and EL-WT is shown as a control.

4.5 Kinetic analysis of GroEL ring exchange

To study the kinetics of GroEL ring exchange, I set up a dual-color fluorescence cross-correlation spectroscopy (dcFCCS) assay using two populations of the GroEL cysteine mutant EL-E315C (residue in the apical substrate binding domain), one labeled with the fluorophore Atto532 (green) and the other with Atto655 (red) (Haldar et al., 2015). Equimolar amounts of the labeled GroEL (0.5 µM each) were mixed and permitted to undergo ring separation and exchange in the presence of GroES, unfolded DM-MBP and ATP at 25°C (Figure 4.6A). The reaction was stopped at different time points by addition of Apyrase (Apy) to rapidly hydrolyze the remaining ATP, followed by dcFCCS measurement. MR formed with an apparent $t_{1/2}$ of ~22 s (Figure 4.6B). However, due to the concentration-dependent nature of ring re-association, this experimental setup may underestimate the kinetics of GroEL ring separation.

To acquire the rate of ring dissociation independent of GroEL concentration, I next performed an exchange reaction as above until equilibrium was reached. The preformed double-labeled MR complex was then incubated with excess unlabeled GroEL in the presence of GroES and unfolded DM-MBP to monitor the decay of the dcFCCS signal (Figure 4.6C). About 70% of the complexes showed a fast ring

separation with a $t_{1/2}$ of ~12 s (Figure 4.6D). The remaining complexes (~30%) showed a slow rate of ring separation (Figure 4.6D), suggesting that a fraction of the labeled MR complexes were not fully active. The ATPase rate for the fluorescently labeled GroEL in the presence of GroES and DM-MBP at 25°C is ~50 min^{-1} (Figure 4.6E), which is equivalent to ATP hydrolysis per tetradecamer being completed in ~17 s. Therefore, ring separation allowing exchange takes place on the time-scale of the ATPase cycle of the chaperonin system.

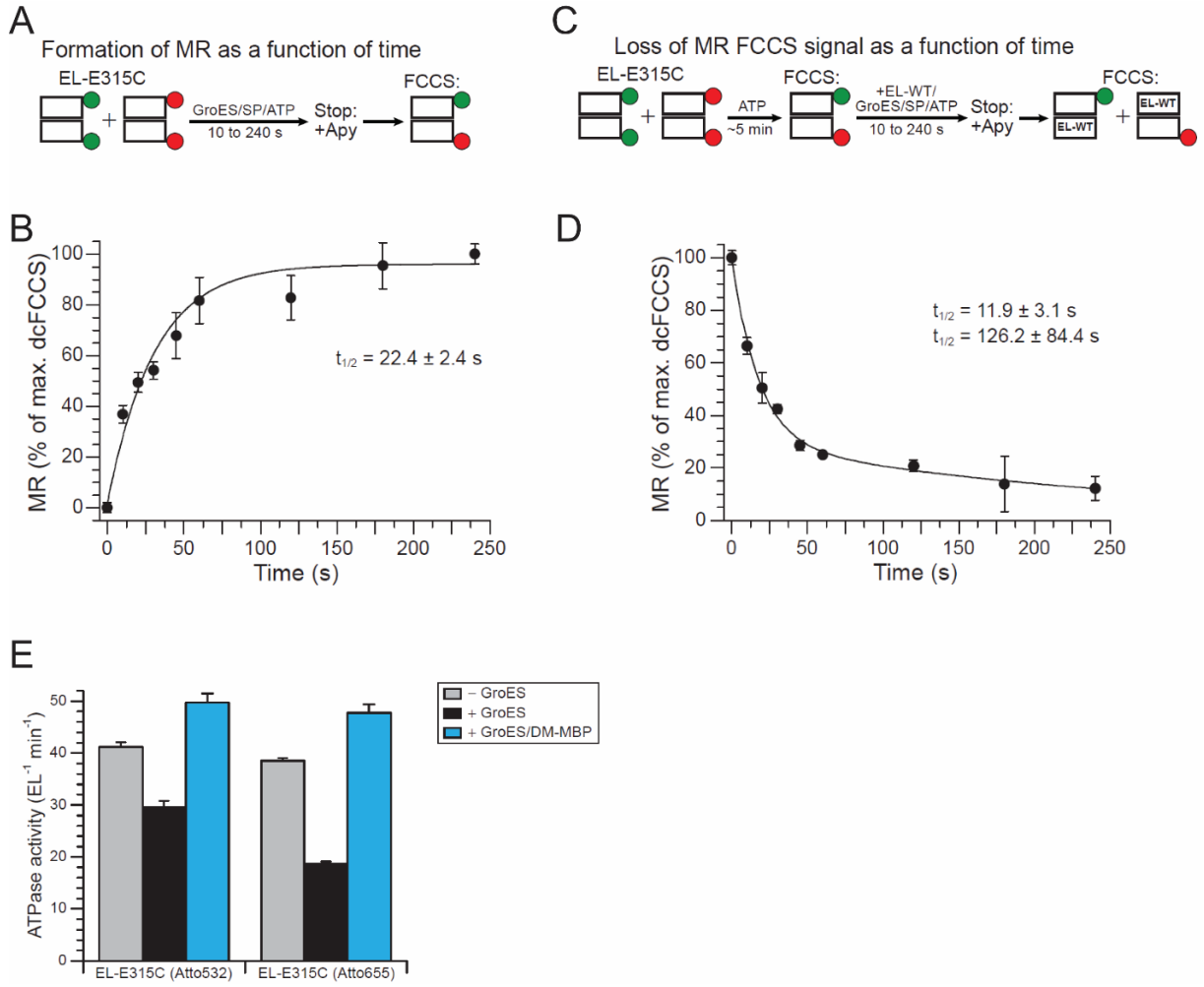

Figure 4.6 Kinetic analysis of GroEL ring exchange.

(A) Schematic of the kinetic analysis of MR formation in the dcFCCS assay. Equimolar concentrations of red- and green-labeled EL-E315C were mixed in the presence of GroES, unfolded DM-MBP, and ATP. Reaction aliquots were stopped by addition of Apy at time points from 10 to 240 s and assayed using dcFCCS. (B) MR formation as in (A). EL-E315C labeled

with Atto532 and EL-E315C labeled with Atto655 (0.5 µM each) were incubated with GroES (2 µM). The reaction was started by adding denatured DM-MBP (1 µM) and ATP (5 mM). At each time point, a 10 µl aliquot of the reaction was stopped by addition of 2.5 U Apy and diluted 15-fold for dcFCCS assay. Data represent the mean ± SEM of three independent experiments. (C) Schematic of the kinetic analysis of MR dissociation in the dcFCCS assay. Double-labeled MR was prepared by mixing equimolar concentrations of E315C (Atto532) and E315C (Atto655) with ATP for 5 min. ATP was removed using two Bio-spin 6 columns. Double-labeled MR was incubated with excess unlabeled EL-WT, GroES, and denatured DM-MBP. The reaction was started by addition of ATP and stopped at different time points by addition of Apy, followed by dcFCCS analysis. (D) MR dissociation as in (C). Double-labeled MR (5 nM tetradecamer) was incubated with unlabeled EL-WT (1 µM), GroES (2.1 µM), and DM-MBP (1 µM). The reaction was started by adding ATP (5 mM). At each time point, a 10 µl aliquot of the reaction was stopped by addition of 2.5 U Apy and diluted 15-fold for dcFCCS assay. Data represent the mean ± SEM of three independent experiments. (E) ATPase activity of EL-E315C labeled with Atto532 or Atto655 alone, in the presence of GroES or in the presence of GroES and excess non-native DM-MBP. ATPase activities were measured photometrically at 25°C.

4.6 Preventing ring separation and exchange by inter-ring disulfide bridges

To study the possible functional importance of ring separation and exchange, I generated a cysteine mutant of GroEL in which the two rings are covalently linked by disulfide bonds. In the structure of apo GroEL (PDB: 1XCK), residue Ala109 of helix D in the equatorial domain of one ring engages in van der Waals contact with Ala109 in the subunit of the opposing ring, which is critical for conveying negative inter-ring allostery (Gruber and Horovitz, 2016; Saibil et al., 2013). I mutated Ala109 to Cys in order to link the two rings. The resulting mutant EL-A109C readily acquired inter-ring disulfide bonds upon expression in *E. coli*, indicating that the selected Cys residues are properly arranged for disulfide bond formation. Disulfide-bonded GroEL subunit dimers were visualized using mass spectrometry and SDS-PAGE under non-reducing condition (Figures 4.7A and 4.7B). We further solved the crystal structure of EL-A109C at 3.2 Å resolution by molecular replacement (PDB:

5OPW; Figure 4.7C and Table 4.1). The inter-ring disulfide bonds between opposing A109C residues are clearly detected with a length of ~2 Å (Figures 4.7C and 4.7D). EL-A109C with disulfide bonds, denoted as EL-SS, showed essentially identical structure to EL-WT (PDB: 1XCK) with an overall root-mean-square deviation (r.m.s.d.) between Cα atoms of 1.128 Å.

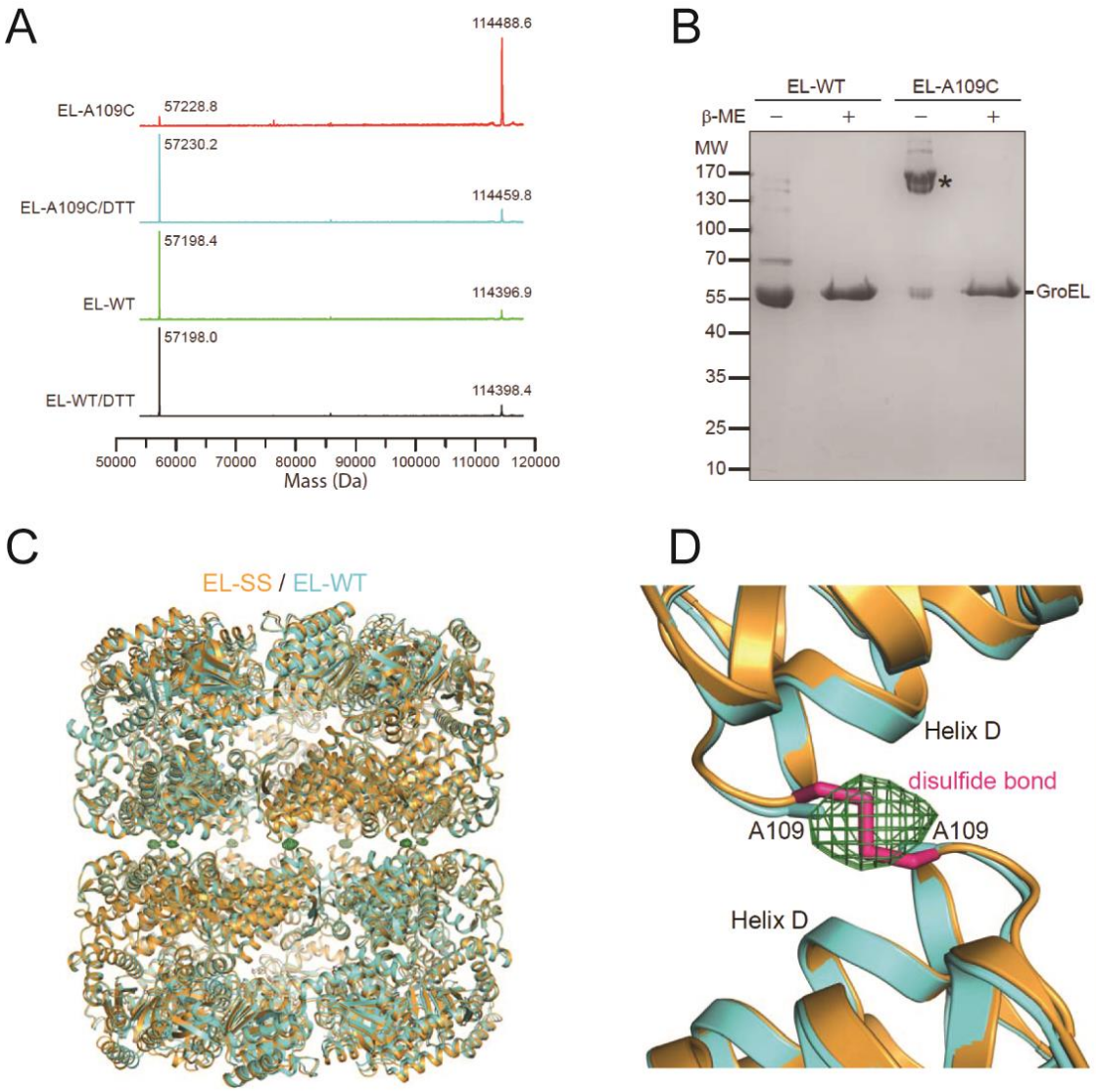

Figure 4.7 The mutant EL-A109C with inter-ring disulfide bridges.
(A) Mass spectroscopic analysis of EL-A109C (EL-SS) under non-reducing and reducing conditions. The molecular masses of the cysteine-bonded dimer and reduced monomer are indicated in Daltons (Da) (theoretical masses: 114457.4 Da and 57229.7 Da, respectively). EL-WT analyzed under the same conditions is shown as a control (57197.7 Da for the monomer of EL-WT). (B) SDS-PAGE (12%) analysis of EL-WT and EL-SS in the absence or presence of

β-mercaptoethanol (β-ME). Samples were not heated prior to SDS-PAGE. Asterisk indicates the position of the disulfide-bonded EL-SS dimer. (C) Overlay of the crystal structures of EL-WT (PDB: 1XCK) and disulfide-bonded EL-SS in aquamarine and orange, respectively. The green meshwork at the equator shows the omit electron density for the disulfide bonds. (D) A close-up of one inter-ring contact. The cysteine moiety (pink) is shown in stick representation.

Table 4.1 Data collection and refinement statistics for crystal structures

Dataset	**EL-A109C**	**EL-A109C:GroES$_2$**
PDB code	5OPW	5OPX
Data collection		
Beamline	ESRF ID30A-1	ESRF ID30A-1
Wavelength	0.9660	0.9660
Space group	$P2_1$	$P2_12_12_1$
Cell dimensions		
a, *b*, *c* (Å)	135.695, 262.047, 149.213	217.567, 230.504, 235.391
α, β, γ (°)	90, 100.81, 90	90, 90, 90
Resolution (Å) *	49.35 – 3.19 (3.25 – 3.19)	49.37 – 3.64 (3.7 – 3.64)
R_{pim} *	0.109 (0. 570)	0.080 (0. 557)
I / σ *	6.3 (1.4)	7.9 (1.4)
Completeness (%)*	99.5 (93.7)	99.8 (99.9)
Redundancy *	3.5 (3.1)	4.9 (5.0)
Refinement		
Resolution (Å)	50 – 3.19	50 – 3.64
No. reflections	160056	125728
R_{work} / R_{free}	0.2446 / 0.2524	0.2312 / 0.2560
No. atoms	53984	63865
Protein	53984	63403
Ligand/ion	0	462
Water	0	0
B-factors (Å^2)	83.96	137.06
Protein	83.96	138.38
Ligand/ion	–	80.67
Water	–	–
r.m.s.d.		
Bond lengths (Å)	0.005	0.011
Bond angles (°)	0.822	1.588

*Values in parentheses are for highest-resolution shell.

As predicted, EL-SS lost the ability of MR formation, even in the presence of 10 mM DTT as detected by native-PAGE (Figures 4.8A and 4.8B), which is consistent with the solvent-inaccessible structure of the disulfide bond (8.3% solvent exposure). To confirm that it is the buried disulfide bridge but not the 109 position inhibiting ring exchange, I generated the control mutant EL-A109S. EL-A109S behaved like EL-WT in terms of MR formation (Figure 4.8A).

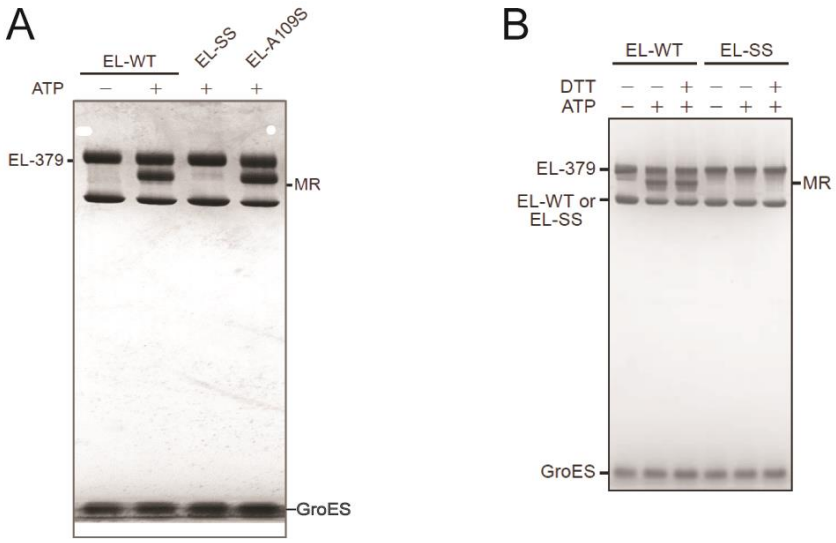

Figure 4.8 Inter-ring disulfide bridges prevent ring separation.
(A) MR formation of EL-379 with EL-SS or EL-A109S in the presence of GroES and ATP at 25°C monitored using native-PAGE. MR formation of EL-379 and EL-WT is shown as control. (B) Analysis of MR formation between EL-WT or EL-SS and EL-379 in the absence or presence of 10 mM DTT and absence or presence of ATP at 25°C. Note that the inter-ring disulfide bonds of EL-SS remain intact in the presence of DTT (in the absence of denaturant), preventing ring separation and exchange.

From the steady-state measurements of ATPase rates, both EL-SS and EL-A109S preserved positive intra-ring and negative inter-ring allostery of their ATPase functions (Figures 4.9A and 4.9B). Therefore, the function of the residue 109 inter-ring contact in conveying the negative cooperativity via helix D is maintained (Gruber and Horovitz, 2016; Saibil et al., 2013), indicating that inter-ring communication is not grossly disturbed in EL-SS mutant. The ATPase activity of EL-SS was about twice that of EL-WT but was reduced to the same level as EL-WT

in the presence of GroES (Figure 4.9C). Furthermore, EL-SS and EL-A109S showed the same binding affinity for non-native SP as EL-WT (Figure 4.9D). In brief, EL-SS allows us to explore the functional consequences of a failure in ring separation.

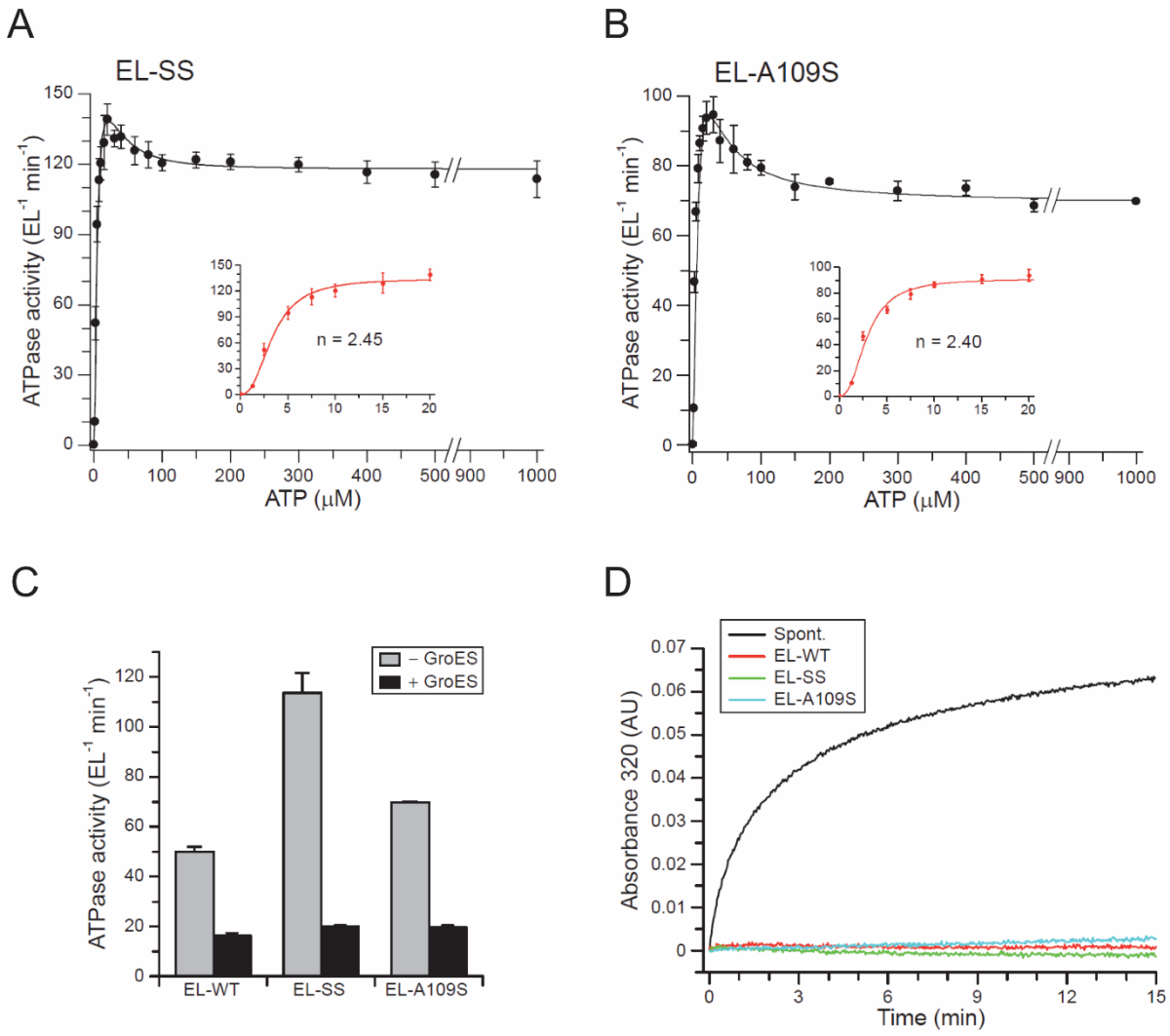

Figure 4.9 Characterization of EL-SS and EL-A109S.
(A and B) ATPase rates of EL-SS (A) and EL-A109S (B) as a function of ATP concentration. ATPase activities were measured photometrically at 25°C and fitted to equation (1). Insert shows the ATPase rate at low ATP concentrations up to 20 μM and fitted to the Hill equation (2). Data represent the mean ± SEM of three independent experiments. (C) ATPase activity of EL-SS and EL-A109S (100 nM each) in the absence or presence of GroES (200 nM) measured in HS buffer containing 1 mM ATP at 25°C. ATPase activity of EL-WT is shown as a control. Data represent the mean ± SEM of three independent experiments. (D) Prevention of Rho aggregation by EL-WT, EL-SS, and EL-A109S. Rho aggregation was measured at an equimolar

ratio of GroEL to Rho by monitoring turbidity at 320 nm. Measurements are normalized to 0 at the start point.

4.7 Failure of ring separation results in formation of symmetric GroEL:GroES$_2$ complexes

In the sequential model of the chaperonin reaction, the major populated class is the asymmetric GroEL:GroES complex. Symmetric GroEL:GroES$_2$ complexes are either missing or happen only transiently (Hayer-Hartl et al., 2016). To test whether preventing ring separation shifts the proportions of asymmetric and symmetric particles, I again applied dcFCCS. The GroES mutant 98C, which carries an additional cysteine at the C-terminus, was labeled with the green fluorophore Atto532 (ES-532) and red Atto655 (ES-655). In this assay, the formation of symmetric particles is reflected by a quantifiable cross-correlation signal generated by the co-diffusion through the confocal volume of two differentially fluorescent-labeled GroES molecules bound to GroEL (Figure 4.10A) (Haldar et al., 2015). The ATP hydrolysis-deficient mutant EL-D398A populating 100% symmetric complexes with GroES was taken as a reference (Koike-Takeshita et al., 2014; Sameshima et al., 2008). As reported previously, EL-WT formed negligible amounts of symmetric complexes both in the absence and presence of saturating non-native DM-MPB (Figures 4.10B and 4.10C) (Haldar et al., 2015), which supports the sequential reaction cycle. Interestingly, EL-SS, failing to undergo ring separation (Figures 4.8A and 4.8B), formed large amounts of symmetric complexes similar to the EL-D398A control, while the ring separation-competent EL-A109S behaved like EL-WT (Figures 4.10B and 4.10C). Formation of symmetric complexes by EL-SS was also confirmed using negative stain EM (Figure 4.11). Therefore, transient ring separation and exchange ensures that the GroEL rings function sequentially,

avoiding the formation of symmetric complexes. In further support of this conclusion, the mutant EL-E461K which is defective in negative inter-ring cooperativity and ring separation (Figures 4.5D and 4.5E), also formed substantial amounts of symmetric complexes during the reaction cycle (Figure 4.10D), especially at higher temperature. Interestingly, EL-E461K was reported to be deficient in mMDH folding in a temperature-dependent manner (Sot et al., 2002).

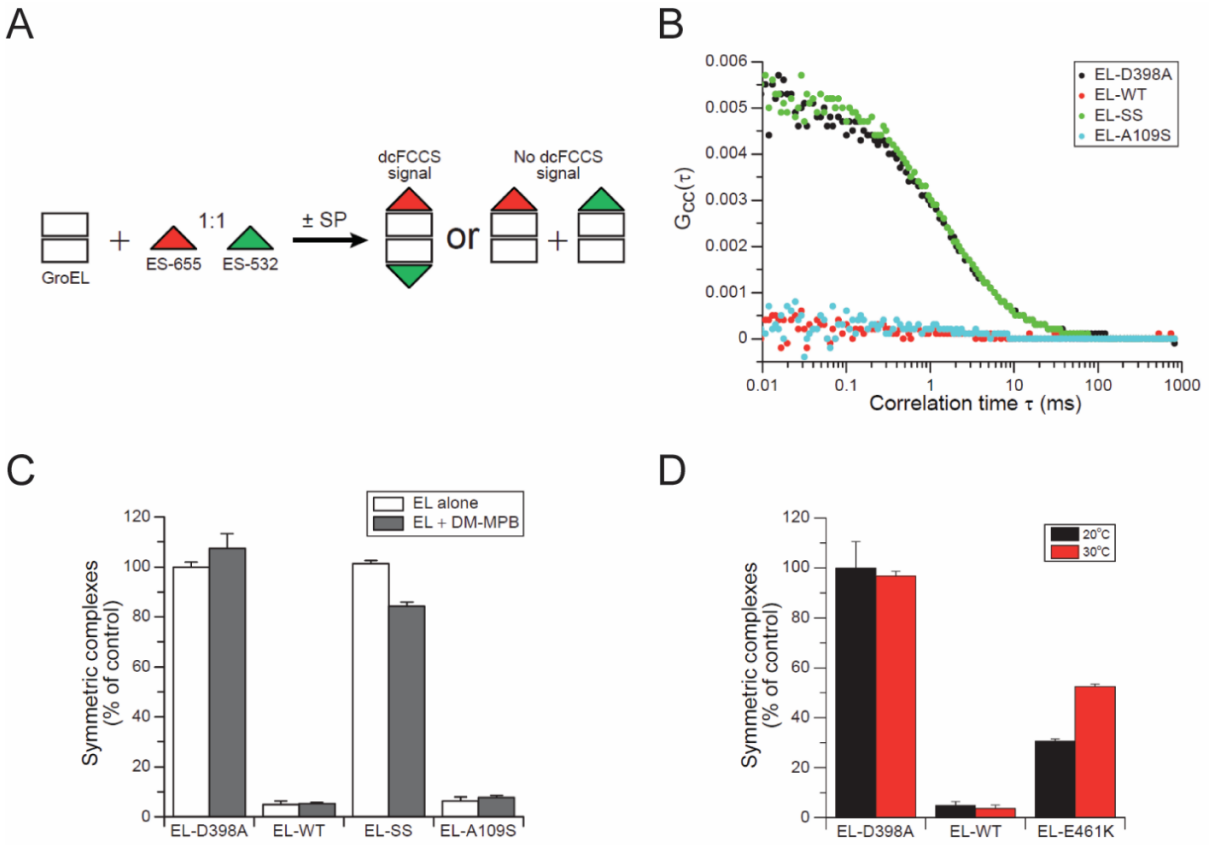

Figure 4.10 Transient ring separation prevents the formation of symmetric GroEL:GroES$_2$ complexes.

(A) Schematic of the dcFCCS experiment. Cross-correlation of Atto655-labeled ES-98C (ES-655) and Atto532-labeled ES-98C (ES-532) bound to GroEL indicates the formation of symmetric GroEL:GroES$_2$ complexes. (B) A 1:1 mixture of ES-655 and ES-532 (50 nM each) was added to HS buffer containing GroEL variants (50 nM). Complex formation was initiated by the addition of ATP (10 mM), and the cross-correlation was measured for 60 min at 20°C. (C) Quantitation of symmetric complexes in the absence or presence of unfolded DM-MBP, performed as in (B). In the absence of DM-MBP the cross-correlation was measured for 60 min and in the presence of DM-MBP for 30 min. The cross-correlation signal obtained with EL-

D398A:$GroES_2$ complexes was set to 100%. Data represent the mean ± SEM of three independent experiments. (D) A 1:1 mixture of ES-655 and ES-532 (50 nM each) was added to HS buffer containing the indicated GroEL variants (50 nM). Complex formation was initiated by the addition of ATP (10 mM), and the cross-correlation was measured for 60 min at 20°C and 30°C. Quantitation of symmetric complexes was performed as in (C). The cross-correlation signal obtained with EL-D398A:$GroES_2$ complexes is set to 100%. Data represent the mean ± SEM of three independent experiments.

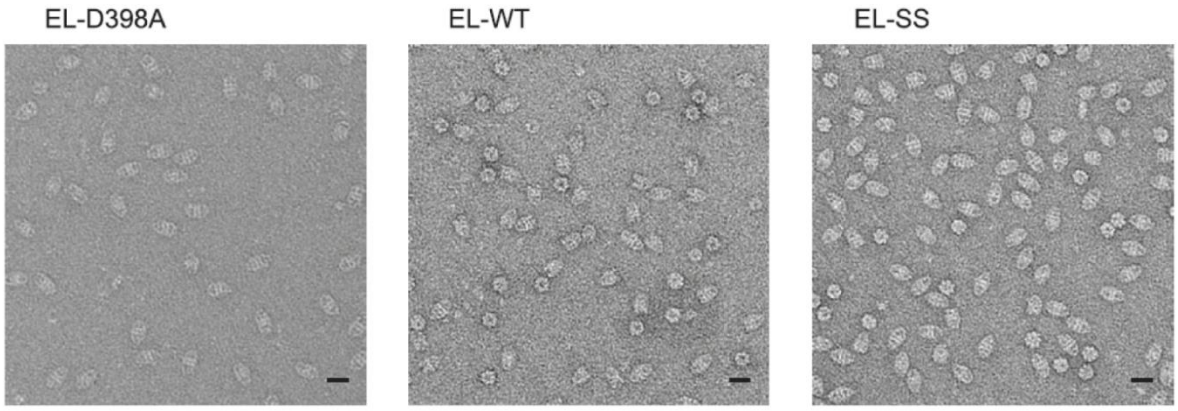

Figure 4.11 GroEL/ES complexes checked by EM.
Electron micrographs of negatively-stained EL-D398A (left), EL-WT (middle) and EL-SS (right). 50 nM GroEL tetradecamer and 100 nM GroES heptamer were incubated in HS buffer containing 1 mM ATP at 25°C for 2 min. Scale bar, 200 Å. EL-SS forms mainly symmetric EL-SS:$GroES_2$ complexes.

Previous studies have shown that GroEL:$GroES_2$ complexes formed by EL-D398A with ATP or EL-WT with ATP·BeF_x are non-cycling (Fei et al., 2014; Koike-Takeshita et al., 2014), which means GroES is stably bound to GroEL. To determine whether EL-SS formed dynamic complexes with GroES, a 20-fold excess of unlabeled GroES was added to preformed double-labeled, symmetric complexes in the dcFCCS assay (Figure 4.12A). In contrast to the non-cycling EL-D398A:$GroES_2$, GroES addition to EL-SS:$GroES_2$ complexes caused displacement of the labeled GroES, as reflected by the loss of the cross-correlation signal (Figure 4.12B). The dynamic cycling of EL-SS was also proved by the ATPase activity in the presence of GroES (Figure 4.9C).

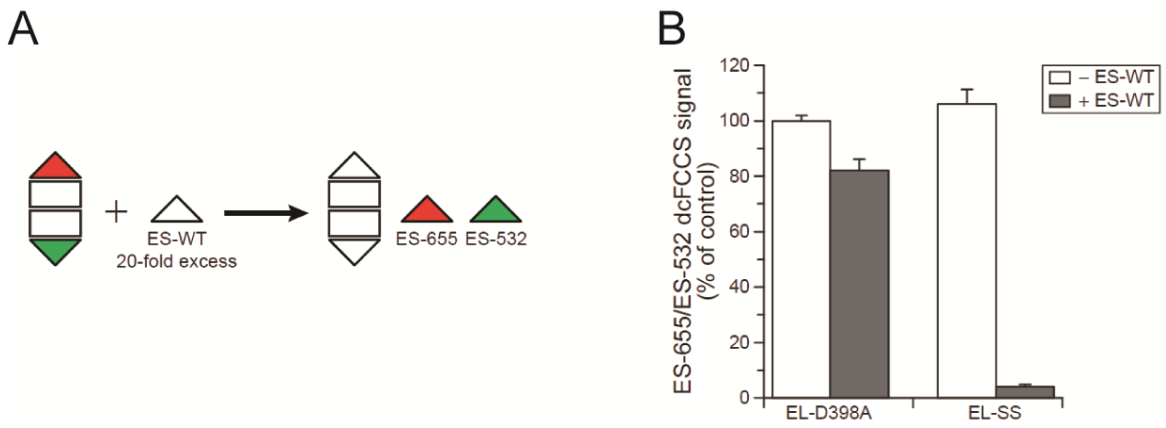

Figure 4.12 EL-SS forms dynamic GroEL:GroES$_2$ complexes.
(A) Schematic of the dcFCCS experiment, monitoring loss of cross-correlation signal upon displacement of fluorescent-labeled GroES by unlabeled GroES. (B) A 20-fold excess of unlabeled GroES was added to the symmetric complexes consisting of either EL-D398A or EL-SS with bound ES-655 and ES-532. After incubation for 3 min, the cross-correlation signal was measured for a time window of 60 min at 20°C. Data represent the mean ± SEM of three independent experiments.

To exclude the possibility that the inter-ring disulfide bridges in EL-SS populate symmetric complexes by topologically restricting the inter-ring interface, we also solved the crystal structure of the EL-SS:GroES$_2$ complex with bound ADP·BeF$_x$ (a mimic of bound ATP prior to hydrolysis) at 3.65 Å resolution (Figure 4.13A and Table 4.1). Compared to the apo states of EL-SS and EL-WT, the equatorial domains in the symmetric complex are obviously re-oriented (Figures 4.7C and 4.13B). However, the symmetric complex of EL-SS:GroES$_2$ was highly similar to that of the symmetric complex formed by EL-WT and GroES in the presence of ADP·BeF$_x$ (PDB: 4PKO) (Fei et al., 2014) (Figure 4.13C), with r.m.s.d. values (Cα atoms) of 2.16 Å (overall) and an average of 1.59 Å (0.92–2.45 Å) for individual chains. Thus, the disulfide bridges linking the two GroEL rings do not restrain conformational changes that occur during ATP binding, which is consistent with EL-SS preserving negative inter-ring cooperativity (Figure 4.9A). Therefore,

the EL-SS mutant would allow us to study the function of ring exchange as well as the behavior of symmetric GroEL:GroES$_2$.

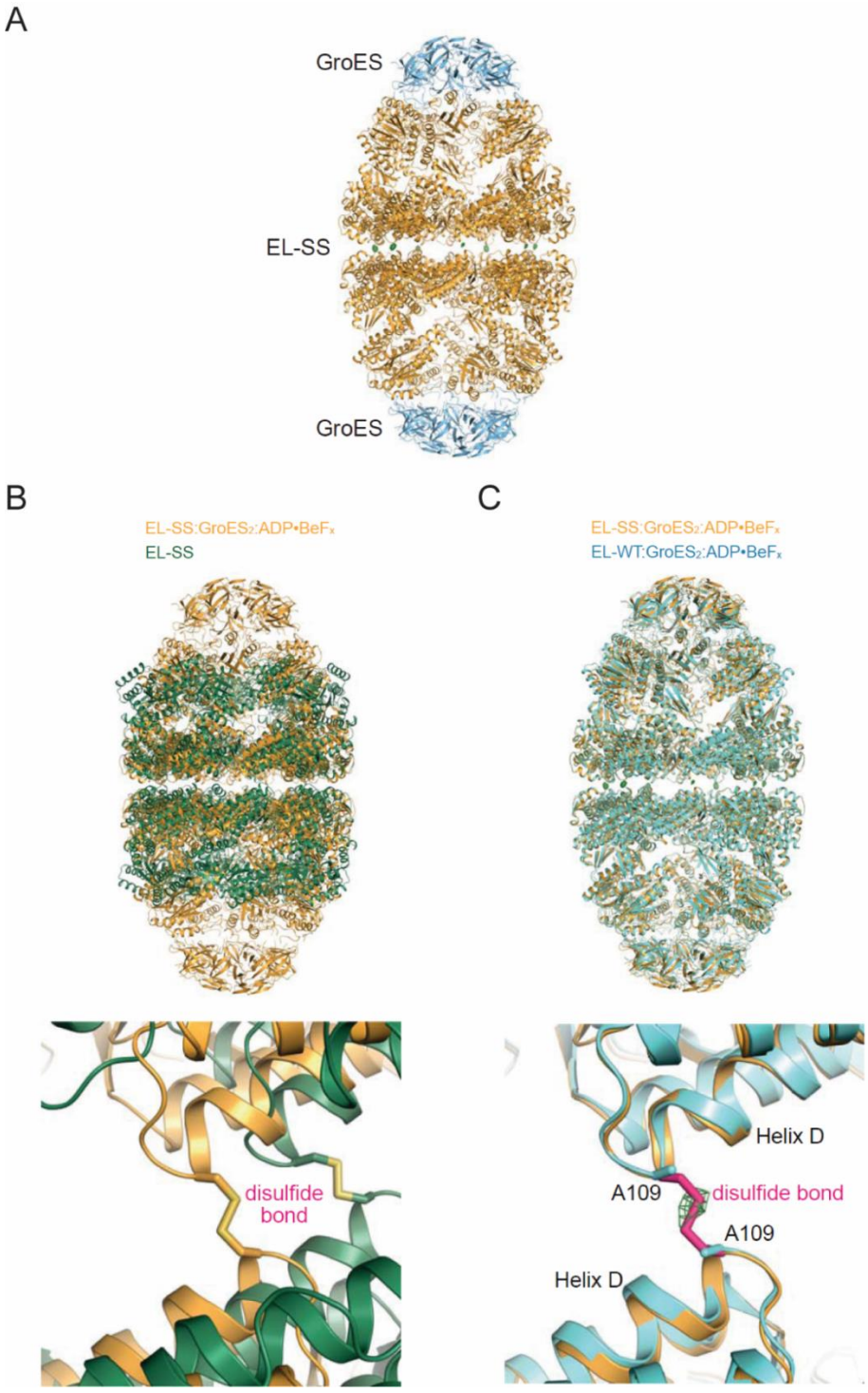

Figure 4.13 Structure of the EL-SS:GroES$_2$ complex.

(A) Crystal structure of the EL-SS:GroES$_2$ complex. Protein is represented in ribbon representation. GroEL and GroES subunits are indicated in orange and light blue, respectively. Omit density for the disulfide bonds across the equator is shown as green meshwork. (B-C) Superposition of the EL-SS:GroES$_2$:ADP·BeF$_x$ complex with EL-SS (B) and EL-WT:GroES$_2$:ADP·BeF$_x$ (C). The EL-SS:GroES$_2$:ADP·BeF$_x$ complex (PDB: 5OPX) is shown in orange, EL-SS (PDB: 5OPW) in green, and EL-WT:GroES$_2$:ADP·BeF$_x$ (PDB: 4PKO) in teal. Close-ups show one inter-ring contact in detail.

4.8 Dynamics of the GroEL/ES cycle measured using stopped-flow fluorescence resonance energy transfer (Stopped-flow FRET)

As with many other cellular machines, the chaperonin nano-machine has evolved elegant regulations to coordinate the binding and release of GroES and SP. The measurement for the real-time association and dissociation between GroEL and GroES would clearly show the influence of ring separation and exchange on chaperonin cycling. Here, I measured the kinetics of GroES association and dissociation using stopped-flow FRET.

The GroEL apical domain cysteine mutants EL-E315C or EL-A109C/E315C were labeled with the acceptor fluorophore Atto647N (EL$_A$-WT or EL$_A$-SS, respectively; ~2.2 fluorophores per tetradecamer), and the GroES mutant 98C was labeled with the donor fluorophore Atto532 (ES$_D$; ~1.1 fluorophores per heptamer). Association was measured upon rapid mixing of EL$_A$-WT or EL$_A$-SS with ES$_D$/ATP in the absence or presence of an excess of unfolded DM-MBP, and the increase in acceptor fluorescence was monitored (Figure 4.14A). Overall, similar pseudo-first-order association rates were observed for EL$_A$-WT and EL$_A$-SS, independently of the presence of SP (k_{ass} ~22 s^{-1}; t$_{½}$ ~30 ms) (Figures 4.14B and 4.14C). Notably, EL$_A$-SS showed a higher amplitude of acceptor fluorescence than EL$_A$-WT, consistent with the formation of symmetric complexes when ring separation is prohibited (Figure 4.10).

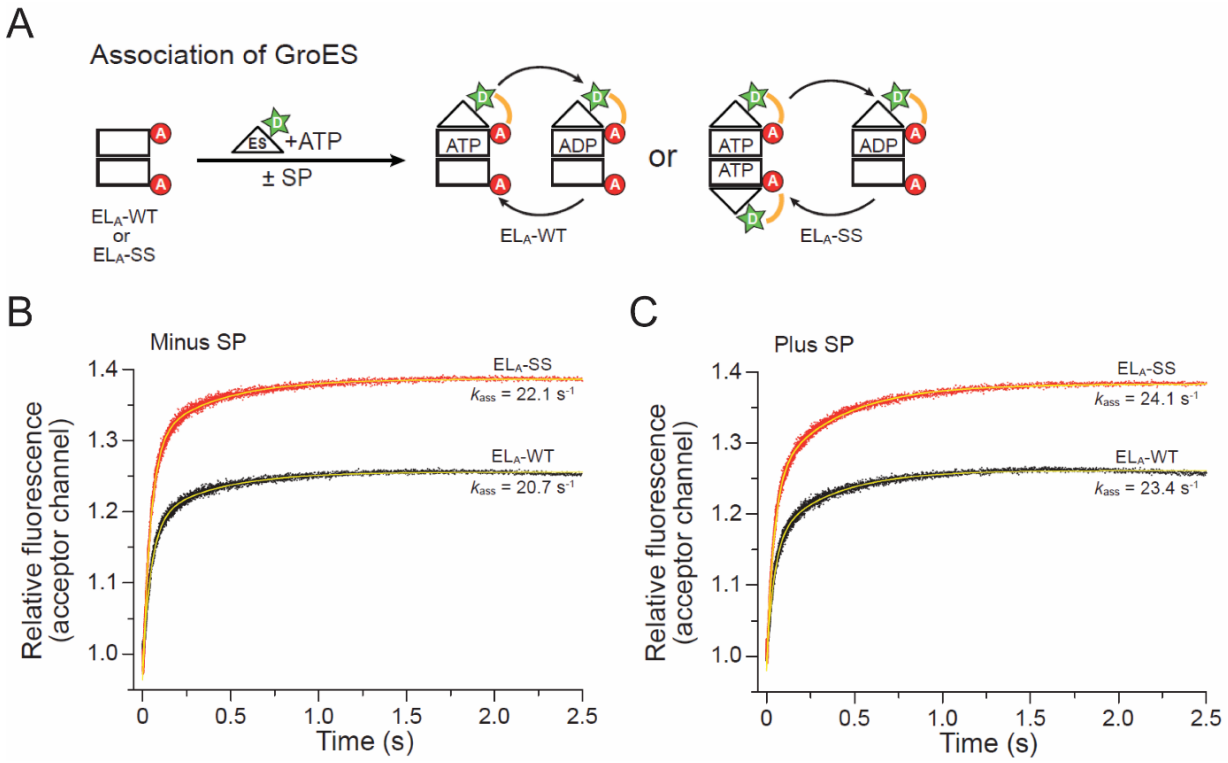

Figure 4.14 Association dynamics of the GroEL/ES system.
(A) Schematic of association dynamics of GroES with GroEL analyzed using stopped-flow FRET. EL_A-WT and EL_A-SS, EL-E315C and EL-A109C/E315C labeled with the acceptor fluorophore Atto647N, respectively; ES_D, ES-98C labeled with the donor fluorophore Atto532. (B and C) Association of ES_D with EL_A-WT or EL_A-SS in the absence (B) or presence (C) of excess unfolded DM-MBP monitored upon rapid mixing. To obtain pseudo-first-order association, a 10-fold excess of ES_D (2 µM) over EL_A (0.2 µM) was used (K_d of the GroEL/ES interaction in the presence of ATP is ~ 17 nM) (Hayer-Hartl et al., 1995). The transfer of energy as ES_D binds to EL_A is measured as an increase in the acceptor fluorescence intensity. The data were fitted using a single exponential model (yellow lines).

Next, I measured the dissociation rate of GroEL/ES complexes under steady-state conditions. EL_A-WT and ES_D were first incubated with ATP for ~1 min, and then unlabeled competitor GroES was added in a 20-fold excess by rapid mixing (Figure 4.15A). In the absence of unfolded DM-MBP, the dissociation of ES_D reflected by the decrease in acceptor fluorescence, followed a single exponential decline with a k_{diss} of 0.10 s^{-1} ($t_{½}$ ~7 s) (Figure 4.15B), consistent with the ATPase rate of EL_A-WT/ES_D (Figure 4.15D). The labeled EL_A-WT and EL_A-SS showed

ATPase activities of ~48 and ~113 ATP min^{-1} alone, ~25 and ~52 ATP min^{-1} with ES_D, and ~75 and ~90 ATP min^{-1} with ES_D/DM-MBP, respectively. The apparent GroES dissociation rate was ~2-times faster with EL_A-SS (k_{diss} of 0.20 s^{-1}; $t_{½}$ ~3.5 s), and the amplitude of acceptor fluorescence was ~2-fold higher (Figure 4.15B), indicating rapid GroES cycling on both GroEL rings in parallel. Note that the single or double-exponential fit of the dissociation kinetics was imperfect, suggesting a stochastic nature of the cycling process with multiple co-existing sub-states. In the presence of unfolded DM-MBP, the dissociation of GroES from EL_A-WT was stimulated ~3.5-fold (k_{diss} of 0.37 s^{-1}; $t_{½}$ ~2.0 s) (Figure 4.15C). In contrast, SP showed little effect on GroES dissociation from EL_A-SS (k_{diss} of 0.23 s^{-1}; $t_{½}$ ~3.0 s) (Figure 4.15C), which is presumably due to the simultaneous occupancy of both GroEL rings with GroES hampering DM-MBP binding. In summary, both rings of EL-SS are simultaneously active in GroES binding and release, as proposed for the non-sequential chaperonin model (Yang et al., 2013).

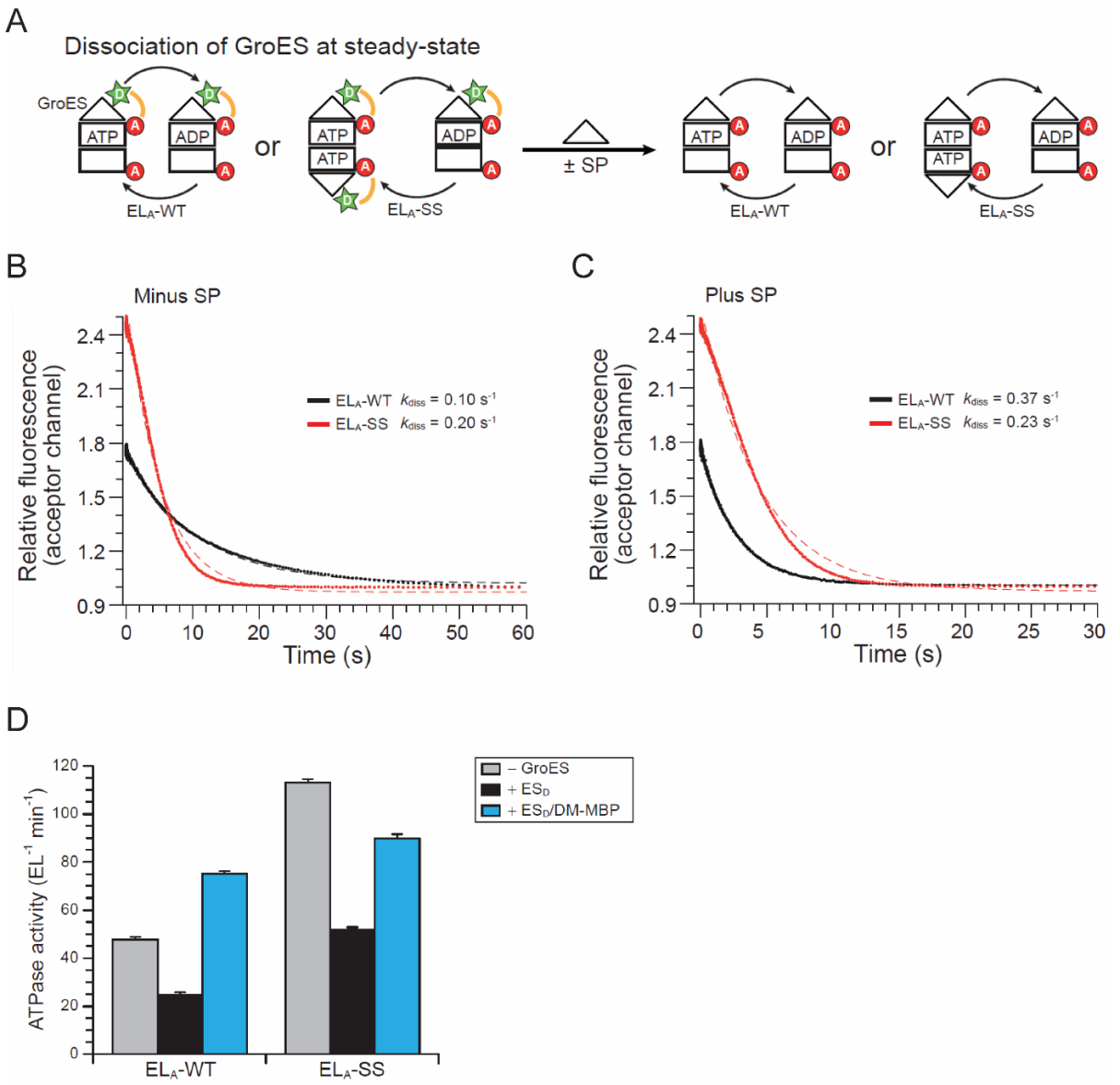

Figure 4.15 Release of GroES from GroEL during a steady-state reaction.
(A) Schematic of the analysis of GroES dissociation from EL-WT or EL-SS at steady state analyzed using stopped-flow FRET. EL$_A$-WT and EL$_A$-SS, EL-E315C and EL-A109C/E315C labeled with the acceptor fluorophore Atto647N, respectively; ES$_D$, ES-98C labeled with the donor fluorophore Atto532. (B and C) Dissociation of ES$_D$ from EL$_A$-WT or EL$_A$-SS under steady-state cycling conditions. EL$_A$ (0.2 µM), ES$_D$ (0.4 µM), and ATP (10 mM) were incubated for ~1 min, followed by addition of a 20-fold molar excess of unlabeled GroES by rapid mixing either without (B) or together with (C) a 10-fold excess of unfolded DM-MBP over GroEL. The loss of energy transfer as ES$_D$ was replaced by unlabeled GroES is measured as a decrease in acceptor fluorescence intensity. The data were fitted by a single exponential model (dotted lines). The fit was imperfect for GroES dissociation from EL-SS and could not be improved by introducing additional parameters. (D) ATPase activity of EL$_A$-WT or EL$_A$-SS alone, in the

presence of ES_D, or in the presence of ES_D and excess non-native DM-MBP. ATPase activities were measured photometrically at 25°C.

4.9 Ring separation and exchange influences SP refolding

To determine how ring separation contributes to the overall efficiency of protein folding assisted by chaperonin, I studied the refolding of three chaperonin SPs by EL-SS: monomeric Rho, dimeric mMDH, and tetrameric *E. coli* dihydrodipicolinate synthase (DapA; ~31 kDa subunits). All three SPs are stringently dependent on GroEL/ES for folding.

GuHCl-denatured SP was diluted into buffer containing either EL-WT, EL-SS, or EL-A109S, and the refolding was started by addition of GroES and ATP. EL-SS refolded Rho with similar kinetics and yield as EL-WT and EL-A109S (Figure 4.16A), indicating that EL-SS is folding-active. Next, I tested the ability of EL-SS to refold the dimeric mMDH and tetrameric DapA. Interestingly, the refolding rate of mMDH and DapA with EL-SS was ~2-3 times slower than with EL-WT or EL-A109S, and the yield was also significantly reduced by ~50% and ~30%, respectively (Figures 4.16B and 4.16C).

Since EL-SS populates symmetric GroEL:$GroES_2$ complexes, we asked whether this would influence the refolding process. I diluted denatured Rho into the actively cycling reaction of GroEL/ES and ATP. A defect for Rho refolding was apparent. The refolding with EL-SS was reduced by ~50% compared to ~20% with EL-WT (Figure 4.16D). This defect of EL-SS clearly indicates that populating symmetric GroEL:$GroES_2$ complexes would limit the availability of GroEL rings for binding non-native SP, resulting in SP aggregation. Therefore, these refolding experiments with stringent SPs clearly indicate that ring separation and exchange,

avoiding symmetric GroEL:GroES$_2$ complexes being populated, is important for chaperonin function.

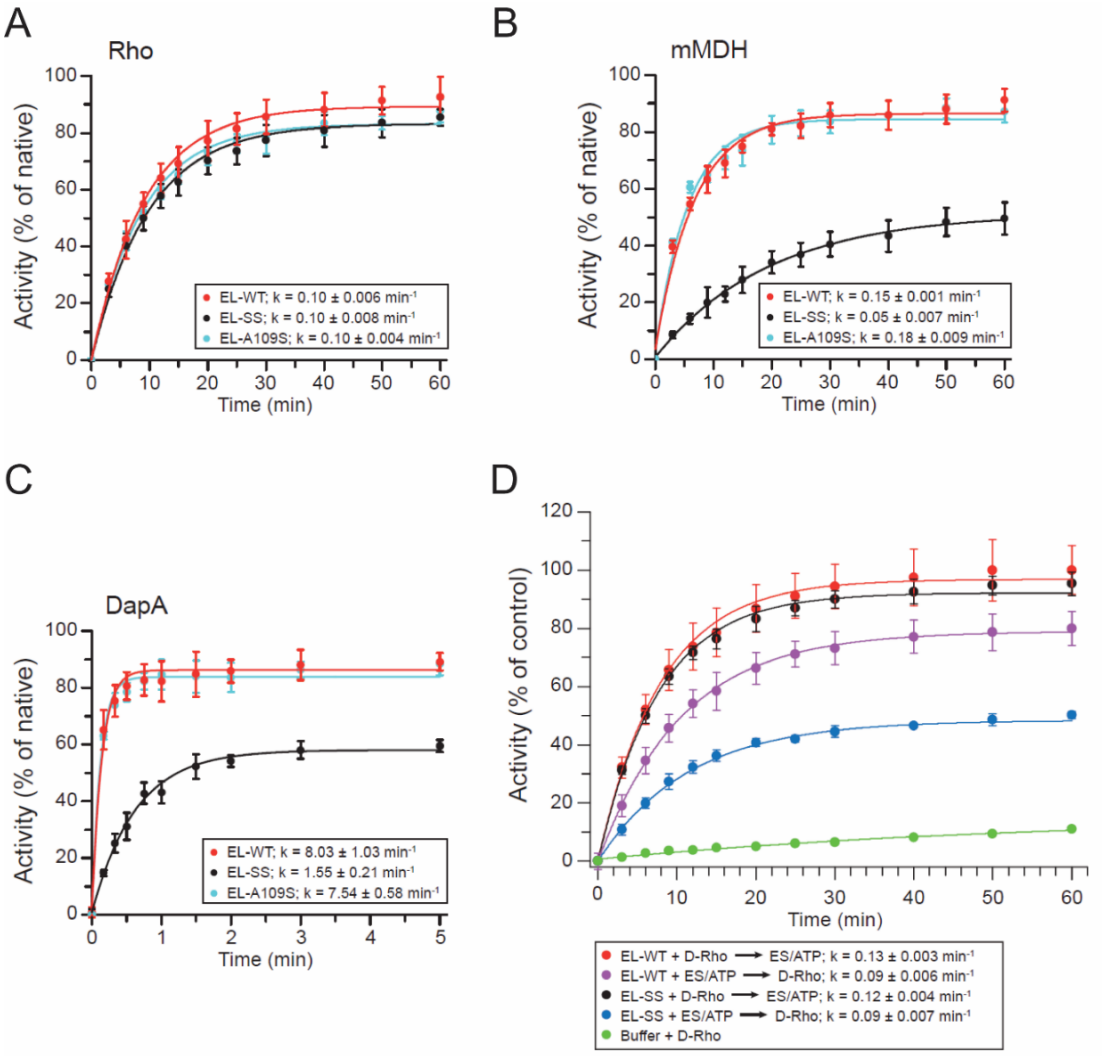

Figure 4.16 Chaperonin functionality in SPs refolding in the absence or presence of ring separation.

(A and B) GroEL/ES-assisted refolding of Rho (A) and mMDH (B). Denatured SP was diluted from GuHCl into HS buffer containing 1 µM GroEL/2 µM GroES (final SP concentration 0.5 µM), followed by addition of 10 mM ATP to initiate refolding at 25°C. Refolding reactions were stopped by addition of CDTA at the indicated time points. Refolding yields are plotted as % enzyme activities of native enzyme control. Single exponential rates are indicated. Data represent the mean ± SEM of three independent experiments. (C) GroEL/ES-assisted refolding of DapA was measured as above, except that denatured DapA was diluted into DapA refolding buffer containing 2 µM GroEL/4 µM GroES (final DapA concentration 0.2 µM). Refolding reactions were stopped by addition of CDTA and incubated for 60 min at 25°C to allow for assembly prior to the enzyme assay. Data represent the mean ± SEM of three independent

experiments. (D) Chaperonin-assisted refolding of Rho in a cycling reaction. Denatured Rho was diluted from GuHCl into HS buffer (final concentration 1 µM) containing actively cycling EL-WT or EL-SS (1 µM)/GroES (2 µM)/ATP (10 mM) at 25°C. In control reactions, Rho was diluted into HS buffer containing EL-WT or EL-SS, and refolding was initiated by addition of GroES and ATP. Refolding in the absence of GroEL is also shown. Refolding reactions were stopped by addition of CDTA at the indicated time points. Refolding yields are plotted as % enzyme activities of EL-WT control. Single exponential rates are indicated. Data represent the mean ± SEM of three independent experiments.

4.10 Ring separation is required for efficient SP release

In contrast to monomeric Rho, the oligomeric mMDH and DapA require the assembly of folded subunits upon release from the chaperonin cage. To understand the defect of EL-SS in the refolding of oligomeric SPs, the fate of mMDH was monitored in the chaperonin reaction. Size-exclusion chromatography (SEC) of GroEL:SP complexes showed that EL-SS and EL-WT bound denatured mMDH with similar efficiency (Figure 4.17A). After 1 h of refolding in the presence of GroES and ATP, BeF_x was added to stably close both folding chambers (Figure 4.17B). SEC showed that EL-SS together with GroES still encapsulated ~65% of mMDH compared to less than 20% in the case of EL-WT (Figures 4.17C). A similar result was also observed with monomeric Rho (Figures 4.17D), indicating that EL-SS is defective in SP release during the functional cycle.

To further test this possibility, I took advantage of previous findings that folding of some SPs involves multiple rounds of binding and release of folding intermediates from chaperonin (Mayhew et al., 1996; Weissman et al., 1994). When the non-native intermediates are released from GroEL into free solution, they will be efficiently trapped by the GroEL mutant N265A (EL-Trap), which does not bind GroES and cannot release SP (Motojima and Yoshida, 2010) (Figure 4.17E). Adding a 5-fold molar excess of EL-Trap 20 s after initiating Rho refolding with EL-

WT/GroES reduced the refolding yield by ~70% (Figure 4.17F). In contrast, the refolding with EL-SS was inhibited by EL-Trap only by ~30% (Figure 4.17F), confirming that Rho is not efficiently released from EL-SS into free solution and spends more time encapsulated in the EL-SS:GroES cage. Taken together, these data suggest that transient ring separation is necessary for the chaperonin system to effectively eject SP and thus allow the timely assembly of folded subunits into functional complexes.

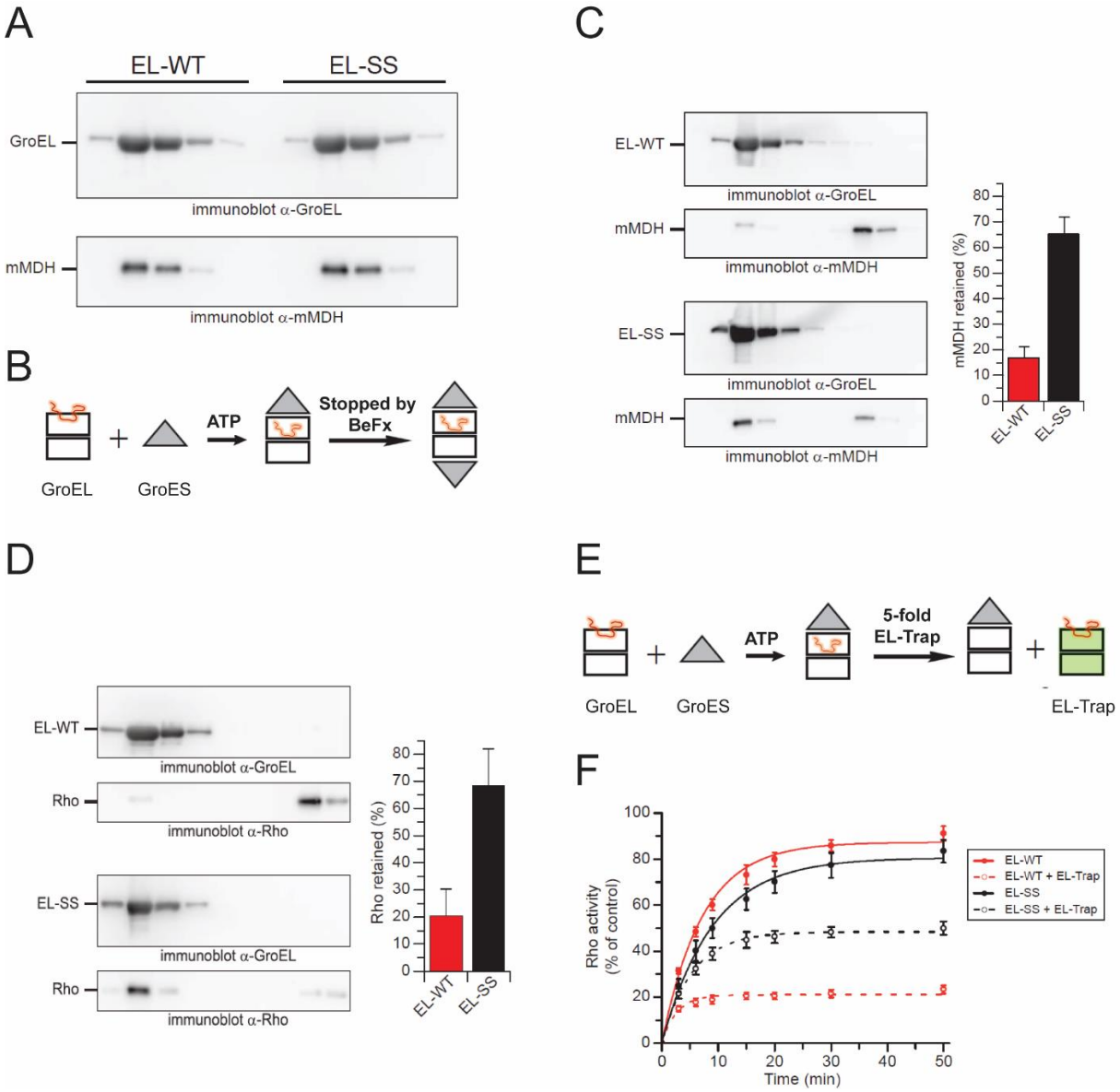

Figure 4.17 Ring separation required for efficient SP release.

(A) EL-WT and EL-SS have similar binding affinities for denatured SP. GuHCl-denatured mMDH was diluted (200-fold) into HS buffer containing EL-WT or EL-SS (1 μM each) to a final concentration of 0.5 μM (monomer). Reactions were analyzed using SEC. GroEL containing fractions were analyzed using SDS-PAGE and immunoblotting with anti-GroEL and anti-mMDH antibodies. (B) Schematic of SP encapsulation after the refolding reaction. At the end of the refolding, BeF_x was added to stably close both folding chambers. (C-D) SEC analysis of the chaperonin-assisted refolding reaction of mMDH (C) and Rho (D). Refolding was carried out as in Figures 4.16A and 4.16B for 60 min (mMDH) or 40 min (Rho), followed by addition of BeF_x to form stable GroEL:$GroES_2$ complexes. Fractions were analyzed using SDS-PAGE and immunoblotting with anti-mMDH (C), anti-Rho (D), and anti-GroEL (C and D) antibodies. The amount of mMDH and Rho retained within the chaperonin was quantified using densitometry (C and D, right panel), with the sum of the retained and free SP set to 100%. Data represent the mean ± SEM of three independent experiments. (E) Schematic of trap experiment. Rho refolding was initiated by addition of ATP. At 20 s after ATP, 5-fold excess of EL-Trap was added to compete for binding of Rho intermediate. (F) Intermittent release of non-native Rho during GroEL/ES-assisted refolding. Rho refolding was performed with EL-WT/GroES or EL-SS/GroES. When indicated, a 5-fold molar excess of EL-Trap over GroEL was added 20 s after initiating refolding with ATP (dotted lines). Data represent the mean ± SEM of three independent experiments.

Next, I tested whether the retained SP in EL-SS cage reaches its native-like state. To do this, the refolding was stopped at the end of the reaction with CDTA. After the cage open, mMDH was incubated for assembly before SEC (Figure 4.18A). SEC showed that most Rho (~90%) and mMDH (~80) were released from GroEL (Figures 4.18B and 4.18C), suggesting that the EL-SS cage is competent for protein folding.

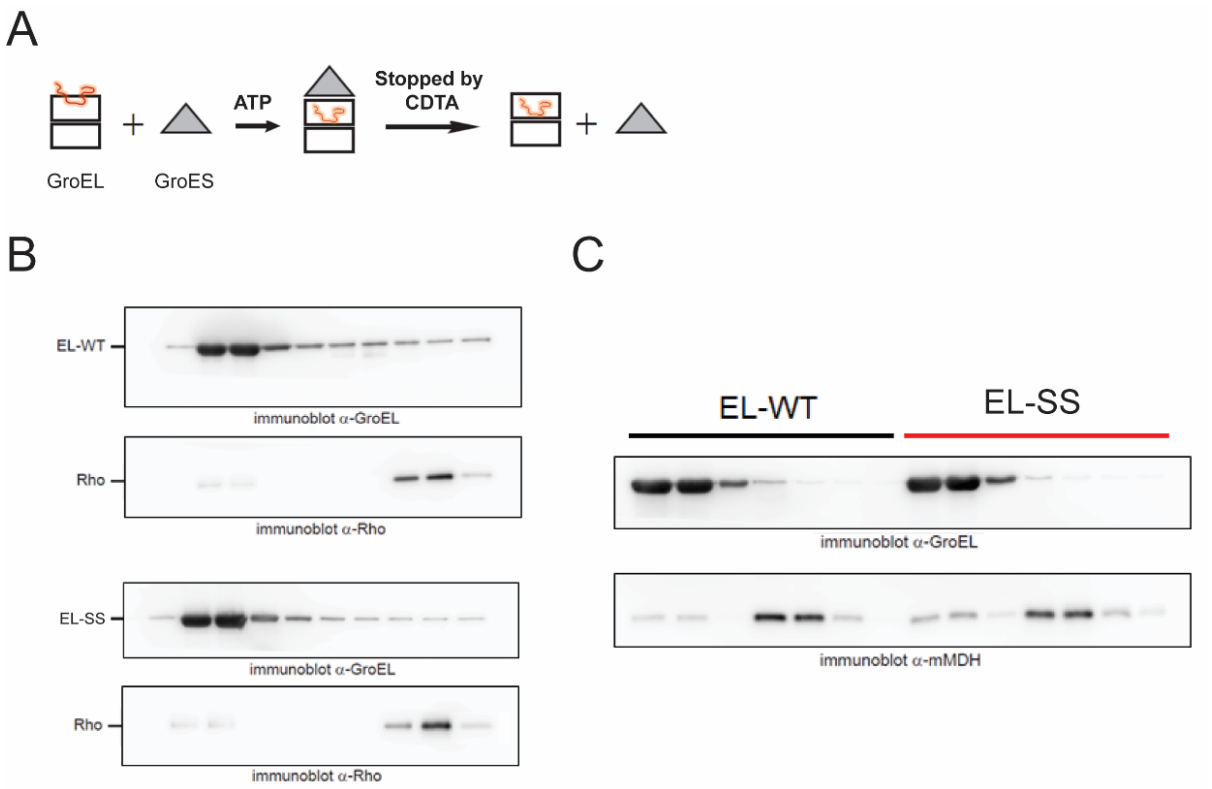

Figure 4.18 The retained SPs are properly folded.
(A) Schematic of SP release after the refolding reaction. At the end of the refolding, CDTA was added to open folding chambers and allow for the release of SPs from GroEL cage. (B-C) SEC analysis of the chaperonin-assisted refolding reaction of Rho (B) and mMDH (C). Refolding was carried out as in Figures 4.16A and 4.16B for 60 min (mMDH) or 40 min (Rho), followed by addition of CDTA to open GroEL cage. Fractions were analyzed using SDS-PAGE and immunoblotting.

4.11 Significance of ring separation *in vivo*

GroEL/ES is essential in *E. coli* (Fayet et al., 1989), consistent with the fact that a subset of cytosolic proteins have an obligate chaperonin requirement for folding (Hayer-Hartl et al., 2016). Many of the known GroEL substrates are oligomeric. To test whether GroEL ring separation is necessary *in vivo*, I took advantage of an MC4100 *E. coli* strain in which the *groE* promoter is replaced with the *araC* gene and the pBAD promoter, and therefore allows the depletion of endogenous GroEL/ES in the absence of arabinose (Kerner et al., 2005). GroES/EL-WT,

GroES/EL-SS, or GroES/EL-A109S was introduced by a single-copy plasmid encoding GroES/EL-WT, GroES/EL-SS, or GroES/EL-A109S under the IPTG-inducible lac UV5 promoter. Thiol-trapping experiments (Leichert and Jakob, 2004) demonstrated that the inter-ring disulfide bonds in EL-SS form in the cytosol, which is consistent with their solvent inaccessibility in the crystal structure (8.3% solvent exposure) (Figure 4.19A). Since the UV5 promoter is leaky, cell growth on glucose was observed without IPTG induction (Figure 4.19B). Importantly, the cell growth with EL-SS was ~100-fold slower than cells expressing EL-WT or EL-A109S at 25°C, 37°C, and 42°C, although the protein level of EL-SS was about 2-fold higher than that of ELWT or EL-A109S (Figures 4.19C and 4.19D). Note that these constructs are not heat-inducible, which accounts for the growth deficiency of EL-WT and EL-A109S cells at 42°C compared to 37°C. Consistently, upon induction with IPTG (Figures 4.19C and 4.19D), EL-WT and EL-A109S cells grew substantially better at 42°C, while EL-SS-expressing cells induced with IPTG still grew much slower at 42°C (Figure 4.19B).

Taken together, these results indicate that the capacity of protein folding mediated by EL-SS *in vivo* is substantially reduced and becomes limiting for growth at GroEL levels similar to those in WT cells (Figures 4.19C and 4.19D). EL-SS overexpression can compensate for the loss of the WT protein at permissive temperatures, but not under stress conditions at 42°C when the requirement for chaperonin function is greatly increased. This deficiency of the EL-SS mutant is consistent with transient ring separation being required to support the sequential GroEL/ES cycle, which allows for efficient SP flux through the chaperonin system.

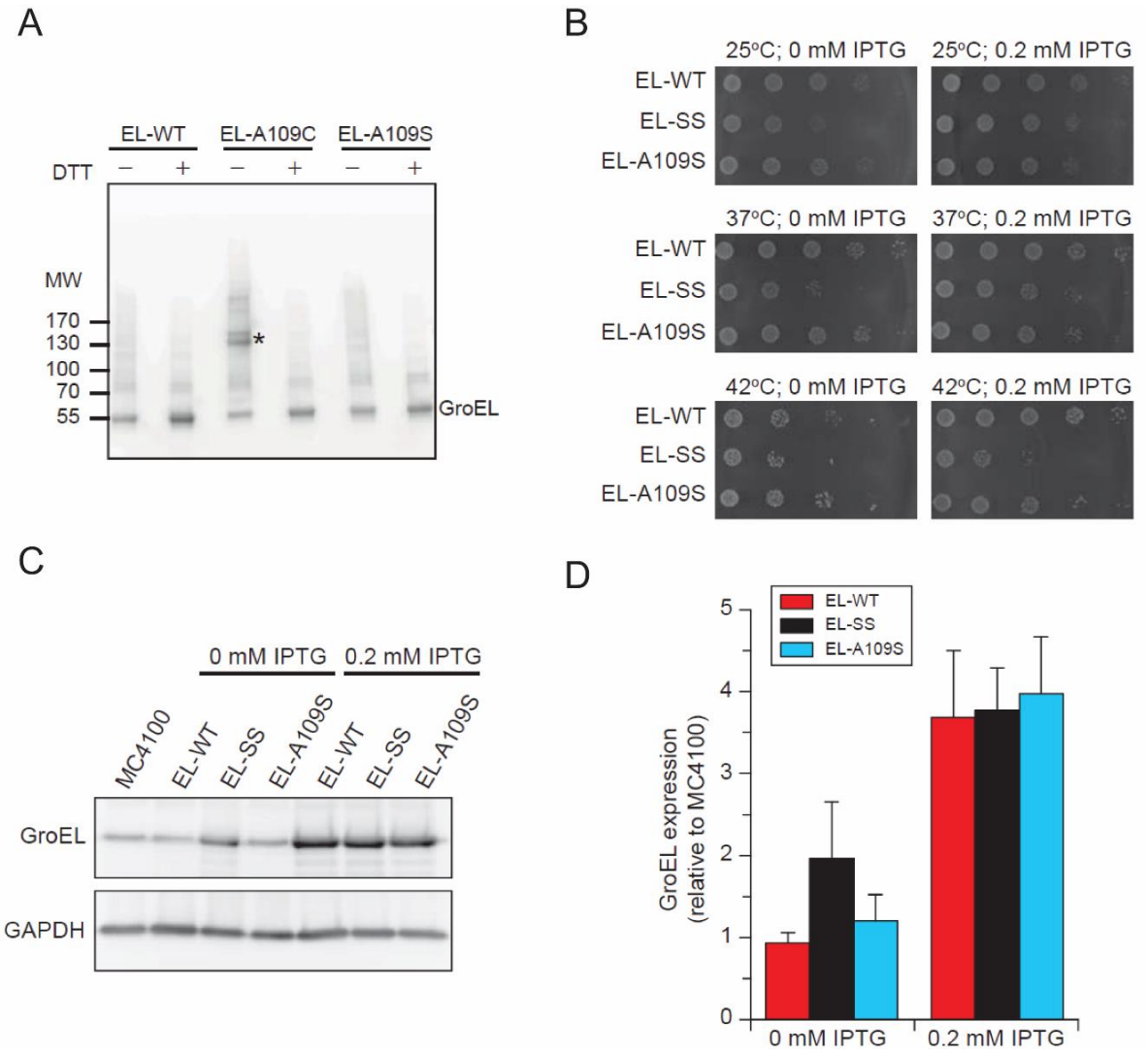

Figure 4.19 Growth phenotype of GroEL-mutant strains.

(A) Formation of disulfide bonds in EL-A109C *in vivo* as detected by thiol-trapping. EL-WT and mutant cells were grown with 0.2 mM IPTG to an OD_{600} of 0.6 at 37°C. Cells were harvested directly into ice-cold 100% (w/v) TCA and free thiols were alkylated with iodoacetamide as described (Leichert and Jakob, 2004; see STAR Methods for details). Reactions were finally dissolved in SDS buffer without or with DTT and analyzed using 4–20% SDS-PAGE (Bio-Rad) and anti-GroEL immunoblotting. Samples were not heated prior to SDS-PAGE. (B) Single-copy plasmids encoding the indicated proteins were transformed into *E. coli* MC4100 SC3 Kan^R cells in which the expression of the chromosomal groES/groEL operon was under the pBAD promoter and shut off in the absence of arabinose. Serial dilutions of cells (10^1- to 10^5-fold) were plated on LB plates in the absence or presence of IPTG for expression of the GroEL variants and GroES at 25°C, 37°C, and 42°C. (C) *In vivo* levels of GroEL variants as in (B) upon expression in the absence or presence of IPTG at 37°C. The expression of the chromosomal GroEL is shown as a control. Equivalent amounts of total cellular protein were analyzed using GroEL immunoblotting. GAPDH is shown as a loading control. (D) Quantification of GroEL in

(C). The level of endogenous GroEL in the *E. coli* MC4100 strain is set to 1. Data represent the mean ± SEM of three independent experiments.

5 Discussion

In this thesis, I have investigated the GroEL/ES reaction cycle in chaperonin-assisted protein folding. The main result of my work is that the two heptameric rings of GroEL show transient separation, resulting in ring exchange between GroEL complexes (Yan et al., 2018). Transient ring separation and exchange occurs on the time scale of the GroEL/ES ATPase cycle, suggesting that it is an integral element of the chaperonin reaction. It serves to avoid formation of symmetric GroEL:$GroES_2$ complexes and ensures the two rings function alternately, which allows for the efficient release of folded SP and rebinding of non-native SP. Ring separation is a consequence of inter-ring negative allostery of GroEL (Gruber and Horovitz, 2016; Saibil et al., 2013). Notably, this basic step of the chaperonin cycle has not been previously investigated and thus my work has revealed novel mechanistic insights regarding the chaperonin reaction.

5.1 The sequential GroEL/ES reaction cycle

A model of the GroEL/ES reaction that incorporates the findings described here is shown in Figure 5.1. SP folds inside the *cis*-ring of an asymmetric GroEL:GroES complex during the time required for the ATP hydrolysis in the *cis*-ring (steps 1 and 2). The portion of SP (red) folded per encapsulation cycle differs for specific proteins (steps 2a and 2b). While folding continues in the *cis*-ring, the *trans*-ring can accept another unfolded SP (black). Ring separation takes place after ATP hydrolysis in the *cis*-ring and is triggered upon cooperative ATP binding (but not hydrolysis) to the *trans*-ring (step 3). The rings are separated as a result of steric clashes that underlie inter-ring negative allostery, leading to the dissociation of ADP and GroES from the

former *cis*-ring (steps 3a and 3b). Folded SP is released from the cage (step 3a) while not-yet folded SP rebinds for another folding attempt (step 3b), with cellular crowding promoting rebinding to the same GroEL molecule (Elcock, 2003; Martin and Hartl, 1997). Upon ATP binding to what was previously the *trans*-ring, unfolded SP (black) is released from the apical domains into the GroEL chamber and is encapsulated by GroES (step 3c). The rings reassemble into double-ring complexes rapidly after ADP release from the former *cis*-ring (steps 4 and 5). Reassembly may occur either without (4a and 4b) or with ring exchange (5a and 5b) between GroEL complexes. SP folding again continues in the newly formed *cis*-ring with various possible ring combinations, completing the cycle.

The model proposed above suggests that single GroEL-rings, with and without bound GroES, coexist with GroEL double-rings in the chaperonin cycle. Small amounts of single-rings have actually been observed using electron microscopy (Llorca et al., 1998; Ranson et al., 2006). Regarding Hsp60, the GroEL homolog in mitochondria, single-rings are more frequently detected and are proposed to occur in equilibrium with double-rings (Levy-Rimler et al., 2001). What would be the expected portion of single-rings in a continuous chaperonin reaction? We can try to calculate this based on kinetic data. GroEL takes ~17 s to hydrolyze 14 ATP molecules in the presence of GroES and saturated SP at 25°C (Figure 4.6E) (Gupta et al., 2014). GroES takes about 0.5–1.0 s to dissociate from GroEL upon ATP binding to the *trans*-ring (Rye et al., 1999; Sharma et al., 2008). Assuming that sing-rings reassemble into double-ring complexes immediately upon GroES dissociation from the *cis*-ring (Figure 5.1, steps 3a and 3b), the single-ring population would add up to at most 10% of total GroEL. Given a total cellular concentration of GroEL complex of ~3 μM (tetradecamer) (Ellis and Hartl, 1996), the single-ring population would reach ~0.3 μM (heptamer). Depending on the diffusion coefficient of single-

ring GroEL and assuming that diffusion in the crowed cell is about 10-times slower than in aqueous solution (Theillet et al., 2014), single-rings would nevertheless encounter one another within ~20–50 milliseconds. Based on ring separation and exchange not being disturbed by biologically relevant concentrations of crowding agent (30% Ficoll 70) (Figure 4.2), ring exchange should take place with a high likelihood *in vivo*.

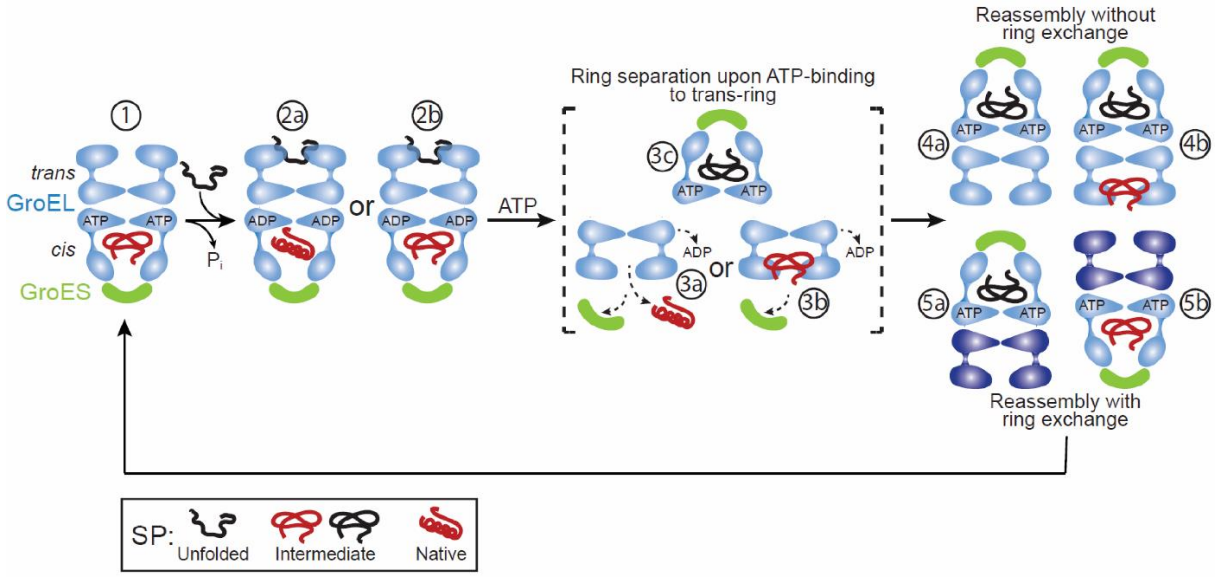

Figure 5.1 Model of the GroEL/ES Reaction Cycle.
The sequential cycle of GroEL/ES in protein folding is shown schematically. Transient ring separation is triggered upon ATP binding to the *trans*-ring of the asymmetric GroEL:7ADP:GroES complexes (step 3). Ring reassembly occurs after ADP and GroES dissociation from the former *cis*-ring, thereby avoiding inter-ring steric clashes (steps 4 and 5). Reassembly with a ring from a different GroEL complex (dark blue) permits recaptured non-native SP to be rapidly encapsulated (step 5b versus 4b).

5.2 Ring separation is a consequence of inter-ring negative allostery upon ATP binding

Allostery is a process by which biological macromolecules (mostly proteins) transmit the binding effect at one site to another, often distal, functional site. It is a

strategy to regulate protein activity and has even been referred to as the "second secret of life" (Fenton, 2008; Gruber and Horovitz, 2016; Motlagh et al., 2014). A quantitative description of allostery is fundamental for understanding most processes beyond the molecular level, e.g., cellular signaling (Freiburger et al., 2011) and diseases (Nussinov et al., 2013).

The chaperonin GroEL/ES belongs to a class of macromolecular assemblies termed "protein machines". In this nano-machine system, ordered conformational changes fueled by ATP binding and hydrolysis result in highly organized temporal and spatial functions (Yifrach and Horovitz, 2000). The ATP-induced conformational changes are reflected by ATP binding with intra-ring positive and inter-ring negative cooperativities shown by the steady-state measurements of ATPase activities at different ATP concentrations (Gruber and Horovitz, 2016; Yifrach and Horovitz, 1995). Intra-ring positive cooperativity for EL-WT was shown by the sigmoid pattern at lower ATP concentrations (Hill coefficient n = ~2.8), and inter-ring negative allostery was reflected by a small but clearly measurable decrease from the maximum ATPase rate as the ATP concentration was raised above ~20 μM (Figure 4.5A). Here, I tested the dependence of ring exchange on the conformational changes with a series of GroEL mutants displaying defects in either positive or negative allostery.

Two mutants, EL-D155A (Danziger et al., 2003) and EL-D155A/R197A (White et al., 1997), defective in positive intra-ring cooperativity but preserving negative inter-ring allostery (Cabo-Bilbao et al., 2006; Sewell et al., 2004), form MR complexes with a similar efficiency to EL-WT (Figure 4.5). In contrast, the mutant EL-E461K which abolishes the negative cooperativity between rings but maintains intra-ring positive cooperativity, fails to form MR (Figure 4.5). Therefore, negative inter-ring cooperativity is required for ring separation. Steric effects primarily form

the structural basis for negative allosteric cooperativity (Cui and Karplus, 2008). Conformational changes in the equatorial domains of the GroEL *trans*-ring upon ATP binding to the GroEL:7ADP:GroES complex are known to weaken inter-ring association (Cui and Karplus, 2008; Ranson et al., 2001), as the ATP induced conformational changes would twist the equatorial domains and thereby result in van der Waals clashes. Ring separation would also be anticipated to take place in the reaction cycle of mitochondrial Hsp60. Intriguingly, a recent crystal structure of the human Hsp60 mutant E321K, unable to cycle Hsp10 (the mitochondrial GroES homolog), displays extensive inter-ring contacts and has been suggested to capture a unique state preceding the dissociation of the double-ring complex into single rings (PDB 4PJ1) (Nisemblat et al., 2015). In this mutant complex, both rings are in the ADP and Hsp10-bound state and double the inter-ring contact surface area compared to the asymmetric GroEL:7ADP:GroES complex. In contrast, EL-E461K has a reduced inter-ring contact surface area of 1341 $Å^2$ (PDB: 2EU1) (Cabo-Bilbao et al., 2006) compared to 2588 $Å^2$ in EL-WT (PDB: 1XCK) (Bartolucci et al., 2005). Lacking strong inter-ring interactions, E461K cannot generate strong van der Waals clashes upon nucleotide binding, thus failing to trigger ring separation and exchange. Therefore, the steric clashes underlying negative inter-ring cooperativity structurally determine ring separation and exchange.

5.3 Ring separation bypasses the formation of a symmetric GroEL:GroES$_2$ complex

Despite intense research, functional coordination between the two rings is only partially understood. Two main models have been proposed: sequential versus simultaneous action of GroEL rings (Hayer-Hartl et al., 2016) (Figure 2.8). In the sequential model, the two GroEL rings function alternately due to the inter-ring

negative allostery, and the asymmetric GroEL:GroES complex is the folding-active species (Gruber and Horovitz, 2016; Hayer-Hartl et al., 1995; Saibil et al., 2013). In the simultaneous model, GroES binds simultaneously to both GroEL rings and dissociates stochastically upon ATP hydrolysis with SP catalyzing nucleotide exchange, resulting in a symmetric GroEL-$GroES_2$ complex as the major populated species (Sameshima et al., 2008; Yang et al., 2013; Ye and Lorimer, 2013).

In previous work from this laboratory, the dcFCCS method was developed to accurately measure the occurrence of different GroEL/ES complexes in solution (Haldar et al., 2015). In this assay, the formation of symmetric particles is indicated by the co-diffusion through the confocal volume of two differentially fluorescent-labeled GroES molecules bound to GroEL, resulting in a quantifiable cross-correlation signal (Figure 4.10). EL-WT formed negligible amounts of symmetric complexes both in the absence and presence of saturating non-native SP. A novel mutant, EL-SS, in which inter-ring disulfide bonds form as a result of the A109C mutation but otherwise essentially identical to EL-WT, completely loses the ability to execute ring separation and MR formation (Figure 4.7). Unexpectedly, EL-SS formed high amounts of dynamic and cycling symmetric complexes (Figure 4.10). These findings suggest that transient ring separation ensures the GroEL rings function sequentially, avoiding symmetric complexes from being populated.

To characterize the kinetics of GroEL/ES cycling, I measured the kinetics of GroES association and dissociation using stopped-flow FRET. GroES association and dissociation rates to EL-WT and EL-SS were shown to be similar (Figures 4.14 and 4.15). In addition, the crystal structure of the symmetric complex of EL-SS:$GroES_2$ with bound ADP·BeF_x (PDB: 5OPX) was highly similar to that of the symmetric complex formed by EL-WT and GroES in the presence of ADP·BeF_x (PDB: 4PKO) (Fei et al., 2014) (Figure 4.13). In summary, both rings of EL-SS are

simultaneously active in binding and unbinding GroES, as proposed for the non-sequential chaperonin model (Yang et al., 2013). Thus EL-SS will constitute an excellent tool with which to probe the function of symmetric GroEL:$GroES_2$, and may yield insights beyond those reported studies using non-cycling GroEL:$GroES_2$ complexes (Fei et al., 2014; Koike-Takeshita et al., 2008).

5.4 Function of GroEL ring separation

What are the physiological contributions of ring separation and exchange to the chaperonin reaction? My investigation of EL-SS, in which the two rings are covalently linked by disulfide bonds, indicates that transient ring separation transforms the negative allosteric coupling of the GroEL rings into a functionally productive reaction cycle. EL-SS, even though maintaining negative inter-ring allostery (Figure 4.9A), has been deprived of the coordination of wild-type GroEL, in which the *cis*-ring is folding-active while the *trans*-ring receives a new SP molecule (Figure 5.1). Instead, both rings of EL-SS cycle GroES rapidly and simultaneously, populating symmetric GroEL:$GroES_2$ complexes. As a result, ejection of folded SP from the GroEL/ES cage becomes less efficient, which heavily decreases oligomeric assembly of SP into functional complexes (Figures 4.16 and 4.17). Additionally, GroES binding to both rings simultaneously reduced the capacity to accept unfolded SP (Figure 4.16D). Ring exchange could also enhance the folding of SPs requiring multiple encapsulation rounds to reach their native state. Without ring exchange, rebound non-native SP (red) (Figure 5.1, step 3b) would have to halt in the bound state on the *trans*-ring until the *cis*-ring has hydrolyzed the bound ATP (Figure 5.1, step 4b). In contrast, exchange with an open ring would permit the rebound SP to be encapsulated and folded without any delay (Figure 5.1, step 5b). Importantly, the capacity of EL-SS to mediate protein folding *in vivo* is

also substantially reduced and becomes limiting for growth at GroEL levels similar to those in WT cells (Figure 4.19). Overexpression of EL-SS can compensate for the loss of the WT protein, but not under stress conditions at 42°C when the demand for chaperonin function is strongly increased. This phenotype of the EL-SS mutant is consistent with ring separation being required to support the sequential GroEL/ES cycle, allowing for efficient SP flux through the chaperonin system *in vivo*.

The reaction cycle of EL-SS/GroES largely resembles the non-sequential (symmetric) cycle which was recently suggested as the general behavior of chaperonin in the presence of SP (Figure 2.8B) (Yang et al., 2013). However, I could not detect significant amounts of symmetric GroEL:$GroES_2$ complexes for EL-WT in the absence or presence of SP (this study and Haldar et al., 2015). The finding that EL-SS cannot functionally replace EL-WT for *E. coli* growth suggests that the sequential cycle prevails *in vivo*.

6 References

Akerfelt, M., Morimoto, R.I., and Sistonen, L. (2010). Heat shock factors: integrators of cell stress, development and lifespan. Nat Rev Mol Cell Biol *11*, 545-555.

Ali, M.M., Roe, S.M., Vaughan, C.K., Meyer, P., Panaretou, B., Piper, P.W., Prodromou, C., and Pearl, L.H. (2006). Crystal structure of an Hsp90-nucleotide-p23/Sba1 closed chaperone complex. Nature *440*, 1013-1017.

Anfinsen, C.B. (1973). Principles that govern the folding of protein chains. Science *181*, 223-230.

Anfinsen, C.B., Harrington, W.F., Hvidt, A., Linderstrom-Lang, K., Ottesen, M., and Schellman, J. (1955). Studies on the structural basis of ribonuclease activity. Biochim Biophys Acta *17*, 141-142.

Apetri, A.C., and Horwich, A.L. (2008). Chaperonin chamber accelerates protein folding through passive action of preventing aggregation. Proc Natl Acad Sci U S A *105*, 17351-17355.

Balchin, D., Hayer-Hartl, M., and Hartl, F.U. (2016). *In vivo* aspects of protein folding and quality control. Science *353*, aac4354.

Bartolucci, C., Lamba, D., Grazulis, S., Manakova, E., and Heumann, H. (2005). Crystal structure of wild-type chaperonin GroEL. J Mol Biol *354*, 940-951.

Baumketner, A., Jewett, A., and Shea, J.E. (2003). Effects of confinement in chaperonin assisted protein folding: rate enhancement by decreasing the roughness of the folding energy landscape. J Mol Biol *332*, 701-713.

Bowler, M.W., Nurizzo, D., Barrett, R., Beteva, A., Bodin, M., Caserotto, H., Delageniere, S., Dobias, F., Flot, D., Giraud, T., *et al.* (2015). MASSIF-1: a beamline dedicated to the fully automatic characterization and data collection from crystals of biological macromolecules. J Synchrotron Radiat *22*, 1540-1547.

Braig, K., Otwinowski, Z., Hegde, R., Boisvert, D.C., Joachimiak, A., Horwich, A.L., and Sigler, P.B. (1994). The crystal structure of the bacterial chaperonin GroEL at 2.8 A. Nature *371*, 578-586.

Brinker, A., Pfeifer, G., Kerner, M.J., Naylor, D.J., Hartl, F.U., and Hayer-Hartl, M. (2001). Dual function of protein confinement in chaperonin-assisted protein folding. Cell *107*, 223-233.

Bukau, B., Deuerling, E., Pfund, C., and Craig, E.A. (2000). Getting newly synthesized proteins into shape. Cell *101*, 119-122.

Burston, S.G., Weissman, J.S., Farr, G.W., Fenton, W.A., and Horwich, A.L. (1996). Release of both native and non-native proteins from a cis-only GroEL ternary complex. Nature *383*, 96-99.

Cabo-Bilbao, A., Spinelli, S., Sot, B., Agirre, J., Mechaly, A.E., Muga, A., and Guerin, D.M. (2006). Crystal structure of the temperature-sensitive and allosteric-defective chaperonin GroELE461K. J Struct Biol *155*, 482-492.

Calloni, G., Chen, T., Schermann, S.M., Chang, H.C., Genevaux, P., Agostini, F., Tartaglia, G.G., Hayer-Hartl, M., and Hartl, F.U. (2012). DnaK functions as a central hub in the *E. coli* chaperone network. Cell Rep *1*, 251-264.

Chakraborty, K., Chatila, M., Sinha, J., Shi, Q., Poschner, B.C., Sikor, M., Jiang, G., Lamb, D.C., Hartl, F.U., and Hayer-Hartl, M. (2010). Chaperonin-catalyzed rescue of kinetically trapped states in protein folding. Cell *142*, 112-122.

Chaudhry, C., Farr, G.W., Todd, M.J., Rye, H.S., Brunger, A.T., Adams, P.D., Horwich, A.L., and Sigler, P.B. (2003). Role of the gamma-phosphate of ATP in triggering protein folding by GroEL-GroES: function, structure and energetics. EMBO J *22*, 4877-4887.

Chaudhuri, T.K., Farr, G.W., Fenton, W.A., Rospert, S., and Horwich, A.L. (2001). GroEL/GroES-mediated folding of a protein too large to be encapsulated. Cell *107*, 235-246.

Chaudhuri, T.K., Verma, V.K., and Maheshwari, A. (2009). GroEL assisted folding of large polypeptide substrates in *Escherichia coli*: Present scenario and assignments for the future. Prog Biophys Mol Biol *99*, 42-50.

Chen, V.B., Arendall, W.B., 3rd, Headd, J.J., Keedy, D.A., Immormino, R.M., Kapral, G.J., Murray, L.W., Richardson, J.S., and Richardson, D.C. (2010).

MolProbity: all-atom structure validation for macromolecular crystallography. Acta Crystallogr D Biol Crystallogr *66*, 12-21.

Cheng, M.Y., Hartl, F.U., Martin, J., Pollock, R.A., Kalousek, F., Neupert, W., Hallberg, E.M., Hallberg, R.L., and Horwich, A.L. (1989). Mitochondrial heat-shock protein hsp60 is essential for assembly of proteins imported into yeast mitochondria. Nature *337*, 620-625.

Clare, D.K., Vasishtan, D., Stagg, S., Quispe, J., Farr, G.W., Topf, M., Horwich, A.L., and Saibil, H.R. (2012). ATP-triggered conformational changes delineate substrate-binding and -folding mechanics of the GroEL chaperonin. Cell *149*, 113-123.

Corsepius, N.C., and Lorimer, G.H. (2013). Measuring how much work the chaperone GroEL can do. Proc Natl Acad Sci U S A *110*, E2451-2459.

Cui, Q., and Karplus, M. (2008). Allostery and cooperativity revisited. Protein Sci *17*, 1295-1307.

Danziger, O., Rivenzon-Segal, D., Wolf, S.G., and Horovitz, A. (2003). Conversion of the allosteric transition of GroEL from concerted to sequential by the single mutation Asp-155 -> Ala. Proc Natl Acad Sci U S A *100*, 13797-13802.

del Alamo, M., Hogan, D.J., Pechmann, S., Albanese, V., Brown, P.O., and Frydman, J. (2011). Defining the specificity of cotranslationally acting chaperones by systematic analysis of mRNAs associated with ribosome-nascent chain complexes. PLoS Biol *9*, e1001100.

Ditzel, L., Lowe, J., Stock, D., Stetter, K.O., Huber, H., Huber, R., and Steinbacher, S. (1998). Crystal structure of the thermosome, the archaeal chaperonin and homolog of CCT. Cell *93*, 125-138.

Dobson, C.M., Andrej Šali, and Karplus, M. (1998). Protein Folding: A Perspective from Theory and Experiment. Angew Chem Int Ed *37*, 868-893.

Elcock, A.H. (2003). Atomic-level observation of macromolecular crowding effects: escape of a protein from the GroEL cage. Proc Natl Acad Sci U S A *100*, 2340-2344.

Ellis, R.J. (2001). Macromolecular crowding: an important but neglected aspect of the intracellular environment. Curr Opin Struct Biol *11*, 114-119.

Ellis, R.J., and Hartl, F.U. (1996). Protein folding in the cell: competing models of chaperonin function. FASEB J *10*, 20-26.

Ellis, R.J., and Minton, A.P. (2006). Protein aggregation in crowded environments. Biol Chem *387*, 485-497.

Emsley, P., and Cowtan, K. (2004). Coot: model-building tools for molecular graphics. Acta Crystallogr D Biol Crystallogr *60*, 2126-2132.

England, J.L., Lucent, D., and Pande, V.S. (2008). A role for confined water in chaperonin function. J Am Chem Soc *130*, 11838-11839.

Ewalt, K.L., Hendrick, J.P., Houry, W.A., and Hartl, F.U. (1997). *In vivo* observation of polypeptide flux through the bacterial chaperonin system. Cell *90*, 491-500.

Fayet, O., Ziegelhoffer, T., and Georgopoulos, C. (1989). The groES and groEL heat shock gene products of *Escherichia coli* are essential for bacterial growth at all temperatures. J Bacteriol *171*, 1379-1385.

Fei, X., Yang, D., LaRonde-LeBlanc, N., and Lorimer, G.H. (2013). Crystal structure of a GroEL-ADP complex in the relaxed allosteric state at 2.7 A resolution. Proc Natl Acad Sci U S A *110*, E2958-2966.

Fei, X., Ye, X., LaRonde, N.A., and Lorimer, G.H. (2014). Formation and structures of GroEL:GroES2 chaperonin footballs, the protein-folding functional form. Proc Natl Acad Sci U S A *111*, 12775-12780.

Fenton, A.W. (2008). Allostery: an illustrated definition for the 'second secret of life'. Trends Biochem Sci *33*, 420-425.

Fenton, W.A., Kashi, Y., Furtak, K., and Horwich, A.L. (1994). Residues in chaperonin GroEL required for polypeptide binding and release. Nature *371*, 614-619.

Figueiredo, L., Klunker, D., Ang, D., Naylor, D.J., Kerner, M.J., Georgopoulos, C., Hartl, F.U., and Hayer-Hartl, M. (2004). Functional characterization of an archaeal GroEL/GroES chaperonin system: significance of substrate encapsulation. J Biol Chem *279*, 1090-1099.

Freiburger, L.A., Baettig, O.M., Sprules, T., Berghuis, A.M., Auclair, K., and Mittermaier, A.K. (2011). Competing allosteric mechanisms modulate substrate binding in a dimeric enzyme. Nat Struct Mol Biol *18*, 288-294.

Fridmann, Y., Ulitzur, S., and Horovitz, A. (2000). *In vivo* and *in vitro* function of GroEL mutants with impaired allosteric properties. J Biol Chem *275*, 37951-37956.

Fujiwara, K., Ishihama, Y., Nakahigashi, K., Soga, T., and Taguchi, H. (2010). A systematic survey of *in vivo* obligate chaperonin-dependent substrates. EMBO J *29*, 1552-1564.

Gamerdinger, M., Hanebuth, M.A., Frickey, T., and Deuerling, E. (2015). The principle of antagonism ensures protein targeting specificity at the endoplasmic reticulum. Science *348*, 201-207.

Genevaux, P., Keppel, F., Schwager, F., Langendijk-Genevaux, P.S., Hartl, F.U., and Georgopoulos, C. (2004). *In vivo* analysis of the overlapping functions of DnaK and trigger factor. EMBO Rep *5*, 195-200.

Georgescauld, F., Popova, K., Gupta, A.J., Bracher, A., Engen, J.R., Hayer-Hartl, M., and Hartl, F.U. (2014). GroEL/ES chaperonin modulates the mechanism and accelerates the rate of TIM-barrel domain folding. Cell *157*, 922-934.

Georgopoulos, C. (2006). Toothpicks, serendipity and the emergence of the *Escherichia coli* DnaK (Hsp70) and GroEL (Hsp60) chaperone machines. Genetics *174*, 1699-1707.

Gloge, F., Becker, A.H., Kramer, G., and Bukau, B. (2014). Co-translational mechanisms of protein maturation. Curr Opin Struct Biol *24*, 24-33.

Goldberg, M.E. (1985). The second translation of the genetic message: protein folding and assembly. Trends Biochem Sci *10*, 388-391.

Goloubinoff, P., Gatenby, A.A., and Lorimer, G.H. (1989). GroE heat-shock proteins promote assembly of foreign prokaryotic ribulose bisphosphate carboxylase oligomers in *Escherichia coli*. Nature *337*, 44-47.

Gruber, R., and Horovitz, A. (2016). Allosteric Mechanisms in Chaperonin Machines. Chem Rev *116*, 6588-6606.

Gupta, A.J., Haldar, S., Milicic, G., Hartl, F.U., and Hayer-Hartl, M. (2014). Active cage mechanism of chaperonin-assisted protein folding demonstrated at single-molecule level. J Mol Biol *426*, 2739-2754.

Haldar, S., Gupta, A.J., Yan, X., Milicic, G., Hartl, F.U., and Hayer-Hartl, M. (2015). Chaperonin-Assisted Protein Folding: Relative Population of Asymmetric and Symmetric GroEL:GroES Complexes. J Mol Biol *427*, 2244-2255.

Hartl, F.U. (1996). Molecular chaperones in cellular protein folding. Nature *381*, 571-579.

Hartl, F.U., Bracher, A., and Hayer-Hartl, M. (2011). Molecular chaperones in protein folding and proteostasis. Nature *475*, 324-332.

Hartl, F.U., and Hayer-Hartl, M. (2002). Molecular chaperones in the cytosol: from nascent chain to folded protein. Science *295*, 1852-1858.

Hayer-Hartl, M. (2000). Assay of malate dehydrogenase. A substrate for the *E. coli* chaperonins GroEL and GroES. Methods Mol Biol *140*, 127-132.

Hayer-Hartl, M., Bracher, A., and Hartl, F.U. (2016). The GroEL-GroES Chaperonin Machine: A Nano-Cage for Protein Folding. Trends Biochem Sci *41*, 62-76.

Hayer-Hartl, M.K., Martin, J., and Hartl, F.U. (1995). Asymmetrical interaction of GroEL and GroES in the ATPase cycle of assisted protein folding. Science *269*, 836-841.

Hayer-Hartl, M.K., Weber, F., and Hartl, F.U. (1996). Mechanism of chaperonin action: GroES binding and release can drive GroEL-mediated protein folding in the absence of ATP hydrolysis. EMBO J *15*, 6111-6121.

Hessling, M., Richter, K., and Buchner, J. (2009). Dissection of the ATP-induced conformational cycle of the molecular chaperone Hsp90. Nat Struct Mol Biol *16*, 287-293.

Hoffmann, A., Bukau, B., and Kramer, G. (2010). Structure and function of the molecular chaperone Trigger Factor. Biochim Biophys Acta *1803*, 650-661.

Horovitz, A., and Willison, K.R. (2005). Allosteric regulation of chaperonins. Curr Opin Struct Biol *15*, 646-651.

Horwich, A.L., Apetri, A.C., and Fenton, W.A. (2009). The GroEL/GroES cis cavity as a passive anti-aggregation device. FEBS Lett *583*, 2654-2662.

Horwich, A.L., Fenton, W.A., Chapman, E., and Farr, G.W. (2007). Two families of chaperonin: physiology and mechanism. Annu Rev Cell Dev Biol *23*, 115-145.

Ishii, N., Taguchi, H., Sasabe, H., and Yoshida, M. (1995). Equatorial split of holo-chaperonin from Thermus thermophilus by ATP and K^+. FEBS Lett *362*, 121-125.

Jewett, A.I., Baumketner, A., and Shea, J.E. (2004). Accelerated folding in the weak hydrophobic environment of a chaperonin cavity: creation of an alternate fast folding pathway. Proc Natl Acad Sci U S A *101*, 13192-13197.

Jewett, A.I., and Shea, J.E. (2010). Reconciling theories of chaperonin accelerated folding with experimental evidence. Cell Mol Life Sci *67*, 255-276.

Kaiser, C.M., Chang, H.C., Agashe, V.R., Lakshmipathy, S.K., Etchells, S.A., Hayer-Hartl, M., Hartl, F.U., and Barral, J.M. (2006). Real-time observation of trigger factor function on translating ribosomes. Nature *444*, 455-460.

Karagoz, G.E., and Rudiger, S.G. (2015). Hsp90 interaction with clients. Trends Biochem Sci *40*, 117-125.

Kerner, M.J., Naylor, D.J., Ishihama, Y., Maier, T., Chang, H.C., Stines, A.P., Georgopoulos, C., Frishman, D., Hayer-Hartl, M., Mann, M., *et al.* (2005). Proteome-wide analysis of chaperonin-dependent protein folding in *Escherichia coli*. Cell *122*, 209-220.

Kim, Y.E., Hipp, M.S., Bracher, A., Hayer-Hartl, M., and Hartl, F.U. (2013). Molecular chaperone functions in protein folding and proteostasis. Annu Rev Biochem *82*, 323-355.

Kinoshita, M. (2006). Roles of entropic excluded-volume effects in colloidal and biological systems: Analyses using the three-dimensional integral equation theory. Chem Eng Sci *61*, 2150-2160.

Koike-Takeshita, A., Arakawa, T., Taguchi, H., and Shimamura, T. (2014). Crystal structure of a symmetric football-shaped GroEL:$GroES_2$-ATP_{14} complex determined at 3.8A reveals rearrangement between two GroEL rings. J Mol Biol *426*, 3634-3641.

Koike-Takeshita, A., Yoshida, M., and Taguchi, H. (2008). Revisiting the GroEL-GroES reaction cycle via the symmetric intermediate implied by novel aspects of the GroEL(D398A) mutant. J Biol Chem *283*, 23774-23781.

Koplin, A., Preissler, S., Ilina, Y., Koch, M., Scior, A., Erhardt, M., and Deuerling, E. (2010). A dual function for chaperones SSB-RAC and the NAC nascent polypeptide-associated complex on ribosomes. J Cell Biol *189*, 57-68.

Labbadia, J., and Morimoto, R.I. (2015). The biology of proteostasis in aging and disease. Annu Rev Biochem *84*, 435-464.

Landry, S.J., Zeilstra-Ryalls, J., Fayet, O., Georgopoulos, C., and Gierasch, L.M. (1993). Characterization of a functionally important mobile domain of GroES. Nature *364*, 255-258.

Leichert, L.I., and Jakob, U. (2004). Protein thiol modifications visualized *in vivo*. PLOS Biol *2*, e333.

Leitner, A., Joachimiak, L.A., Bracher, A., Monkemeyer, L., Walzthoeni, T., Chen, B., Pechmann, S., Holmes, S., Cong, Y., Ma, B., *et al.* (2012). The molecular architecture of the eukaryotic chaperonin TRiC/CCT. Structure *20*, 814-825.

Levinthal, C. (1968). Are there pathways for protein folding? J Chim Phys Physico-Chimie Biol *65*, 44–45.

Levy-Rimler, G., Bell, R.E., Ben-Tal, N., and Azem, A. (2002). Type I chaperonins: not all are created equal. FEBS Lett *529*, 1-5.

Levy-Rimler, G., Viitanen, P., Weiss, C., Sharkia, R., Greenberg, A., Niv, A., Lustig, A., Delarea, Y., and Azem, A. (2001). The effect of nucleotides and mitochondrial chaperonin 10 on the structure and chaperone activity of mitochondrial chaperonin 60. Eur J Biochem *268*, 3465-3472.

Li, J., Soroka, J., and Buchner, J. (2012). The Hsp90 chaperone machinery: conformational dynamics and regulation by co-chaperones. Biochim Biophys Acta *1823*, 624-635.

Lin, M.M., and Zewail, A.H. (2012). Hydrophobic forces and the length limit of foldable protein domains. Proc Natl Acad Sci U S A *109*, 9851-9856.

Lin, Z., Madan, D., and Rye, H.S. (2008). GroEL stimulates protein folding through forced unfolding. Nat Struct Mol Biol *15*, 303-311.

Lindquist, S. (2009). Protein folding sculpting evolutionary change. Cold Spring Harb Symp Quant Biol *74*, 103-108.

Llorca, O., Galan, A., Carrascosa, J.L., Muga, A., and Valpuesta, J.M. (1998). GroEL under heat-shock. Switching from a folding to a storing function. J Biol Chem *273*, 32587-32594.

Lucent, D., Vishal, V., and Pande, V.S. (2007). Protein folding under confinement: a role for solvent. Proc Natl Acad Sci U S A *104*, 10430-10434.

Martin, J., and Hartl, F.U. (1997). The effect of macromolecular crowding on chaperonin-mediated protein folding. Proc Natl Acad Sci U S A *94*, 1107-1112.

Martin, J., Langer, T., Boteva, R., Schramel, A., Horwich, A.L., and Hartl, F.U. (1991). Chaperonin-mediated protein folding at the surface of groEL through a 'molten globule'-like intermediate. Nature *352*, 36-42.

Mayer, M.P. (2010). Gymnastics of molecular chaperones. Mol Cell *39*, 321-331.

Mayer, M.P. (2013). Hsp70 chaperone dynamics and molecular mechanism. Trends Biochem Sci *38*, 507-514.

Mayhew, M., da Silva, A.C., Martin, J., Erdjument-Bromage, H., Tempst, P., and Hartl, F.U. (1996). Protein folding in the central cavity of the GroEL-GroES chaperonin complex. Nature *379*, 420-426.

Molugu, S.K., Hildenbrand, Z.L., Morgan, D.G., Sherman, M.B., He, L., Georgopoulos, C., Sernova, N.V., Kurochkina, L.P., Mesyanzhinov, V.V., Miroshnikov, K.A., *et al.* (2016). Ring Separation Highlights the Protein-Folding Mechanism Used by the Phage EL-Encoded Chaperonin. Structure *24*, 537-546.

Motlagh, H.N., Wrabl, J.O., Li, J., and Hilser, V.J. (2014). The ensemble nature of allostery. Nature *508*, 331-339.

Motojima, F., and Yoshida, M. (2010). Polypeptide in the chaperonin cage partly protrudes out and then folds inside or escapes outside. EMBO J *29*, 4008-4019.

Muller, B.K., Zaychikov, E., Brauchle, C., and Lamb, D.C. (2005). Pulsed interleaved excitation. Biophys J *89*, 3508-3522.

Murshudov, G.N., Skubak, P., Lebedev, A.A., Pannu, N.S., Steiner, R.A., Nicholls, R.A., Winn, M.D., Long, F., and Vagin, A.A. (2011). REFMAC5 for the refinement of macromolecular crystal structures. Acta Crystallogr D Biol Crystallogr *67*, 355-367.

Nelson, D.L., and Cox, M.M. (2005). Principles of Biochemistry. *4th edition*.

Nisemblat, S., Yaniv, O., Parnas, A., Frolow, F., and Azem, A. (2015). Crystal structure of the human mitochondrial chaperonin symmetrical football complex. Proc Natl Acad Sci U S A *112*, 6044-6049.

Nussinov, R., Tsai, C.J., and Ma, B. (2013). The underappreciated role of allostery in the cellular network. Annu Rev Biophys *42*, 169-189.

Ostermann, J., Horwich, A.L., Neupert, W., and Hartl, F.U. (1989). Protein folding in mitochondria requires complex formation with hsp60 and ATP hydrolysis. Nature *341*, 125-130.

Poso, D., Clarke, A.R., and Burston, S.G. (2004). A kinetic analysis of the nucleotide-induced allosteric transitions in a single-ring mutant of GroEL. J Mol Biol *338*, 969-977.

Powers, E.T., Morimoto, R.I., Dillin, A., Kelly, J.W., and Balch, W.E. (2009). Biological and chemical approaches to diseases of proteostasis deficiency. Annu Rev Biochem *78*, 959-991.

Preissler, S., and Deuerling, E. (2012). Ribosome-associated chaperones as key players in proteostasis. Trends Biochem Sci *37*, 274-283.

Radaev, S., and Sun, D.P. (2002). Crystallization of protein-protein complexes. J Appl Cryst *35*, 674-676.

Ranson, N.A., Clare, D.K., Farr, G.W., Houldershaw, D., Horwich, A.L., and Saibil, H.R. (2006). Allosteric signaling of ATP hydrolysis in GroEL-GroES complexes. Nat Struct Mol Biol *13*, 147-152.

Ranson, N.A., Dunster, N.J., Burston, S.G., and Clarke, A.R. (1995). Chaperonins can catalyse the reversal of early aggregation steps when a protein misfolds. J Mol Biol *250*, 581-586.

Ranson, N.A., Farr, G.W., Roseman, A.M., Gowen, B., Fenton, W.A., Horwich, A.L., and Saibil, H.R. (2001). ATP-bound states of GroEL captured by cryo-electron microscopy. Cell *107*, 869-879.

Retzlaff, M., Hagn, F., Mitschke, L., Hessling, M., Gugel, F., Kessler, H., Richter, K., and Buchner, J. (2010). Asymmetric activation of the hsp90 dimer by its cochaperone aha1. Mol Cell *37*, 344-354.

Rohl, A., Rohrberg, J., and Buchner, J. (2013). The chaperone Hsp90: changing partners for demanding clients. Trends Biochem Sci *38*, 253-262.

Rutherford, S.L., and Lindquist, S. (1998). Hsp90 as a capacitor for morphological evolution. Nature *396*, 336-342.

Rye, H.S., Burston, S.G., Fenton, W.A., Beechem, J.M., Xu, Z., Sigler, P.B., and Horwich, A.L. (1997). Distinct actions of cis and trans ATP within the double ring of the chaperonin GroEL. Nature *388*, 792-798.

Rye, H.S., Roseman, A.M., Chen, S., Furtak, K., Fenton, W.A., Saibil, H.R., and Horwich, A.L. (1999). GroEL-GroES cycling: ATP and nonnative polypeptide direct alternation of folding-active rings. Cell *97*, 325-338.

Saibil, H.R., Fenton, W.A., Clare, D.K., and Horwich, A.L. (2013). Structure and allostery of the chaperonin GroEL. J Mol Biol *425*, 1476-1487.

Sameshima, T., Ueno, T., Iizuka, R., Ishii, N., Terada, N., Okabe, K., and Funatsu, T. (2008). Football- and bullet-shaped GroEL-GroES complexes coexist during the reaction cycle. J Biol Chem *283*, 23765-23773.

Scheufler, C., Brinker, A., Bourenkov, G., Pegoraro, S., Moroder, L., Bartunik, H., Hartl, F.U., and Moarefi, I. (2000). Structure of TPR domain-peptide complexes: critical elements in the assembly of the Hsp70-Hsp90 multichaperone machine. Cell *101*, 199-210.

Schmidt, M., Rutkat, K., Rachel, R., Pfeifer, G., Jaenicke, R., Viitanen, P., Lorimer, G., and Buchner, J. (1994). Symmetric complexes of GroE chaperonins as part of the functional cycle. Science *265*, 656-659.

Schultz, C.P. (2000). Illuminating folding intermediates. Nat Struct Biol *7*, 7-10.

Sewell, B.T., Best, R.B., Chen, S., Roseman, A.M., Farr, G.W., Horwich, A.L., and Saibil, H.R. (2004). A mutant chaperonin with rearranged inter-ring electrostatic contacts and temperature-sensitive dissociation. Nat Struct Mol Biol *11*, 1128-1133.

Sharma, S., Chakraborty, K., Muller, B.K., Astola, N., Tang, Y.C., Lamb, D.C., Hayer-Hartl, M., and Hartl, F.U. (2008). Monitoring protein conformation along the pathway of chaperonin-assisted folding. Cell *133*, 142-153.

Shiseki, K., Murai, N., Motojima, F., Hisabori, T., Yoshida, M., and Taguchi, H. (2001). Synchronized domain-opening motion of GroEL is essential for communication between the two rings. J Biol Chem *276*, 11335-11338.

Sot, B., Galan, A., Valpuesta, J.M., Bertrand, S., and Muga, A. (2002). Salt bridges at the inter-ring interface regulate the thermostat of GroEL. J Biol Chem *277*, 34024-34029.

Taguchi, H., Amada, K., Murai, N., Yamakoshi, M., and Yoshida, M. (1997). ATP, K+-dependent heptamer exchange reaction produces hybrids between GroEL and chaperonin from Thermus thermophilus. J Biol Chem *272*, 18155-18160.

Taipale, M., Jarosz, D.F., and Lindquist, S. (2010). HSP90 at the hub of protein homeostasis: emerging mechanistic insights. Nat Rev Mol Cell Biol *11*, 515-528.

Taipale, M., Krykbaeva, I., Koeva, M., Kayatekin, C., Westover, K.D., Karras, G.I., and Lindquist, S. (2012). Quantitative analysis of HSP90-client interactions reveals principles of substrate recognition. Cell *150*, 987-1001.

Tang, Y.C., Chang, H.C., Chakraborty, K., Hartl, F.U., and Hayer-Hartl, M. (2008). Essential role of the chaperonin folding compartment *in vivo*. EMBO J *27*, 1458-1468.

Tang, Y.C., Chang, H.C., Roeben, A., Wischnewski, D., Wischnewski, N., Kerner, M.J., Hartl, F.U., and Hayer-Hartl, M. (2006). Structural features of the GroEL-GroES nano-cage required for rapid folding of encapsulated protein. Cell *125*, 903-914.

Teufel, D.P., Johnson, C.M., Lum, J.K., and Neuweiler, H. (2011). Backbone-driven collapse in unfolded protein chains. J Mol Biol *409*, 250-262.

Theillet, F.X., Binolfi, A., Frembgen-Kesner, T., Hingorani, K., Sarkar, M., Kyne, C., Li, C., Crowley, P.B., Gierasch, L., Pielak, G.J., *et al.* (2014). Physicochemical properties of cells and their effects on intrinsically disordered proteins (IDPs). Chem Rev *114*, 6661-6714.

Thirumalai, D., and Lorimer, G.H. (2001). Chaperonin-mediated protein folding. Annu Rev Biophys Biomol Struct *30*, 245-269.

Tissieres, A., Mitchell, H.K., and Tracy, U.M. (1974). Protein synthesis in salivary glands of Drosophila melanogaster: relation to chromosome puffs. J Mol Biol *84*, 389-398.

Todd, M.J., Lorimer, G., and Thirumalai, D. (1996). Chaperonin-facilitated protein folding: optimization of rate and yield by an iterative annealing mechanism. Proc Natl Acad Sci U S A *93*, 4030–4035.

Todd, M.J., Walke, S., Lorimer, G., Truscott, K., and Scopes, R.K. (1995). The single-ring Thermoanaerobacter brockii chaperonin 60 (Tbr-EL7) dimerizes to Tbr-EL14.Tbr-ES7 under protein folding conditions. Biochemistry *34*, 14932-14941.

Tokuriki, N., and Tawfik, D.S. (2009). Chaperonin overexpression promotes genetic variation and enzyme evolution. Nature *459*, 668-673.

Tyagi, N.K., Fenton, W.A., Deniz, A.A., and Horwich, A.L. (2011). Double mutant MBP refolds at same rate in free solution as inside the GroEL/GroES chaperonin chamber when aggregation in free solution is prevented. FEBS Lett *585*, 1969-1972.

Vabulas, R.M., and Hartl, F.U. (2005). Protein synthesis upon acute nutrient restriction relies on proteasome function. Science *310*, 1960-1963.

Vagin, A.A., and Isupov, M.N. (2001). Spherically averaged phased translation function and its application to the search for molecules and fragments in electron-density maps. Acta Crystallogr D Biol Crystallogr *57*, 1451-1456.

van den Berg, B., Ellis, R.J., and Dobson, C.M. (1999). Effects of macromolecular crowding on protein folding and aggregation. EMBO J *18*, 6927-6933.

Verba, K.A., Wang, R.Y., Arakawa, A., Liu, Y., Shirouzu, M., Yokoyama, S., and Agard, D.A. (2016). Atomic structure of Hsp90-Cdc37-Cdk4 reveals that Hsp90 traps and stabilizes an unfolded kinase. Science *352*, 1542-1547.

Viitanen, P.V., Lorimer, G.H., Seetharam, R., Gupta, R.S., Oppenheim, J., Thomas, J.O., and Cowan, N.J. (1992). Mammalian mitochondrial chaperonin 60 functions as a single toroidal ring. J Biol Chem *267*, 695-698.

Walter, P., and Ron, D. (2011). The unfolded protein response: from stress pathway to homeostatic regulation. Science *334*, 1081-1086.

Wandinger, S.K., Richter, K., and Buchner, J. (2008). The Hsp90 chaperone machinery. J Biol Chem *283*, 18473-18477.

Weaver, J., Jiang, M., Roth, A., Puchalla, J., Zhang, J., and Rye, H.S. (2017). GroEL actively stimulates folding of the endogenous substrate protein PepQ. Nat Commun *8*, 15934.

Weaver, J., and Rye, H.S. (2014). The C-terminal tails of the bacterial chaperonin GroEL stimulate protein folding by directly altering the conformation of a substrate protein. J Biol Chem *289*, 23219-23232.

Weber, F., and Hayer-Hartl, M. (2000). Refolding of bovine mitochondrial rhodanese by chaperonins GroEL and GroES. Methods Mol Biol *140*, 117-126.

Weissman, J.S., Kashi, Y., Fenton, W.A., and Horwich, A.L. (1994). GroEL-mediated protein folding proceeds by multiple rounds of binding and release of nonnative forms. Cell *78*, 693-702.

White, H.E., Chen, S., Roseman, A.M., Yifrach, O., Horovitz, A., and Saibil, H.R. (1997). Structural basis of allosteric changes in the GroEL mutant Arg197-->Ala. Nat Struct Biol *4*, 690-694.

Willmund, F., del Alamo, M., Pechmann, S., Chen, T., Albanese, V., Dammer, E.B., Peng, J., and Frydman, J. (2013). The cotranslational function of ribosome-associated Hsp70 in eukaryotic protein homeostasis. Cell *152*, 196-209.

Woerner, A.C., Frottin, F., Hornburg, D., Feng, L.R., Meissner, F., Patra, M., Tatzelt, J., Mann, M., Winklhofer, K.F., Hartl, F.U., *et al.* (2016). Cytoplasmic protein aggregates interfere with nucleocytoplasmic transport of protein and RNA. Science *351*, 173-176.

Xu, Z., Horwich, A.L., and Sigler, P.B. (1997). The crystal structure of the asymmetric GroEL-GroES-$(ADP)_7$ chaperonin complex. Nature *388*, 741-750.

Yan X., Shi Q., Bracher A., Miličić G., Singh A.K., Hartl F.U., Hayer-Hartl M. (2018). GroEL ring separation and exchange in the chaperonin reaction. Cell *172*, 605-617.

Yang, D., Ye, X., and Lorimer, G.H. (2013). Symmetric GroEL:GroES2 complexes are the protein-folding functional form of the chaperonin nanomachine. Proc Natl Acad Sci U S A *110*, E4298-4305.

Ybarra, J., and Horowitz, P.M. (1995). Inactive GroEL monomers can be isolated and reassembled to functional tetradecamers that contain few bound peptides. J Biol Chem *270*, 22962-22967.

Ye, X., and Lorimer, G.H. (2013). Substrate protein switches GroE chaperonins from asymmetric to symmetric cycling by catalyzing nucleotide exchange. Proc Natl Acad Sci U S A *110*, E4289-4297.

Yifrach, O., and Horovitz, A. (1995). Nested cooperativity in the ATPase activity of the oligomeric chaperonin GroEL. Biochemistry *34*, 5303-5308.

Yifrach, O., and Horovitz, A. (2000). Coupling between protein folding and allostery in the GroE chaperonin system. Proc Natl Acad Sci U S A *97*, 1521-1524.

Young, J.C., Barral, J.M., and Ulrich Hartl, F. (2003). More than folding: localized functions of cytosolic chaperones. Trends Biochem Sci *28*, 541-547.

Zhang, G., and Ignatova, Z. (2011). Folding at the birth of the nascent chain: coordinating translation with co-translational folding. Curr Opin Struct Biol *21*, 25-31.

Zimmerman, S.B., and Minton, A.P. (1993). Macromolecular crowding: biochemical, biophysical, and physiological consequences. Annu Rev Biophys Biomol Struct *22*, 27-65.

7 Appendix: the full electrophoresis gels shown in 'Results'

Related to Figure 4.1A

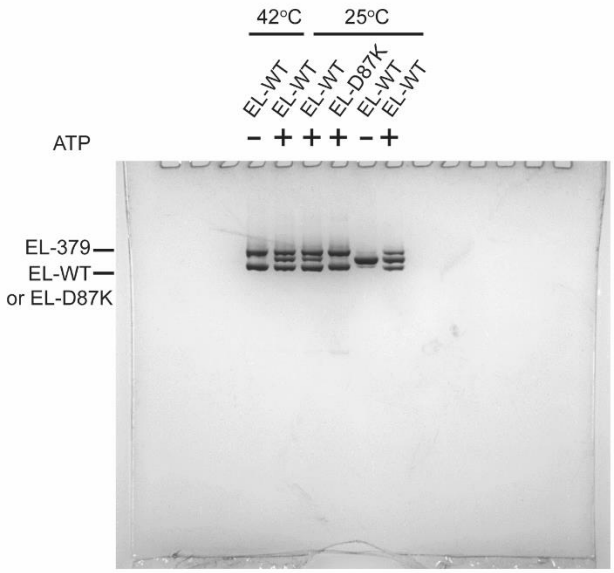

Related to Figure 4.1C

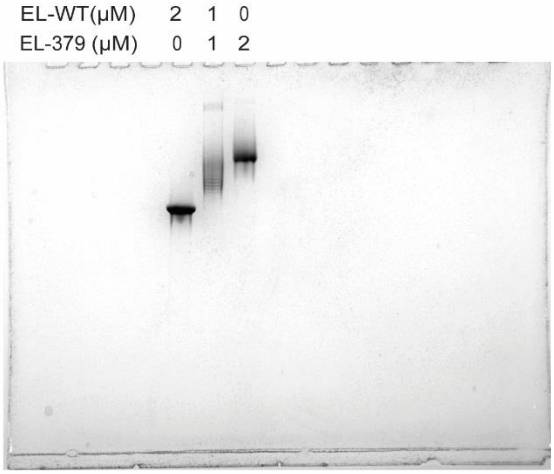

Related to Figures 4.3A and 4.3B

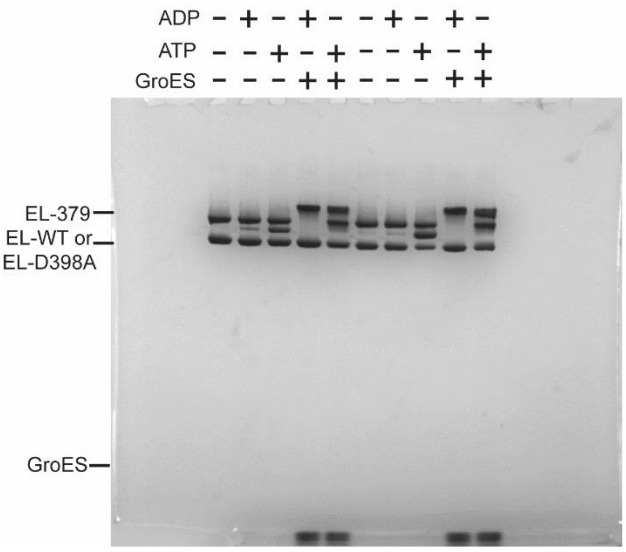

Related to Figures 4.3C

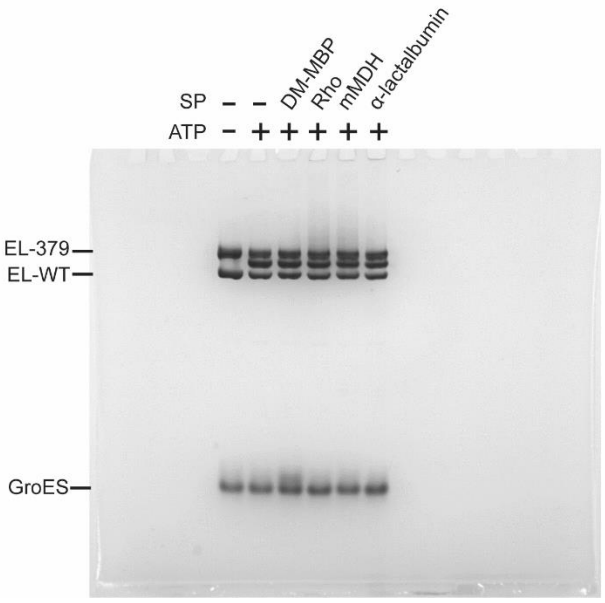

Related to Figure 4.4A

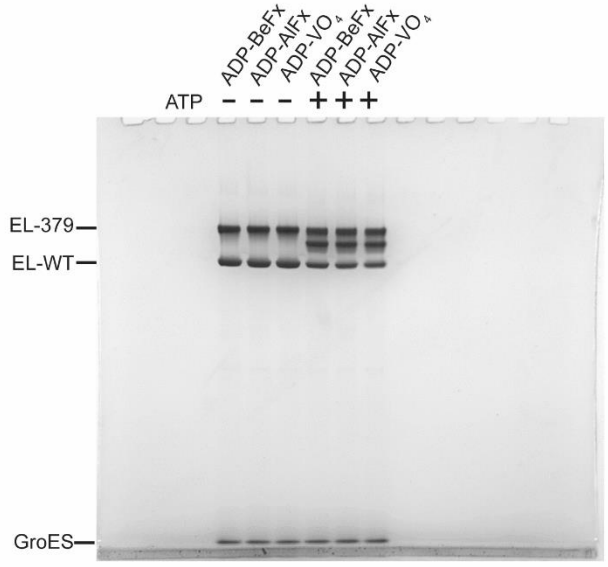

Related to Figure 4.4B

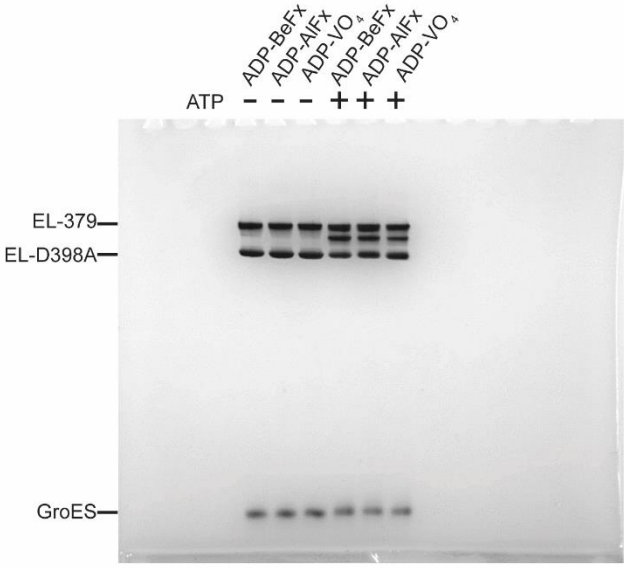

Related to Figure 4.4C

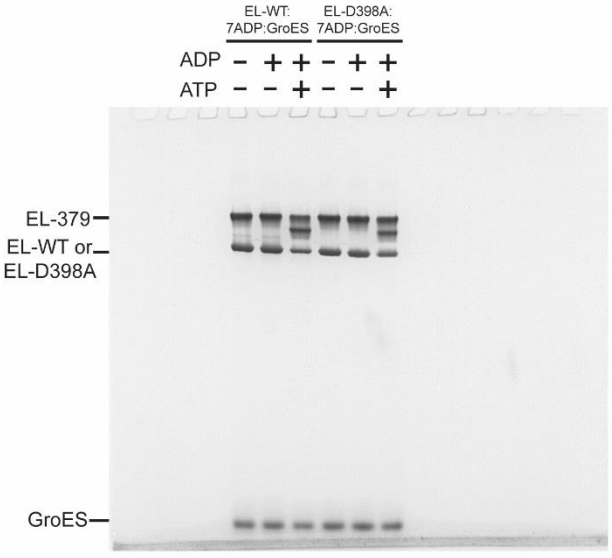

Related to Figures 4.5E

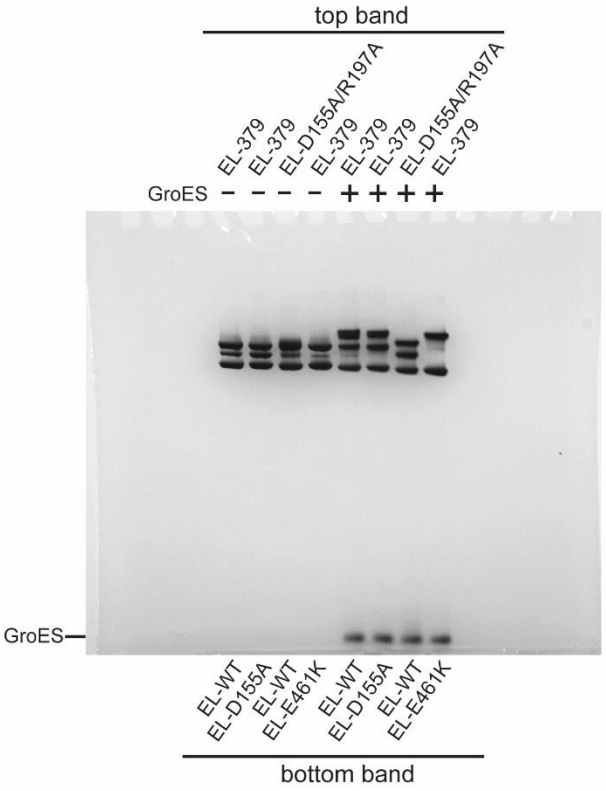

Related to Figure 4.7B

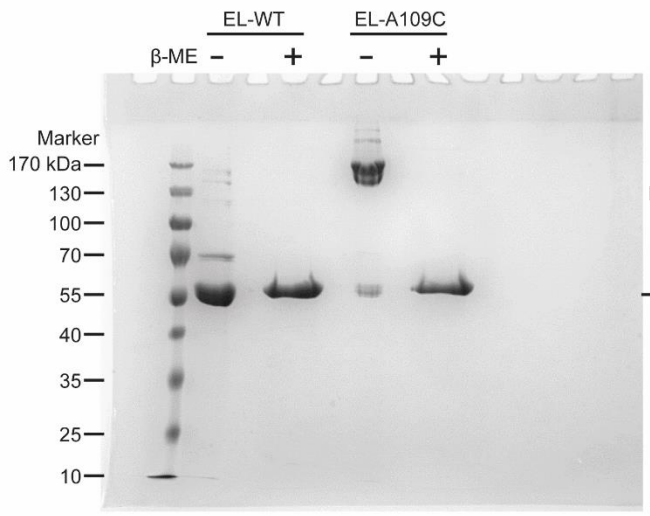

Related to Figure 4.8A

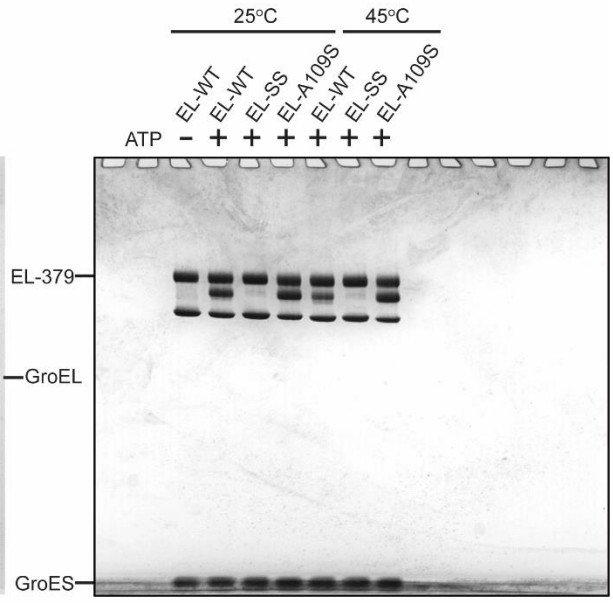

Related to Figure 4.8B